

2016

Circuitry of emotion: integration in orbitofrontal cortex

<https://hdl.handle.net/2144/15267>

"Downloaded from OpenBU. Boston University's institutional repository."

BOSTON UNIVERSITY
SCHOOL OF MEDICINE

Dissertation

CIRCUITRY OF EMOTION: INTEGRATION IN ORBITOFRONTAL CORTEX

by

CLARE TIMBIE

B.S., Tufts University, 2006

Submitted in partial fulfillment of the
requirements for the degree of
Doctor of Philosophy

2014

© 2014 by
CLARE TIMBIE
All rights reserved

Approved by

First Reader

Helen Barbas, Ph.D.
Professor of Health Sciences
Professor of Anatomy and Neurobiology

Second Reader

Jennifer Luebke, Ph.D.
Associate Professor of Anatomy and Neurobiology

Third Reader

Vasileios Zikopoulos, Ph.D.
Assistant Professor of Health Sciences

ACKNOWLEDGMENTS

I thank my mentor, Dr. Helen Barbas for her patience, enthusiasm, and encouragement in training me to be a scientist, and for teaching me how to set and achieve a high standard of excellence in research. I thank the members of my committee and Dr. Alan Peters for helpful comments and stimulating discussions on the project. I thank the members of the Neural Systems lab, including Marcia Feinberg, Dr. Basilis Zikopoulos, Dr. Jamie G. Bunce, Dr. Miguel Angel Garcia-Cabezas, Dr. Yohan John, Olivia Swanson, and Lisa Rycyna for their advice and technical assistance. I thank Dr. Maya Medalla for being my guide through graduate school; I could not ask for a better role model. I thank the MD/PhD community at Boston University for helping me navigate the complexities of the dual degree program.

I thank my friends Elizabeth Herman, Jenna Snow, Ruju Rai, and my sister Anna for their emotional support through this long process. I thank my parents, who have carved their own paths to apply their academic training, and who inspire me to challenge myself.

CIRCUITRY OF EMOTION: INTEGRATION IN ORBITOFRONTAL CORTEX

CLARE TIMBIE

Boston University School of Medicine, 2014

Ph.D. degree requirements completed in 2014

Dual M.D./Ph.D. degrees expected in 2016

Major Professor: Dr. Helen Barbas, Ph.D., Professor of Health Sciences; Anatomy and Neurobiology

ABSTRACT

The amygdala and orbitofrontal cortex are critical sites for processing emotional content. The amygdala sends dense pathways preferentially to the posterior orbitofrontal cortex (pOFC) and to the magnocellular part of the mediodorsal thalamic nucleus (MDmc), which is itself robustly connected with pOFC. This tri-partite circuit is thought to be activated when associating stimuli with emotional value, and is necessary to flexibly adapt behavior to changing circumstances, but its features and synaptic interactions are unknown. Labeling of pathways with distinct neural tracers in rhesus monkeys revealed that amygdalar terminals in pOFC were denser and larger compared to those in other prefrontal cortices. Further, amygdalar terminals in pOFC were even larger than thalamocortical terminals, which are considered highly efficient drivers of cortical neurons. In comparison with thalamocortical pathways, amygdalar terminals innervated more excitatory neurons and were more frequently multisynaptic. These features suggest that the amygdala sends a highly efficient excitatory pathway to pOFC. Among a small proportion of innervated inhibitory neurons, the pathway from the

amygdala to pOFC preferentially targeted the neurochemical classes of calbindin and calretinin inhibitory neurons in the upper layers, which are functionally suited to suppress distracting stimuli and enhance relevant signals. Further, the amygdalar pathway to MDmc targeted thalamocortical relay neurons, including those that project to pOFC, providing a second route for amygdalar signals to reach cortex. Neurochemical and morphological differences among terminals suggest that the direct pathway from the amygdala to pOFC and the indirect route through MDmc arise from separate neuronal populations in the amygdala. In MDmc, axon terminals from the amygdala formed synaptic triads, a thalamic specialization connecting excitatory projection neurons and local inhibitory neurons. This synaptic specialization is akin to what is found in sensory thalamic nuclei connecting peripheral sensory afferents with cortex. By analogy, the amygdala may act as a sensor of affective value, relaying signals about internal states to cortex through MDmc. The synaptic specializations shown here in the circuit that tightly interlinks the amygdala, MDmc, and pOFC shed light on the functional circuitry for emotional behavior and its disruption in psychiatric disorders such as phobias and obsessive compulsive disorder.

TABLE OF CONTENTS

TITLE PAGE	i
COPYRIGHT	ii
APPROVAL PAGE	iii
ACKNOWLEDGMENTS	iv
ABSTRACT	v
TABLE OF CONTENTS	vii
LIST OF TABLES	xi
LIST OF FIGURES	xii
LIST OF ABBREVIATIONS	xiv
CHAPTER ONE: AMYGDALAR PATHWAYS AND EMOTION.....	1
1.1 Overview: Major pathways of the primate amygdala.....	1
1.2 Anatomy of pOFC.....	4
1.2.1 Laminar organization of subcortical input and output.....	4
1.2.2 Inhibitory mechanisms in the cortex.....	6
1.3 Anatomy of the amygdala: connections with the cortex and subcortical structures.	8
1.4 Affective signaling in the amygdala	10
1.5 What signals are sent from the basal amygdala to pOFC?	12
1.6 Structure and function of thalamic MDmc	13

1.7 Thalamic MDmc plays a role in affective learning and social behavior	16
1.8 Disorders related to amygdala – thalamus – pOFC circuit	17
CHAPTER TWO: SPECIALIZED PATHWAYS FROM THE PRIMATE AMYGDALA TO POSTERIOR ORBITOFRONTAL CORTEX	20
2.1 Introduction.....	20
2.2 Materials and Methods.....	22
2.2.1 Surgery, tracer injections, and tissue processing	22
2.2.2 Brightfield and confocal microscopy.....	23
2.2.3 Electron microscopy	28
2.3 Results.....	33
2.3.1 Injection sites in the amygdala and MD	33
2.3.2 Amygdalar terminals were larger in pOFC than in other prefrontal areas	36
2.3.3 Amygdalar terminals were larger than thalamic terminals in pOFC	39
2.3.4 Appositions between amygdalar and thalamic projections with inhibitory neurons.....	41
2.3.5 Postsynaptic targets of amygdalar projections in pOFC.....	47
2.3.6 Synaptic specializations of amygdalar and thalamic boutons.....	50
2.3.7 Comparison of amygdalar synapses with surrounding neuropil.....	51
2.4 Discussion.....	52
2.4.1 Specialized amygdalar pathways target preferentially the pOFC: comparison with ACC	52

2.4.2 Specialized amygdalar ‘drivers’ to the upper layers of pOFC: comparison with the thalamic	55
2.4.3 Amygdalar drivers and feedforward inhibition: a mechanism for gain control	56
2.4.4 Circuits for flexible behavior and their disruption in psychiatric diseases	57

CHAPTER THREE: SEQUENTIAL PATHWAYS LINK THE PRIMATE

AMYGDALA, MEDIODORSAL THALAMUS, AND POSTERIOR

ORBITOFRONTAL CORTEX	60
3.1 Introduction.....	60
3.2 Materials and Methods.....	62
3.2.1 Surgery, tracer injections, and tissue processing	62
3.2.2 Brightfield and confocal microscopy.....	66
3.2.3 Electron microscopy	70
3.3 Results.....	74
3.3.1 Thalamic projection neurons targeting pOFC.....	74
3.3.2 Amygdalar pathways form synapses with excitatory projection neurons in MDmc	76
3.3.3 Amygdalar boutons in MDmc were larger than those in pOFC	81
3.3.4 Amygdalar axons in pOFC and MDmc colocalize with vesicular glutamate transporters.....	81
3.3.5 Amygdalar axons target projection neurons in MDmc that project to pOFC..	84
3.4 Discussion.....	86
3.4.1 Direct and indirect routes connect amygdala with pOFC	88

3.4.2 Divergence of amygdalar pathways to the cortex and to the thalamus.....	90
3.4.3 Amygdalar axons form synaptic triads in MDmc.....	92
3.4.4 Role of thalamus in emotion.....	94
CHAPTER FOUR: CONCLUSION.....	97
4.1 Amygdalar and thalamic pathways converge in pOFC	97
4.2 Sequential pathways link the amygdala with pOFC through MDmc	99
4.3 Functional implications.....	100
BIBLIOGRAPHY.....	101
CURRICULUM VITAE.....	115

LIST OF TABLES

Table 2.1. Injection sites in amygdalar and thalamic nuclei	34
Table 3.1. Injection sites in pOFC, amygdala, and thalamus	63

LIST OF FIGURES

Figure 1.1. Amygdalar pathways in the prefrontal cortex.	2
Figure 1.2. The amygdala targets pOFC directly and also indirectly through MD, which projects to pOFC.	3
Figure 1.3. Extrinsic connections of pOFC.	5
Figure 1.4. Intrinsic connections of pOFC.	7
Figure 1.5. Anatomical organization of amygdalar nuclei.	9
Figure 1.6. Structural and functional organization of thalamic MD.	14
Figure 1.7. Unanswered questions describing the synaptic organization and circuit mechanism of the tripartite circuit connecting the amygdala, thalamus, and pOFC.	19
Figure 2.1. Injection sites in the amygdala and mediodorsal thalamus.	35
Figure 2.2. Amygdalar boutons were densest and largest in pOFC.	38
Figure 2.3. Amygdalar axon boutons in pOFC were larger than in A32 or the thalamic.	40
Figure 2.4. Amygdalar terminals in the upper layers of pOFC were larger than thalamic terminals in the middle layers at the synaptic level.	43
Figure 2.5. Examples of amygdalar and thalamic axons targeting inhibitory neurons in pOFC.	46
Figure 2.6. Excitatory and inhibitory postsynaptic targets of amygdalar boutons in pOFC.	49
Figure 2.7. Summary of features in amygdalar pathway to pOFC, ACC, and 9/46.	53
Figure 3.1. Neural tracers used to label pathways in the amygdala and pOFC.	64
Figure 3.2. Neurons in MD projecting to pOFC colocalized with CB or PV.	75

Figure 3.3. Amygdalar axon terminals formed synapses on MDmc thalamic relay dendrites.....	78
Figure 3.4. Amygdalar axon terminals in MDmc were larger than those in the cortex and frequently multisynaptic.	79
Figure 3.5. Amygdalar axons in MDmc and pOFC express different glutamate transporters.....	82
Figure 3.6. Amygdalar axons in MDmc expressed VGLUT2 more frequently, while those in pOFC expressed more VGLUT1.	83
Figure 3.7. In MDmc, neurons projecting to pOFC overlapped with amygdalar axons...	85
Figure 3.8. Amygdalar signals reach pOFC directly, and indirectly through the thalamus.	87
Figure 4.1. Synaptic specializations in amygdalar pathways to pOFC and MD.	98

LIST OF ABBREVIATIONS

A9/46.....	dorsolateral prefrontal cortical areas 9 and 46
A32.....	medial prefrontal cortical area 32
AB-HRP	avidin-biotin horseradish peroxidase
ACC	anterior cingulate cortex
Amy At.....	amygdalar axon terminal
At.....	axon terminal
BDA	biotinylated dextran amine
BL	basolateral nucleus of amygdala
BM	basomedial nucleus of amygdala
BSA.....	bovine serum albumin
CB	calbindin
CBL.....	Cascade blue
Ce	central nucleus of amygdala
Cim.....	central intermediate nucleus of thalamus
Cl.....	central lateral nucleus of thalamus
cm.....	centimeter
Cn Md	centromedian nucleus of thalamus
Co.....	cortical nucleus of amygdala
CR	calretinin
DAB	diaminobenzidine
Den	dendrite

ECS	enhancement conditioning solution
EM	electron microscope
FE	fluoroemerald
FR	fluororuby
GABA	gamma-aminobutyric acid
IM	intercalated masses of amygdala
L	lateral nucleus of amygdala
LD	lateral dorsal nucleus of thalamus
LY	Lucifer yellow
MD	mediodorsal nucleus of thalamus
MDdc	mediodorsal nucleus of thalamus, densocellular part
MDmc	mediodorsal nucleus of thalamus, magnocellular part
MDmf	mediodorsal nucleus of thalamus, multiform part
MDpc	mediodorsal nucleus of thalamus, parvicellular part
Me	medial nucleus of amygdala
μm	micrometer
mm	millimeter
NGS	normal goat serum
OCD	obsessive-compulsive disorder
OPAl	orbital periallocortex
OPro	orbital proisocortex
P	pyramidal neuron

Pa..... paraventricular nucleus of thalamus

PB.....phosphate buffer

PBS phosphate buffer saline

pOFC..... posterior orbitofrontal cortex

PSD postsynaptic density

PV parvalbumin

Re nucleus reuniens of thalamus

SA spine apparatus

SER..... smooth endoplasmic reticulum

Sm stria medularis

Sp spine

SS spiny stellate neuron

TCthalamocortical

Thal Atthalamic axon terminal

TMBtetramethylbenzidine

TRN..... thalamic reticular nucleus

Tx Triton-X

VCo..... ventral cortical nucleus of amygdala

VGLUT1 vesicular glutamate transporter 1

VGLUT2 vesicular glutamate transporter 2

VL ventrolateral nucleus of thalamus

VPL.....ventral posterolateral nucleus of thalamus

CHAPTER ONE: AMYGDALAR PATHWAYS AND EMOTION

1.1 Overview: Major pathways of the primate amygdala

The amygdala, the brain's emotional sensor, associates stimuli with affective value and projects to subcortical areas for expression of emotions (Davis and Whalen, 2001; Ghashghaei and Barbas, 2002; Price, 2003). Pathways from the amygdala also innervate areas in prefrontal cortex, where signals conveying affective value converge with sensory information and influence executive functions (Ghashghaei et al., 2007). The entire prefrontal cortex is connected with the amygdala (Fig. 1.1). Among prefrontal cortices the medial and orbitofrontal regions have the strongest connections with the amygdala (Ghashghaei et al., 2007). The medial prefrontal region in the anterior cingulate (ACC) has a heavier output to the amygdala compared to input that it receives from the amygdala (Fig. 1.1A, D) (Ghashghaei et al., 2007). The opposite holds for the posterior orbitofrontal cortex (pOFC), an area poised to integrate emotional signals with sensory information (Fig. 1.1C, F) (Ghashghaei et al., 2007). Amygdalar pathways also terminate in the thalamic mediodorsal magnocellular nucleus (MDmc), which is reciprocally connected with prefrontal cortex, providing a second route for the amygdala to influence pOFC (Fig. 1.2) (Porrino et al., 1981). The systems' level and synaptic interactions of this tripartite circuit connecting the amygdala, pOFC, and MDmc remain largely unexplored.

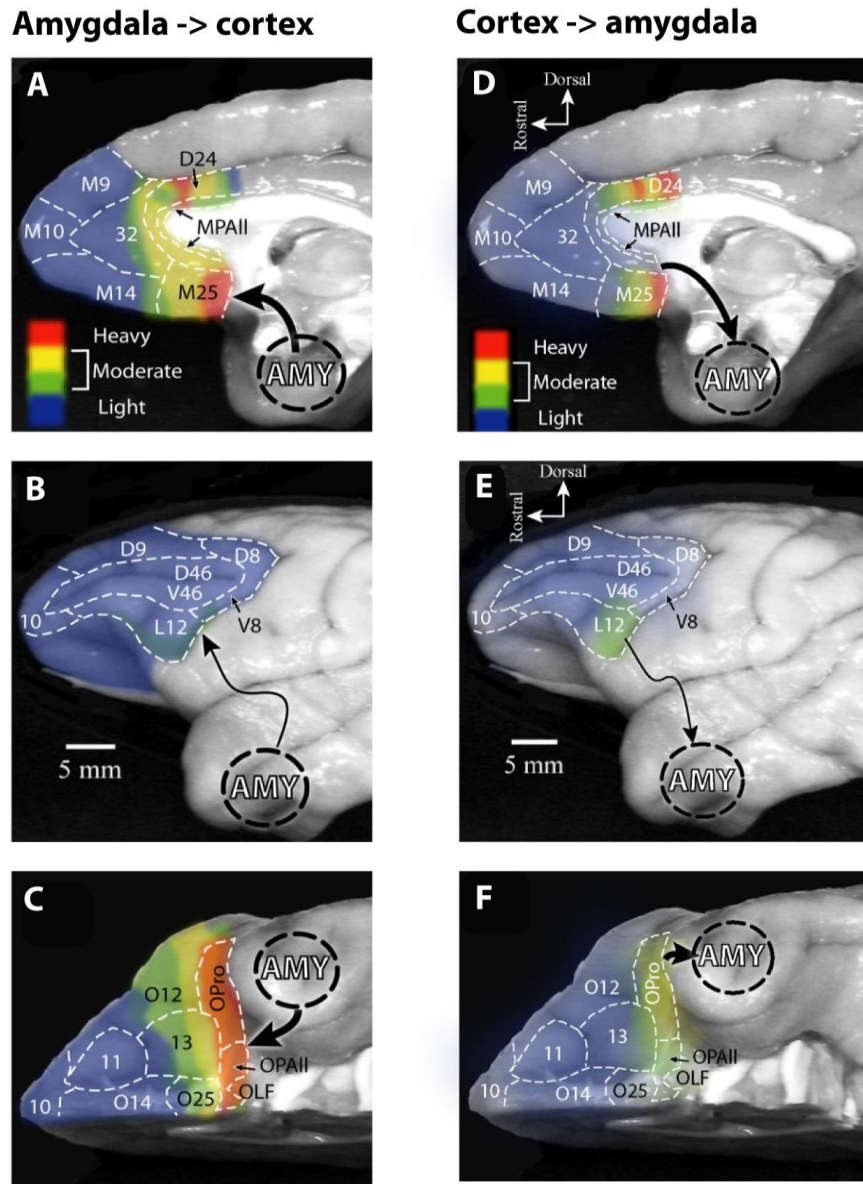


Figure 1.1. Amygdalar pathways in the prefrontal cortex.

Adapted from Ghashghaei et al, 2007. **A-C**, Amygdalar pathways strongly target posterior orbitofrontal and medial prefrontal cortices. **D-F**, Medial prefrontal cortices project robustly to the amygdala, in comparison with dorsolateral and orbitofrontal cortices.

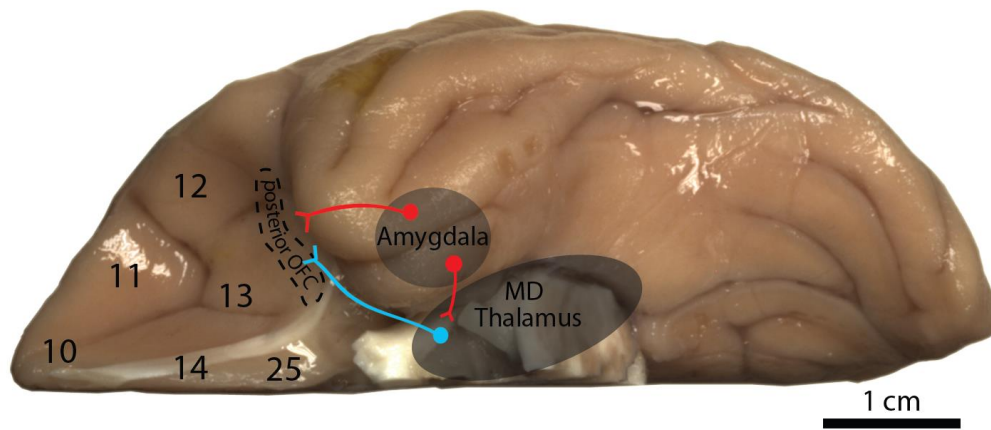


Figure 1.2. The amygdala targets pOFC directly and also indirectly through MD, which projects to pOFC.

1.2 Anatomy of pOFC

1.2.1 Laminar organization of subcortical input and output

In the rhesus monkey, the pOFC includes the orbital preisocortex (OPro), which is dysgranular, and orbital periallocortex (OPAll), which is agranular. Both of these areas are situated posterior to area 13 on the orbital surface of the brain (Fig. 1.1C, F) (Barbas and Pandya, 1989). Posterior orbital and medial prefrontal cortices receive the strongest input from the amygdala among prefrontal cortices (Ghashghaei et al., 2007). In comparison with medial areas, the pOFC is distinguished for receiving more input from the amygdala compared to its output (Fig. 1.1C, F), and also for having specially organized projections to amygdalar nuclei (Ghashghaei and Barbas, 2002; Ghashghaei et al., 2007). The pOFC is also the most multimodal area in prefrontal cortex: it receives sensory information from unimodal sensory association cortices representing all modalities (Fig. 1.3) (reviewed in Barbas et al., 2011). The convergence of widespread inputs from areas associated with sensory and motivational processing, suggests that the pOFC plays a key role in associating sensory information with affective value.

The pOFC is dysgranular, containing four distinguishable layers including layer 1, 2-3, a poorly developed layer 4, and layers 5-6, or agranular, which entirely lacks layer 4 (Fig. 1.4A) (Barbas and Pandya, 1989). Within pOFC, different inputs and outputs are organized in different layers. Amygdalar pathways to pOFC innervate mainly the upper cortical layers 1-3a, and output to the amygdala arises from neurons in layer 5 and to a lesser extent from layer 3 (Ghashghaei et al., 2007). In the amygdala, the pOFC targets the basolateral and basomedial nuclei, and interestingly also innervates the inhibitory

intercalated masses, which inhibit other amygdalar nuclei (Ghashghaei and Barbas, 2002). A major output of the intercalated masses is the central nucleus of the amygdala, which has downstream connections with brainstem and spinal autonomic centers (Price and Amaral, 1981; Barbas et al., 2011). Another major input to the pOFC is from the thalamic MDmc, which terminates mostly in the middle cortical layers (Giguere and Goldman-Rakic, 1988; McFarland and Haber, 2002). Neurons from layers 5 and 6 of pOFC project back to MDmc, with collaterals to the inhibitory thalamic reticular nucleus (Zikopoulos and Barbas, 2006; Xiao et al., 2009). Like the rest of the cortex, the pOFC projects to the striatum through neurons from layer 5, which innervate the medial caudate and nucleus accumbens (Haber et al., 1995). The striatum does not project back to the cortex. However, unlike the rest of the cortex, the frontal cortex receives the output of the striatum through projections from the pallidum and the substantia nigra reticulata, which innervate motor nuclei of the thalamus (ventral lateral and ventral anterior), as well as MD, which projects to the prefrontal cortex (Ilinsky et al., 1985; Russchen et al., 1987; Dermon and Barbas, 1994; McFarland and Haber, 2002; Zikopoulos and Barbas, 2007a).

1.2.2 Inhibitory mechanisms in the cortex

The separation of different pathways within pOFC is relevant because different layers represent different microenvironments, especially with respect to local inhibitory neurons (Fig. 1.4B-E). In the primate cortex, including humans, the calcium-binding proteins calbindin (CB), calretinin (CR), and parvalbumin (PV) label three neurochemical and non-overlapping classes of inhibitory GABAergic neurons (DeFelipe, 1997), which

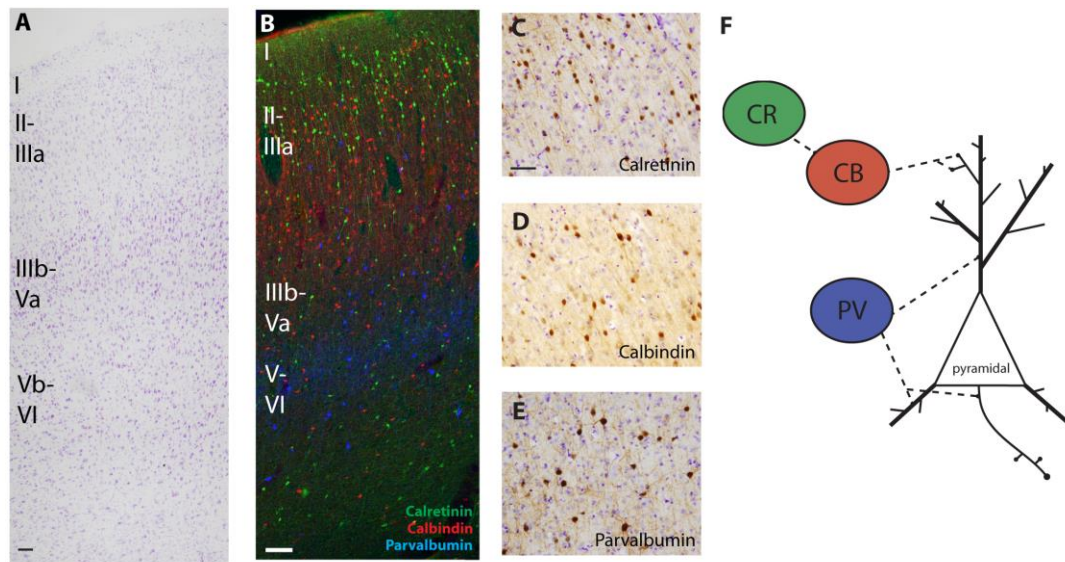


Figure 1.4. Intrinsic connections of pOFC.

A, Nissl stained coronal section through pOFC, shows dysgranular cytoarchitecture in OPro. Scale bar is 100 μm . **B**, Coronal section through pOFC shows the laminar distribution of CB, CR, and PV inhibitory neurons. Scale bar is 100 μm . **C-E**, Higher magnification photographs depict morphology of CR, CB, and PV inhibitory neurons. Scale bar is 50 μm and applies to C-E. **F**, PV neurons provide strong, perisomatic inhibition, while CB neurons target distal dendrites and weakly inhibit pyramidal neurons, and CR neurons inhibit CB neurons in the upper cortical layers.

make up about 20-30% of all neurons in the prefrontal cortex (Dombrowski et al., 2001). Upper cortical layers 1-3a contain more CB and CR inhibitory neurons, while the middle layers 3b-5 are populated with more PV inhibitory neurons (Dombrowski et al., 2001). These neurons differ in their postsynaptic targets: PV neurons provide strong, perisomatic inhibition of neighboring pyramidal (excitatory) neurons, while CB neurons target distal dendrites and weakly inhibit nearby pyramidal neurons (Fig. 1.4F) (DeFelipe, 1997). CR neurons in the upper layers inhibit CB neurons (DeFelipe, 1997). Physiological and computational evidence suggests that CB and CR neurons are especially suited to enhance signal in active cortical columns and reduce noise at the fringes (Constantinidis and Goldman-Rakic, 2002; Wang et al., 2004).

1.3 Anatomy of the amygdala: connections with the cortex and subcortical structures

The pOFC receives a dense excitatory projection from the amygdala, which may convey the affective value of stimuli (Ghashghaei et al., 2007; Murray, 2007). The amygdala is a collection of nuclei in the temporal lobe, which receive sensory information and act as an intermediary between autonomic systems and limbic cortices (Fig. 1.5A). Of these nuclei, the basolateral, basomedial, lateral and cortical nuclei project most strongly to prefrontal cortex (Barbas and De Olmos, 1990; Ghashghaei and Barbas, 2002). The basomedial nucleus (also known as accessory basal) is located medially in the amygdala, and dorsomedial to the basolateral nucleus (Price et al., 1987). The basomedial and basolateral nuclei are comprised of mostly pyramidal-like neurons,

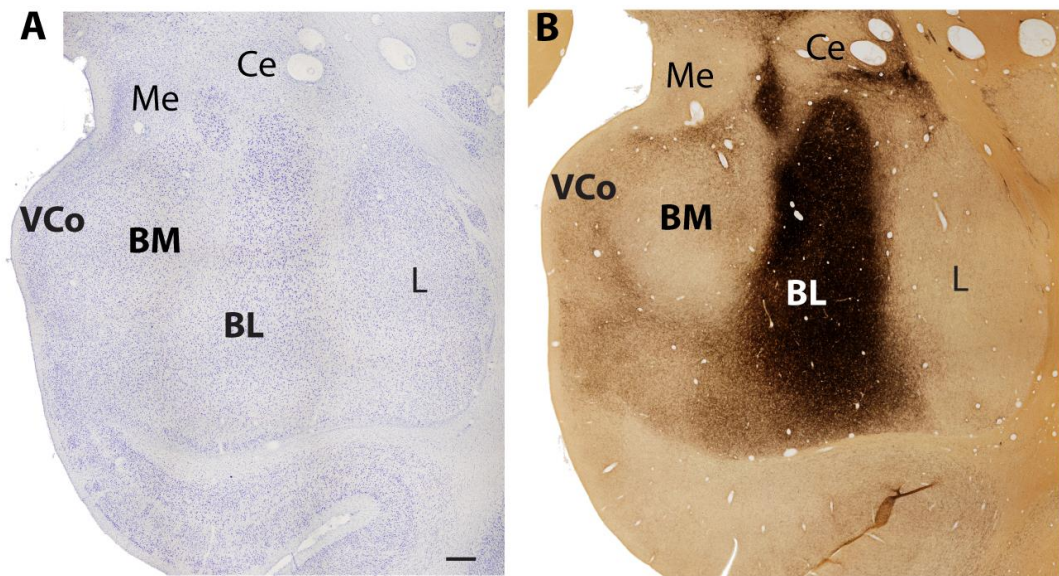


Figure 1.5. Anatomical organization of amygdalar nuclei.

Scale bar is 500 μm and applies to A-B. **A**, Nissl stained coronal section depicts relative position of amygdalar nuclei. **B**, Amygdala section stained for acetylcholinesterase, which is expressed strongly in the basolateral nucleus.

as well as non-spiny stellate cells which are likely intrinsic neurons (reviewed in Price et al., 1987; Pitkanen and Amaral, 1994). Similar to the cortex, amygdalar local inhibitory neurons colocalize with the calcium binding proteins CB, CR, and PV (Pitkanen and Kemppainen, 2002). The basolateral nucleus is distinguished by dense acetylcholinesterase staining, while the basomedial nucleus stains moderately for acetylcholinesterase (Fig. 1.5B) (De Olmos, 1990). Cholinergic fibers in these nuclei arise from neurons found in the nucleus basalis (Mesulam et al., 1983).

Basomedial and basolateral nuclei receive sensory information directly from sensory association cortices, as well as via the lateral nucleus of the amygdala, which relays information from thalamic and cortical sensory areas (reviewed in Price et al., 1987). These nuclei also receive input from hypothalamic nuclei including the ventromedial, lateral preoptic, and lateral hypothalamic areas, and cortical input from entorhinal and prefrontal cortex (Aggleton et al., 1980; reviewed in Price et al., 1987; Barbas, 2007). The basolateral and basomedial nuclei project extensively to the prefrontal cortex, entorhinal cortex, hippocampus, mediodorsal nucleus of the thalamus, basal forebrain, hypothalamus and striatum, as well as within the amygdala to the central, medial and amygdalo-hippocampal transition area (reviewed in Price et al., 1987; Barbas and De Olmos, 1990; Ghashghaei and Barbas, 2002).

1.4 Affective signaling in the amygdala

Electrophysiological studies can shed light on the types of signals that are sent along active pathways. In the basolateral amygdala, different classes of neurons have

distinct intrinsic firing properties. In cats, pyramidal neurons of the basolateral amygdala are either regular spiking or bursting, while local-circuit inhibitory neurons are fast-spiking (Pare et al., 1995; Pare et al., 2003). In the cat basolateral nucleus, bursting neurons predominate, while in the lateral nucleus, regular spiking neurons are more frequent (Pare et al., 1995). Excitatory, glutamatergic amygdalar neurons can also be distinguished by their expression of vesicular glutamate transporters, which are necessary for transporting glutamate into neurotransmitter vesicles (Fremeau, 2001; Otis, 2001). Two major classes of these transporters are VGLUT1 and VGLUT2 (Fremeau, 2001). In mice glutamatergic neurons in the medial and central nuclei express VGLUT2 exclusively while lateral and basolateral neurons mostly express VGLUT1 while some express VGLUT2 (Fremeau, 2001).

The physiological properties of amygdalar neurons have been studied extensively in the context of fear conditioning in rats, a process of learning associations between neutral and aversive stimuli such as acoustic tones (conditioned stimulus) and electric shocks (unconditioned stimulus). Extinction refers to unlearning this association when it no longer signals shock. This type of learning involves synaptic changes in the lateral amygdala, a site of integration between sensory modalities in the amygdala (Romanski et al., 1993). Specifically, neurons in the lateral amygdala change their firing properties in response to conditioned stimuli following fear conditioning, as measured by evoked field potentials and changes in single unit recordings in rats (Quirk et al., 1995; Rogan et al., 1997).

1.5 What signals are sent from the basal amygdala to pOFC?

The lateral amygdala projects to the basolateral nucleus, and neurons here are also responsive to conditioned stimuli. However, in addition to neurons which increase their firing rates in response to conditioned stimuli, the basolateral amygdala in mice also contains neurons which increase their firing rates in response to extinguished stimuli, suggesting that it has a key role in behavioral flexibility (Herry et al., 2008). Neurons in the basolateral amygdala may encode value, as they can modulate their firing rates in response to stimuli associated with rewarding or aversive events in macaque monkeys (reviewed in Morrison and Salzman, 2010). Similarly, neurons in orbitofrontal cortex can encode the relative value of rewards, likely through signals sent by amygdalar pathways (Tremblay and Schultz, 1999; Wallis and Miller, 2003; Hosokawa et al., 2007; Morrison and Salzman, 2011).

Monkeys with excitotoxic lesions of the amygdala are able to learn new reinforcement associations, but show deficits in updating reward value, also known as reinforcement devaluation (Malkova et al., 1997; Izquierdo and Murray, 2007). Amygdala-lesioned monkeys continue responding to stimuli associated with devalued rewards, such as foods the animal has been satiated with previously (Malkova et al., 1997; Izquierdo and Murray, 2007). However, excitotoxic amygdala lesions do not impair unlearning previously rewarded associations or extinguishing previously rewarded responses (Izquierdo and Murray, 2005, 2007; Rudebeck and Murray, 2008). This suggests that the amygdala is critical for updating the internal value of rewards.

Monkeys with transient inactivation of pOFC also show deficits in reinforcer devaluation (West et al., 2011). Unlike amygdalar inactivation, pOFC activity is necessary when the animal must avoid choosing a devalued reward, while amygdalar activity is necessary to update internal values of rewards during satiation (West et al., 2011). This suggests that while the amygdala and pOFC are both required to flexibly adjust behavior to changing rewards, the amygdala is critical for changing representations of reward value, while pOFC is needed to adjust behavior to match current reward values. The synaptic interactions between the amygdala and pOFC underlying this important pathway for flexible behavior have not yet been described.

1.6 Structure and function of thalamic MDmc

In addition to strong pathways to pOFC, the amygdala sends dense pathways to the thalamic MD (Fig. 1.6) (Porrino et al., 1981; Miyashita et al., 2007). The mediodorsal thalamic nucleus of rhesus monkeys has four sectors: the medial magnocellular (MDmc), central parvicellular (MDpc), lateral multiform (MDmf), and posterior densocellular (MDdc) (Olszewski, 1952). Of these, the magnocellular is the most strongly connected with pOFC and the amygdala (Porrino et al., 1981; Aggleton and Mishkin, 1984; Giguere and Goldman-Rakic, 1988; Dermon and Barbas, 1994; Xiao et al., 2009).

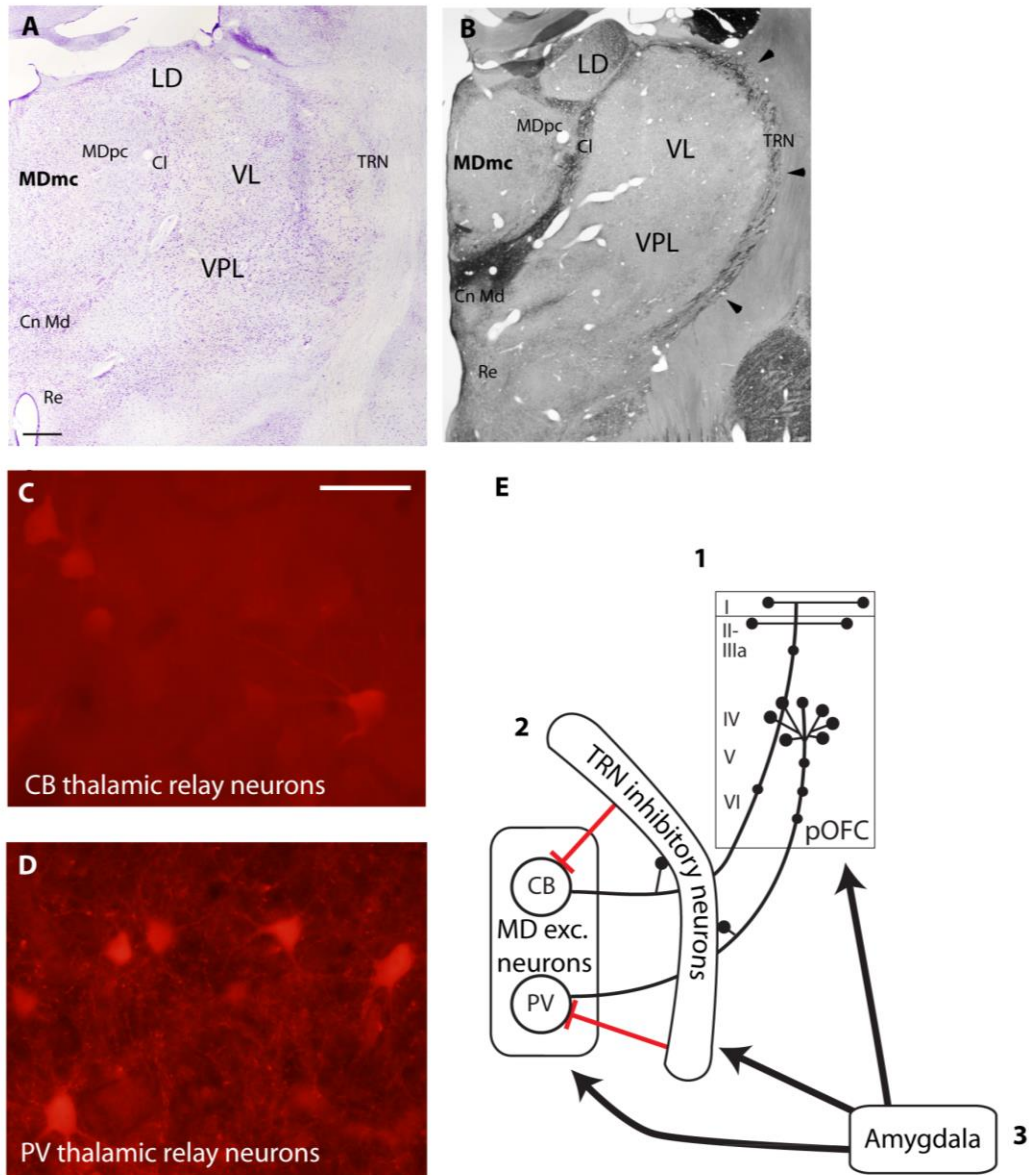


Figure 1.6. Structural and functional organization of thalamic MD.

A, Nissl stained coronal section through the thalamus depicts the relative position of MD. Scale bar is 1 mm and applies to A-B. **B**, Adapted from (Zikopoulos and Barbas, 2007b). Thalamic section stained for acetylcholinesterase, depicts nuclear borders of MD and TRN. **C-D**, Excitatory thalamic relay neurons are labeled with CB or PV in the dorsal thalamus. Scale bar is 50 μ m. **E1**, Schematic depicts the upper and middle layer cortical projections of CB and PV thalamic neurons, respectively; **E2**, TRN neurons inhibit MD projection neurons, and receive collaterals of projection neurons; **E3**, Amygdalar pathways strongly target MD, TRN, and pOFC.

The primate MDmc contains large multipolar neurons, including some that contain CB, PV, or CR (Fig. 1.6C-E) (Jones and Hendry, 1989; Jones, 2009). Unlike in the cortex, these calcium-binding proteins mark different classes of excitatory projection neurons in the thalamus. CB neurons project to the upper cortical layers, while PV neurons innervate the middle layers (Jones, 1998; Jones, 2009). Whether CR neurons provide a third pathway to the cortex has not been addressed.

Additionally, the primate thalamus contains local inhibitory neurons which feature vesicle-containing dendrites that can be both pre- and post-synaptic and are GABAergic (Famiglietti and Peters, 1972; Kultas-Ilinsky and Ilinsky, 1991). Like the rest of the dorsal thalamus, neurons in MD also receive inhibitory input from the thalamic reticular nucleus (TRN, Fig. 1.6E) (Tai et al., 1995). Also like other thalamic nuclei, MD receives the inhibitory output of the basal ganglia, which it communicates to the frontal cortex via thalamocortical projections (Russchen et al., 1987; Carpenter, 1989; McFarland and Haber, 2002). The robust connections with pOFC and the amygdala distinguish MDmc from other thalamic nuclei (Fig. 1.6E).

Thalamic projection neurons have unique physiological properties.

Thalamocortical neurons are capable of switching between a tonic firing mode that transmits signals linearly to cortex, and bursting mode which is associated with oscillatory activity during sleep (reviewed in Steriade and Deschenes, 1984; Jones, 2009). Switching between modes is associated with projections from corticothalamic neurons (reviewed in Jones, 2009). Thalamocortical neurons form two pathways to cortex, which have been called drivers and modulators (Sherman and Guillery, 1998). Drivers convey

signals to cortex that reliably induce a change in the firing rate of postsynaptic neurons. On the other hand, modulators appear to be important for gain control and modulate the response properties of postsynaptic neurons (Sherman and Guillery, 1998; Abbott and Chance, 2005). Thalamocortical driver pathways are thought to terminate in the middle cortical layers, while modulator pathways innervate the upper cortical layers (Jones, 1998). The role of these dual projection systems in emotion with respect to amygdalar and prefrontal pathways has not yet been studied.

1.7 Thalamic MDmc plays a role in affective learning and social behavior

The thalamic MDmc has classically been implicated in memory based on evidence that its damage results in amnesia (Markowitsch, 1982; Zola-Morgan and Squire, 1985). More recently, thalamic lesions have been implicated in emotional processes as well: thalamic MD lesions result in deficits in reward devaluation, similar to deficits following amygdala lesions (Mitchell et al., 2007). Further, in rats, MD lesions result in changes in emotional responses, and the animals appear to be tamer (Waring and Means, 1976). Monkeys show deficits in reward learning following crossed lesions, in which MD is lesioned in one hemisphere and the amygdala and/or OFC are lesioned in the other hemisphere. This paradigm was used to investigate the necessity of interactions between the amygdala, MD, and prefrontal cortex (Gaffan and Murray, 1990; Izquierdo and Murray, 2010).

The thalamic MDmc is involved in updating rewards associated with stimuli, as shown through lesion studies, but what role does it play in this process? Neurons in MD

modulate their firing in response to stimuli that are associated with reward, similar to amygdalar neurons in the basomedial and basolateral nuclei (Oyoshi et al., 1996). This suggests that MD receives input from amygdalar neurons related to stimulus-reward associations.

Amygdalar and thalamic MD pathways converge strongly in pOFC, and in another region associated with attention: the TRN (Fig. 1.6E) (Zikopoulos and Barbas, 2012). Both amygdalar and MD axons innervate robustly and broadly the TRN, which sends inhibitory projections to thalamic nuclei (Zikopoulos and Barbas, 2012). Amygdalar axons innervate neurons in TRN that innervate sensory and higher order thalamic nuclei, including MD. This pattern of innervation suggests that the amygdala may also gate thalamocortical signals to direct attention to emotionally salient stimuli (Zikopoulos and Barbas, 2012).

1.8 Disorders related to amygdala – thalamus – pOFC circuit

Study of the synaptic interactions in this circuit for emotion is needed to understand their potential disruption in psychiatric diseases, such as phobias and obsessive-compulsive disorder (OCD) which affect nodes in this tightly knit circuit. OCD is characterized by obsessive, anxiogenic thoughts and repetitive compulsive behaviors (Greenberg et al., 2010). For example, multiple lines of evidence point to alterations in pathways linking the orbitofrontal cortex, thalamic nuclei, and amygdala in the pathogenesis of OCD (Rauch et al., 1994; Adler et al., 2000; Kim et al., 2001; Lacerda et al., 2003; Kang et al., 2004). Reduced cortical inhibition has been shown in

OCD patients, and therapeutic deep brain stimulation may exert its effect by enhancing cortical inhibition (Greenberg et al., 1998; McCracken and Grace, 2007; Richter et al., 2012). However, the interactions between amygdala and thalamic projections with cortical inhibitory neurons in primates have not yet been studied. In addition to shedding light on the pathogenesis of psychiatric disorders, a detailed understanding of the circuit connecting the amygdala, thalamus, and orbitofrontal cortex is needed to interpret electrophysiological data and build computational models of emotional learning (Fig. 1.7). The following studies were designed to investigate the organization of this important circuit from the level of the system to the synapse.

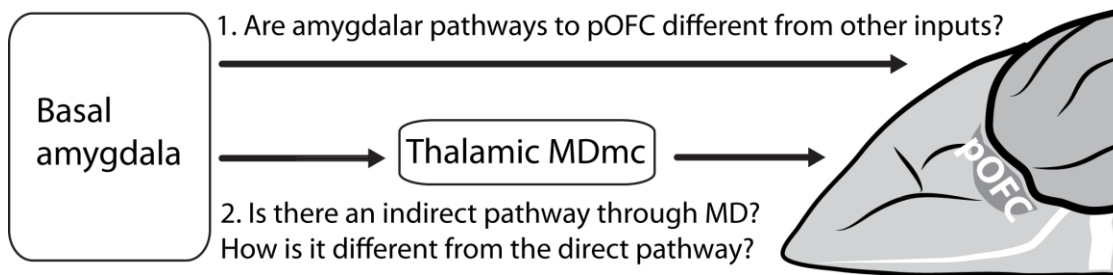


Figure 1.7. Unanswered questions describing the synaptic organization and circuit mechanism of the tripartite circuit connecting the amygdala, thalamus, and pOFC.

CHAPTER TWO: SPECIALIZED PATHWAYS FROM THE PRIMATE AMYGDALA TO POSTERIOR ORBITOFRONTAL CORTEX

2.1 Introduction

Emotions guide decisions and their disruption impairs flexible behavior as in obsessive-compulsive disorder and autism (Bachevalier and Loveland, 2006; Maia et al., 2008). The amygdala has been implicated in emotional processes and through connections with prefrontal cortex (Porrino et al., 1981; Ghashghaei and Barbas, 2002) likely transmits affective valence that influences executive functions (reviewed in Bechara et al., 2000; Murray, 2007).

Pathways from the amygdala terminate most densely in posterior orbitofrontal cortex (pOFC) and anterior cingulate cortex (ACC) (Ghashghaei et al., 2007). The pOFC also receives input representing all sensory modalities from high-order sensory association cortices (reviewed in Cavada et al., 2000; Barbas et al., 2011). As the most multimodal prefrontal region and biased recipient of amygdalar pathways, the pOFC is poised to integrate signals from the external environment and the internal milieu associated with the affective significance of stimuli. In contrast, the ACC is a biased sender of projections to the amygdala (Ghashghaei et al., 2007), mediating emotional expression through pathways to central autonomic structures (reviewed in Devinsky et al., 1995).

Another strong pathway to pOFC is from the mediodorsal thalamic nucleus (MD) and adjacent midline nuclei (Goldman-Rakic and Porrino, 1985; Dermon and Barbas,

1994). The amygdalar and thalamic pathways show opposite laminar innervation in pOFC (Porrino et al., 1981). Amygdalar fibers densely innervate lower layer 1 and layer 2 and to a lesser extent all other layers (Ghashghaei et al., 2007), while MD innervates most densely the middle cortical layers and to a lesser extent the upper layers (McFarland and Haber, 2002). Different layers represent distinct microenvironments. The upper layers (1-3a) include dendrites from pyramidal neurons in layers 2-5 (DeFelipe and Farinas, 1992) and among inhibitory neurons they are populated preferentially with the neurochemical classes of calretinin (CR) and calbindin (CB) neurons. In contrast, the middle layers are preferentially populated with parvalbumin (PV) inhibitory neurons (Gabbott and Bacon, 1996; Dombrowski et al., 2001).

Pathways that terminate in different layers are thought to differ functionally. Sensory thalamic pathways to the middle cortical layers have been called “drivers” because they reliably elicit action potentials in postsynaptic neurons, assuring transmission of signals (Sherman and Guillery, 1998). Pathways that terminate in the upper layers form synapses distally on postsynaptic neurons, mildly change their excitability, and thus have been called “modulators” (Sherman and Guillery, 1998). While the predominant termination pattern of amygdalar fibers in upper pOFC layers suggests a modulatory role, there is evidence that the amygdala can drive cortical neurons, at least in mice (Little and Carter, 2013).

Understanding the features of pathways from the amygdala to distinct prefrontal cortices in comparison with parallel thalamocortical pathways is prerequisite to unraveling core cognitive-emotional interactions that are disrupted in psychiatric

disorders. Key outstanding questions addressed in this study pertain to the strength and potential efficacy of these pathways and interactions with excitatory and distinct classes of inhibitory neurons in prefrontal cortices. We identified specializations in amygdalar pathways to pOFC, suggesting specificity in the information conveyed by this strong pathway for flexible behavior.

2.2 Materials and Methods

2.2.1 Surgery, tracer injections, and tissue processing

Experiments were conducted on six rhesus monkeys (*Macaca mulatta*) aged 2-3.5 years of both sexes injected with 1-2 distinct neural tracers for an overall 10 cases (Table 1). Experiments were conducted according to the *Guide for the Care and Use of Laboratory Animals* (National Research Council, 2011). Experimental methods were approved by the Institutional Animal Care and Use Committee at Boston University School of Medicine, Harvard Medical School, and New England Primate Research Center. Procedures involving animals were designed to reduce the number of animals needed and minimize animal suffering.

Prior to surgery, magnetic resonance images were obtained following animal sedation with ketamine hydrochloride and propofol anesthesia, in order to calculate stereotaxic coordinates for the injection sites. Experiments were conducted under sterile conditions, and animals were continuously monitored for respiratory rate, oxygen saturation, heart rate, and temperature. For surgery, the animals were placed under isoflurane anesthesia and positioned in stereotaxic apparatus (Kopf 1430M, David Kopf

Instruments; Tujunga, CA, USA), and a small opening was made in the skull and dura. We injected 10% dilutions of Lucifer yellow dextran (LY, 4 μ l, 10 kDa, Invitrogen; Carlsbad, CA, USA), fluoroemerald (FE, fluorescein dextran, 3 μ l, 10kDa or a mixture of 3 kDa and 10 kDa; Invitrogen), fluororuby (FR, tetramethylrhodamine dextran, 3 – 4 μ L, mixture of 3 kDa and 10kDa; Invitrogen), biotinylated dextran amine (BDA, 9 μ l, 3 kDa or a mixture of 3 kDa and 10 kDa; Invitrogen) or Cascade Blue dextran (CBL, 6 μ l, mixture of 3 kDa and 10 kDa, Invitrogen) into amygdalar or thalamic nuclei using Hamilton syringes (10 μ l; Reno, NV, USA). After 18 days, the animals were anesthetized with sodium pentobarbital and perfused transcardially with 4% paraformaldehyde, 0.2% glutaraldehyde in 0.1M phosphate buffer saline (PBS), pH 7.4. The brain was removed, cryoprotected in ascending sucrose solutions (10% to 30% sucrose %wt/vol in 0.1M PBS, pH 7.4 with 0.05% sodium azide; Sigma-Aldrich, St. Louis, MO, USA) (Rosene et al., 1986), frozen in isopentane (Fisher Scientific; Pittsburgh, PA, USA), at -80°C, and cut on a freezing microtome (AO Scientific Instruments, Reichert Technologies; Buffalo, NY, USA), in 50 μ m coronal sections forming 10 series. Sections were stored free floating at -20°C in a solution of 30% ethylene glycol, 30% glycerol, 0.05% sodium azide in 0.05 M phosphate buffer, pH 7.4.

2.2.2 Brightfield and confocal microscopy

2.2.2.1 Immunohistochemistry: Free floating sections were incubated for one hour at 4°C in 0.05M glycine (Sigma-Aldrich) and pre-blocked for one hour at 4°C in 5% normal goat serum (NGS, Vector Laboratories; Burlingame, CA, USA), 5% bovine serum

albumin (BSA, Sigma-Aldrich) and 0.2% Triton-X (Sigma-Aldrich) in 0.01M PBS. For cases using BDA tracer, sections were incubated for one hour at 25°C with avidin-biotin horseradish peroxidase (AB-HRP, Vectastain Elite ABC kit, Vector) at a 1:100 dilution in PBS, followed by rinses in PBS (all rinses are 3 x 10 minutes unless otherwise indicated), and tracer was visualized with incubation for 1-3 minutes in diaminobenzidine (DAB substrate kit, Vector). For cases with fluorescent tracer injections, sections were first incubated with avidin-biotin blocking solutions (AB blocking kit, Vector), and then rinsed in PBS and incubated overnight at 4°C with primary antibodies to tracers (FE [Invitrogen, Cat# A889, RRID: AB_221561], FR [Invitrogen, Cat# A6397, RRID: AB_1502299], CBL [Invitrogen, Cat# A5760, RRID: AB_11181009], or LY [Invitrogen Cat# A5750 RRID:AB_1501344] at 1:800 in 1% NGS, 1% BSA, and 0.1% Triton-X in PBS; all rabbit polyclonal IgG). Sections were then rinsed in PBS and incubated for two hours at 25°C with biotinylated secondary antibodies (1:200 in 1% NGS, 1% BSA, and 0.1% Triton-X in PBS; biotinylated goat anti-rabbit IgG, Vector, Cat# BA-1000, RRID: AB_2313606), followed by AB-HRP and DAB, as above.

Sections were rinsed in 0.1M phosphate buffer (PB), pH 7.4, mounted on gelatin-coated glass slides, and dried for at least 10 days. Slides were defatted in a 1:1 chloroform-ethanol mixture for one hour and then rehydrated in a series of ethanols (100%, 95%, 70%) and then water, followed by staining with 0.05% thionin and rinsed again in water. Slides were then dehydrated in a series of ethanols (70%, 95%, 100%), cleared in xylene (Sigma-Aldrich), and coverslipped with Entellan mounting medium (Sigma-Aldrich).

For analysis with confocal microscopy, tissue was incubated in glycine and pre-blocked as above. Tracers and calcium-binding proteins were bound overnight at 4°C with primary antibodies (FE, FR, CBL, or LY: 1:800 in 1% NGS, 1% BSA, and 0.1% Triton-X in PBS; and CB [Swant, Cat# 300, RRID:AB_10000347], CR [Swant, Cat# 6B3, RRID:AB_1000032], or PV [Swant, Cat# 235, RRID:AB_10000343] at 1:2000, mouse monoclonal, Swiss Antibodies; Bellinzona, Switzerland). Next the tissue was rinsed in PBS and incubated overnight at 4°C in secondary antibodies conjugated with fluorescent label (1:100 in 1% NGS, 1% BSA, and 0.1% Triton-X in PBS; Alexa 568 goat anti-rabbit IgG [Invitrogen, Cat# A11011, RRID:AB_143157] or goat anti-mouse IgG [Invitrogen, Cat# A11019, RRID:AB_143162] and Alexa 488 goat anti-mouse IgG [Invitrogen, Cat# A11001, RRID:AB_10566289] or goat anti-rabbit IgG [Invitrogen, Cat# A11008, RRID:AB_143165]). Sections were rinsed in PB, mounted on gelatin-coated glass slides and coverslipped while damp with Prolong Gold Antifade mounting medium (Invitrogen).

In all cases, primary and secondary antibody penetration was enhanced with eight minute runs (three minutes on, two minutes off, three minutes on) in a temperature-controlled variable wattage microwave oven (150W at 4°C, Pelco Biowave with ColdSpot and ThermoCube, Ted Pella; Redding, CA, USA) during each incubation. For three cases (BB, BN, and BO), a method of antigen retrieval was used prior to immunohistochemistry to enhance signal: sections were rinsed in PB, then incubated in 0.01M sodium citrate buffer (pH 8.5) at 35-45°C for 30 minutes, followed by incubation in glycine, pre-blocking and immunohistochemistry as above (Jiao et al., 1999). In

control experiments omission of the primary antibodies and incubating in secondary antibody solutions showed no immunolabeling.

2.2.2.2 Data analysis: We used thionin-stained tissue to determine cytoarchitectonic and laminar boundaries of area OPro and area 32 in prefrontal cortex (Barbas and Pandya, 1989). OPro is dysgranular, contains a layer 2, and has slightly more prominent deep layers compared to upper layers (Barbas and Pandya, 1989). Area 32 (A32) is also dysgranular, has a broad layer 1, and a greater density of neurons in deep layers compared to upper layers (Dombrowski et al., 2001). All analyses were conducted in area OPro and area 32 in the anterior cingulate. We refer to these areas as pOFC (OPro) and ACC (A32) for short, and based on their common references in the primate literature by location.

Columns with DAB-labeled amygdalar or thalamic fibers within pOFC or A32 were photographed at 1000x covering equal volumes of cortex in layer 1, layers 2-3a, layers 3b-5a, and layers 5b-6 (Olympus BX51 and DP70, Olympus; Center Valley, PA, USA). The maximum diameter of each labeled bouton was measured using the program Reconstruct (Synapse Web Reconstruct, RRID:nif-0000-23420) (Fiala, 2005). At least 4 columns were analyzed in order to sample evenly across cortical areas; additional columns were sampled until at least 1000 boutons were identified in each case, which is sufficient to obtain a significant result using a Cohen's *d* power analysis for an effect size of 0.2 (Cohen, 1988). Statistical analyses were performed using Statistica software (version 10, StatSoft; Tulsa, OK, USA). Boutons were classified as large or small using a

k-means cluster analysis for two clusters in each case and each area (cutoff between small and large ranged from 0.91-1.26 μm). We used two-tailed t tests to compare mean diameters across areas and pathways, and ANOVA with Bonferroni post hoc analysis to compare bouton size distributions across areas and pathways.

We determined the density of small and large labeled amygdalar boutons in layers 1, 2-3a, and 3b-5a of pOFC and area 32. For comparison, we also include areas 9/46, which are granular areas with well delineated six layers. We determined densities using a semi-automated method of systematic random sampling using a microscope fitted with a motorized stage and controlled by software (StereoInvestigator 10, MBF Biosciences; Williston, VT, USA; Olympus BX60). After pilot studies to determine the optimal sampling rate for each case and layer we used a counting frame of 50 μm by 50 μm , disector height of 11 μm and a counting frame size that varied from 100 μm by 100 μm to 750 μm by 750 μm to achieve a coefficient of error (Gundersen, $m=1$) less than 0.1. A cutoff of 1 μm was used to distinguish between small and large boutons for all cases and all layers, which is approximately the average of all cutoff values calculated (mean cutoff value = 1.1 μm , $n = 12$ cases). Densities were normalized to the densest area in each case, and we compared normalized densities across areas using ANOVA with Bonferroni post-hoc analysis.

We used laser scanning confocal microscopy (Fluoview FV-300, Olympus; LSM-510, Carl Zeiss Microscopy; Thornwood, NY, USA) to study appositions between fluorescently labeled tracer and dendrites labeled for calcium-binding proteins CR, CB, and PV. Stacks of optical sections 0.3 μm thick were acquired in columns of pOFC

containing labeled fibers in layers 1-3a and 3b-5a, and all labeled boutons and appositions between labeled amygdalar or thalamic boutons and labeled dendrites were counted. Appositions were defined as close contacts between a labeled bouton and labeled dendrite, including an area of colocalization at the point of contact. Alexa 488 conjugates were excited with a 488 nm Argon laser, Alexa 568 conjugates were excited with a 568 nm Krypton laser (Olympus) or 543 nm Helium Neon laser (Zeiss). We used χ^2 tests to compare proportions of labeled axons forming appositions with labeled dendrites across pathways and layers.

2.2.3 Electron microscopy

2.2.3.1 Immunohistochemistry and embedding: To study pathways in the electron microscope (EM), we used triple immunohistochemistry to identify tracers with DAB (which appears as uniform dark precipitate under EM), and calcium binding proteins (CB, PV, or CR) using gold labeling with silver enhancement (forms clumps of round particles) and tetramethylbenzidine (TMB) staining (forms rod-shaped precipitate), modified from previous studies (Medalla et al., 2007). Tissue sections were incubated as above in 0.01M sodium citrate, pH 8.5 (30 minutes at 35°C), 0.05 M glycine (one hour at 4°C), and any BDA tracer was blocked with AB blocking solutions. Background binding was blocked with incubation for one hour at 4°C in 5% NGS, 5% BSA, 0.025% Triton X-100 (Roche Applied Sciences; Indianapolis, IN, USA), 0.1% acetylated BSA-c (Aurion; Wageningen, NL), and 3.5% mouse blocking reagent (MOM basic kit, Vector) in PBS. Sections were then bound overnight at 4°C with antibodies for tracers (FE, FR, or LY:

1:800 in 1% NGS, 1% BSA, 0.1% BSA-c, 0.025% Triton X-100, and 8% MOM protein concentrate [MOM basic kit, Vector] in PBS; rabbit polyclonal IgG, Invitrogen) and one of three calcium binding proteins (CB, CR, or PV: 1:2000, mouse monoclonal IgG, Swant). All primary and secondary antibody incubations included an eight minute microwave run as above.

Sections were rinsed in PBS then incubated for six hours at 25°C with biotinylated secondary antibodies for tracers (1:200 in 1% NGS, 1% BSA, 0.1% BSA-c, 0.025% Triton X-100, 8% MOM protein concentrate, and 0.1% cold water fish gelatin [Aurion] in PBS; biotinylated goat anti-rabbit IgG, Vector) and gold-conjugated secondary antibodies for calcium-binding proteins (1:50 UltraSmall ImmunoGold F(ab) fragment of goat anti-mouse IgG [Aurion, Cat# 800.266, RRID: AB_2315632]).

Sections were then postfixated with 3% glutaraldehyde and 1% paraformaldehyde in PB in a microwave oven (2 minutes at 150W, 4°C). Sections were rinsed in glycine (5 minutes) and rinsed in PB (2 x 10 minutes), followed by enhancement conditioning solution (ECS, 1:10, 2 x 10 minutes, Aurion). Gold-conjugated proteins were visualized by silver enhancement for 60-90 minutes (R-Gent SE-EM, Aurion); the tissue was then rinsed in ECS (2 x 10 minutes) and then PB (2 x 10 minutes). Tracers were visualized with DAB as above. For all rinses following silver enhancement 0.1 M PB pH 7.4 was used, and in some pieces of tissue the order of labeling was reversed to control for any attraction between gold and biotin. Any remaining biotin binding sites were blocked with AB blocking solutions, and then any remaining mouse binding sites were blocked with

incubation for one hour at 4°C in 3.5% mouse blocking reagent, 5% NGS, 5% BSA, 0.025% Triton X-100, and 0.1% BSA-c in PB.

Sections were incubated overnight at 4°C with antibody for a second calcium binding protein (CB, PV, or CR: 1:2000 in 1% NGS, 1% BSA, 0.1% BSA-c, 0.025% Triton X-100, and 8% MOM protein concentrate in PB; mouse monoclonal IgG, Swant), followed by rinses in PB and incubation for 1-2 hours at 25°C in biotinylated secondary antibody (1:200 in 1% NGS, 1% BSA, 0.1% BSA-c, 0.025% Triton X-100, and 8% MOM protein concentrate in PB; biotinylated goat anti-mouse IgG, Vector), then rinsed in PB and incubated in AB-HRP as above. These calcium-binding proteins were visualized with TMB staining as follows: sections were first incubated for 15 minutes in 0.005% TMB (Sigma-Aldrich), 0.004% ammonium chloride (Sigma-Aldrich), and 5% ammonium paratungstate (Sigma-Aldrich) in 0.1M PB, pH 6.0, and then incubated for one to five minutes in the same solution plus 0.005% hydrogen peroxide (Sigma-Aldrich) until staining appeared. The staining was stabilized by incubating sections for 10 minutes in a solution of 0.05% DAB (SigmaFast DAB tablet, Sigma-Aldrich), 0.02% cobalt chloride (Sigma-Aldrich), 0.004% ammonium chloride (Sigma-Aldrich), and 0.005% hydrogen peroxide (Sigma-Aldrich) in 0.1M PB, pH 6.0. Finally sections were rinsed in PB and postfixed in 6% glutaraldehyde and 2% paraformaldehyde in PB with a microwave oven (150W at 15°C) until sample temperature reached 30-35 °C (Jensen and Harris, 1989). We conducted control experiments on tissue by omitting primary antibodies and incubating in secondary antibody solutions and no immunolabeling was observed.

Sections were rinsed in PB (3 x 20 minutes) and postfixed for 15 minutes in 1% osmium tetroxide (Electron Microscopy Sciences, Hatfield, PA, USA) with 1.5% potassium ferrocyanide (Electron Microscopy Sciences) in PB with a microwave oven (100W at 12°C, 2 minutes on, 2 minutes off, 2 minutes on) and rinsed in PB (3 x 2 minutes) and water (3 x 2 minutes). Sections were then rinsed in 50% ethanol (3 x 5 minutes), stained with 1% uranyl acetate (30 minutes in 70% ethanol, Electron Microscopy Sciences), and dehydrated in a series of ethanols (90%, 95%, 100%; 3 x 5 minutes each). For embedding, sections were infiltrated with propylene oxide (2 x 7 minutes, Electron Microscopy Sciences), and then a 1:1 mixture of araldite (Electron Microscopy Sciences) and propylene oxide (one hour). Sections were infiltrated with araldite overnight, followed by flat embedding in araldite in aclar (Ted Pella). Aclar-embedded tissue was cured for 48 hours at 60°C. Small columns of tissue 500-750 µm wide were cut from each section, divided by layer, and re-embedded in araldite blocks and cured for 48 hours at 60°C.

2.2.3.2 Serial sectioning and data analysis: To reconstruct postsynaptic sites, araldite blocks containing embedded tissue from layers 1, 2-3a, or 3b-5a were sectioned at 50 nm using an ultramicrotome (Leica Ultracut UCT, Leica Microsystems; Buffalo Grove, IL, USA) and collected on pioloform coated copper slot grids, to form series of approximately 75-150 sections. Using 80 kV transmission EM at 16000x-26000x (JEOL 100CX; Jeol, Peabody, MA, USA), we exhaustively sampled a few sections to identify approximately 10-30 labeled boutons in each series. Each bouton was photographed in

serial sections through the entire bouton plus in five additional sections before and after. We analyzed labeled boutons using Reconstruct to trace bouton profiles and postsynaptic sites (Fiala, 2005). Synapses, axon terminals, and postsynaptic sites were identified using classical criteria, (Peters et al., 1991), and all labeled boutons and postsynaptic sites that were complete in the series were reconstructed in 3D to determine volumes and area of the postsynaptic density (PSD). Models in 3D were generated in Reconstruct and imported into 3Ds Max for rendering (version 14, Autodesk; San Rafael, CA, USA). We determined extraneous background level of gold labeling in each piece of tissue (Muly et al., 2009; Medalla and Barbas, 2012). In one series for each piece of tissue, enhanced gold particles in mitochondria were counted, and this value was divided by the total volume of mitochondria in the series. The threshold for gold-positive elements was set to twice the density of gold in mitochondria. We compared mean diameters, bouton and spine volumes, and PSD areas across pathways using hierarchically-nested mixed model ANOVA for comparisons including boutons from multiple cases, and proportions of synaptic specializations using Fisher exact tests. We used linear regression to analyze correlation between bouton volume and PSD area or spine volume.

We also used systematic random sampling to analyze unlabeled boutons in the neuropil surrounding labeled amygdalar boutons. In one of every twenty series in case BN-R, we measured the PSD area for all unlabeled asymmetric synapses that were complete in the series, using Reconstruct. We compared the PSD area of unlabeled synapses and labeled amygdalar synapses using a two-tailed t test.

2.3 Results

2.3.1 Injection sites in the amygdala and MD

The pathways studied with neural tracers are shown in Figure 2.1 and listed in Table 2.1. We used cases with large injections in the amygdala (described previously in Ghashghaei et al., 2007) to study the overall pattern of amygdalar pathways, and smaller injections (Fig. 2.1A-D) to study specific aspects of amygdalar pathways at the level of the system and the synapse. The tracer injections in amygdalar nuclei are listed in Table 2.1; they include the basal and cortical nuclei that project extensively to pOFC in rhesus monkeys (Porrino et al., 1981; Barbas and De Olmos, 1990).

For comparison, we studied the pattern of thalamocortical pathways to pOFC and their synaptic interactions with light, confocal, and electron microscopy. Targeted small injections of tracer in two cases were mainly localized in MD magnocellular (MDmc), including its junction with MD parvicellular in one case (MDpc; Fig. 2.1E-G), and part of the paraventricular (Pa) nucleus in another case (Fig. 2.1H, I). A third small injection included caudal MDpc (Fig. 2.1J, K). All of these segments of MD and Pa are connected strongly with pOFC (Dermon and Barbas, 1994). In the third case the tracer spread to part of the habenula (Fig. 2.1J, K), which projects mainly to the brainstem (Shelton et al., 2012); we used this case to study thalamocortical pathways with light microscopy.

Case - Hemisphere	Injection site – division	Tracer	Sex	Age (years)
BB - Left	Amygdala – basomedial, basolateral, anterior	BDA	F	2
BB - Right	Amygdala –basolateral, anterior, basomedial, cortical	BDA	F	2
BD - Left	Amygdala –basolateral, central, lateral, basomedial	BDA	M	2
BD - Right	Amygdala – cortical, medial, basomedial, basolateral	BDA	M	2
BL - Right	Amygdala – cortical, basomedial	FR	M	3
BM - Right	Amygdala –basomedial, cortical	FR	F	3.5
BN - Right	Amygdala – basomedial, basolateral	FE	M	2
BB - Left	Thalamus – mediodorsal magnocellular, mediodorsal parvicellular	FE	F	2
BO - Right	Thalamus – mediodorsal magnocellular, paraventricular, central intermediate	LY	M	3
BN – Right	Thalamus – mediodorsal parvicellular, habenula	CBL	M	2

Table 2.1. Injection sites in amygdalar and thalamic nuclei

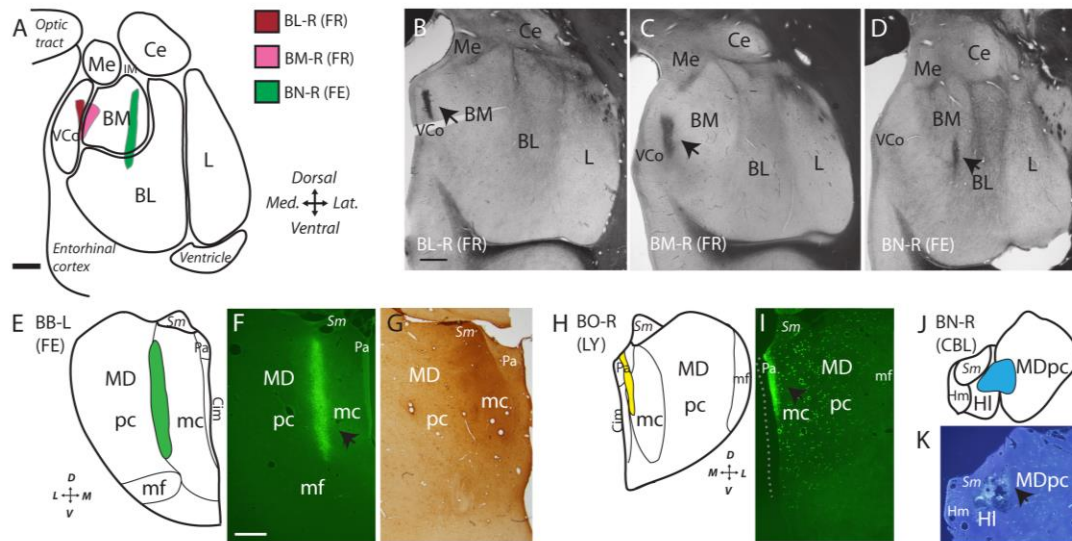


Figure 2.1. Injection sites in the amygdala and mediodorsal thalamus.

Scale bars are 1 mm. **A**, Schematic shows relative position of small injection sites in the amygdala in cases BL-R, BM-R, and BN-R. **B-D**, Fresh tissue sections show tracer in the amygdala (arrows). **E, H, J**, Schematics depict location of tracer injections in thalamic mediodorsal nucleus (cases BB-L, BO-R, and BN-R). **F, I, K**, Fluorescent micrographs show tracer in the thalamus. **G**, Brightfield photomicrograph shows section with injection in MDmc.

2.3.2 Amygdalar terminals were larger in pOFC than in other prefrontal areas

After measuring the major diameter of amygdalar boutons in pOFC and A32 in a large population (n = 31,420 boutons in pOFC; n = 16,967 boutons in A32), we performed a k-means cluster analysis, which separated boutons into two groups by diameter: large and small. We used a cutoff of 1 μm to distinguish between small and large boutons for all cases and all layers, which is approximately the average of all cutoff values calculated (mean cutoff value = 1.1 μm , n = 12 cases). The rationale is based on evidence that bouton size is highly correlated with the number of synaptic vesicles, and the synaptic efficacy of the pathway (for discussion see Germuska et al., 2006). We then compared the density of large amygdalar boutons (≥ 1 μm in diameter) in the three prefrontal sites. We found that pOFC also contained the highest density of large amygdalar boutons (n = 3 cases in each of 3 areas; ANOVA with Bonferroni post-hoc test, $F_{(2,6)} = 8.5$, $p = 0.02$ between pOFC and A9/46; Fig. 2.2).

Next we compared directly the size of amygdalar terminals in pOFC and in A32. We found that amygdalar terminals across all layers in pOFC were larger than those in A32, though not significantly (mean diameter \pm SE, pOFC: 1.0 ± 0.021 μm , n = 6 cases; A32: 0.97 ± 0.0057 μm , n = 3; two-tailed t test, $t_{(7)} = 1.9$, $p = 0.1$). By comparing the frequency of large boutons, we found that the amygdalar projection to pOFC contained significantly more large boutons than A32 (1-1.5 μm diameter; pOFC: n = 6 cases and 8 bins; A32: n = 3 cases and 8 bins; multi-factorial ANOVA with Bonferroni post-hoc test, $F_{(7,56)} = 30.6$, $p = 0.002$; Fig. 2.3A). These data show that pOFC receives denser projections as well as a higher proportion of large terminals from the amygdala compared

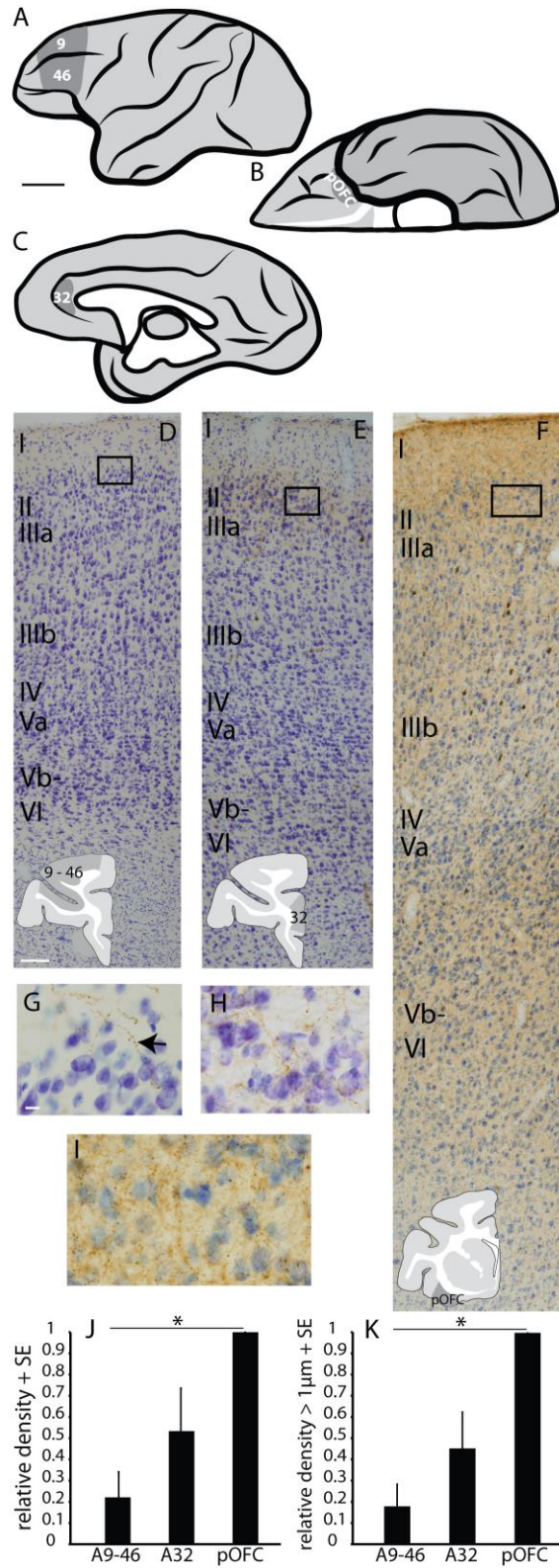


Figure 2.2. Amygdalar boutons were densest and largest in pOFC.

A-C, Areas of study: **A**, Lateral, **B**, Orbital, and **C**, Medial views of a rhesus monkey brain show areas of interest in areas 9/46, OPro (pOFC), and A32 (ACC). Scale bar = 1 cm. **D-F**, Nissl-stained columns of cortex in: **D**, A46; **E**, A32; and **F**, pOFC (area OPro) labeled for amygdalar fibers (insets in G-I). Scale bar = 100 μm and applies to D-F. **G-I**, Amygdalar fibers (arrow) at layer 1-2 border in: **G**, A46; **H**, A32; and **I**, pOFC. Scale bar = 10 μm and applies to G-I. **J**, Relative density of amygdalar boutons in A9/46, A32, and pOFC, normalized to the highest density in each case (pOFC). **K**, Relative density of large amygdalar boutons $\geq 1 \mu\text{m}$ in diameter in A9/46, A32, and pOFC, normalized to the highest density in each case (pOFC). Vertical lines indicate standard error (SE). * $p \leq 0.05$.

to A32, another phylogenetically old prefrontal area that is also strongly connected with the amygdala.

2.3.3 Amygdalar terminals were larger than thalamic terminals in pOFC

We then compared amygdalar terminals in pOFC with terminals from the thalamic MD nucleus, which is the major source of thalamic input to pOFC (Goldman-Rakic and Porrino, 1985; Dermon and Barbas, 1994). Across all layers of pOFC, amygdalar terminals were larger than those from MD (mean diameter \pm SE, amygdalar: $1.0 \pm 0.021 \mu\text{m}$, $n = 6$ cases with 31,420 boutons; thalamic: $0.88 \pm 0.050 \mu\text{m}$, $n = 3$ cases with 7,169 boutons; two-tailed t test, $t_{(7)} = 2.8$, $p = 0.03$). We further characterized the frequency of large boutons and found that compared to boutons from MD, the amygdalar projection to pOFC contained a significantly higher proportion of large boutons (1-1.5 μm diameter; amygdalar: $n = 6$ cases and 8 bins; thalamic: $n = 3$ cases and 8 bins; multi-factorial ANOVA with Bonferroni post-hoc test, $F_{(7, 56)} = 9.5$, $p = 0.0001$; Fig. 2.3B). Next we analyzed the middle cortical layers specifically (layers 3b-5a), which are thought to be the primary recipient of ‘driver’ thalamocortical fibers. We found that amygdalar terminals (mean diameter \pm SE, $1.06 \pm 0.026 \mu\text{m}$, $n = 6$ cases) were significantly larger than the thalamic even in the middle layers (layers 3b-5a: $0.89 \pm 0.047 \mu\text{m}$, $n = 3$; two-tailed t test, $t_{(7)} = 3.1$, $p = 0.02$), consistent with the pattern shown above.

Analysis of boutons measured at the synaptic level in the EM confirmed the data obtained at the light microscope (mean diameter \pm SE, $0.99 \pm 0.033 \mu\text{m}$, $n = 164$ amygdalar boutons from 2 cases; $0.84 \pm 0.041 \mu\text{m}$, $n = 39$ thalamic boutons from 2 cases;

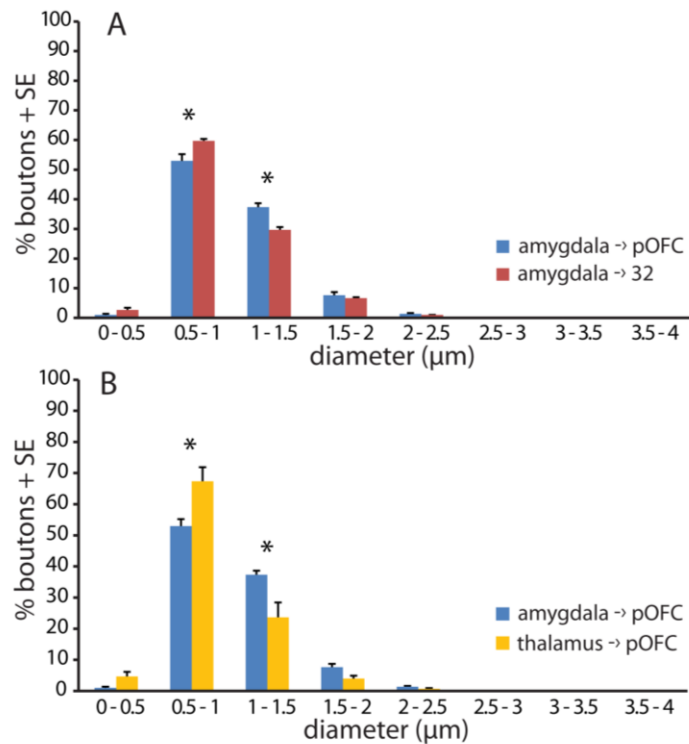


Figure 2.3. Amygdalar axon boutons in pOFC were larger than in A32 or than the thalamic axon boutons.

A, Histogram shows size distribution of amygdalar boutons in A32 (red) and pOFC (blue) across all layers. **B**, Histogram shows size distribution of amygdalar boutons (blue) and thalamic boutons (yellow) in pOFC across all layers. Vertical lines indicate standard error (SE). * $p \leq 0.05$.

hierarchically-nested mixed model ANOVA, $F_{(1, 5.7)} = 10.7$ for fixed effect of injection site, $p = 0.02$; $F_{(2, 199)} = 0.3$ for random effect of case, $p = 0.7$; Fig. 2.4A-H). When reconstructed in 3D, amygdalar boutons were larger in volume (mean volume \pm SE, $0.33 \mu\text{m}^3 \pm 0.035 \mu\text{m}^3$, $n = 152$ boutons from 2 cases) than the thalamic ($0.19 \pm 0.024 \mu\text{m}^3$, $n = 36$ boutons from 2 cases; hierarchically-nested mixed model ANOVA, $F_{(1, 20.6)} = 14.6$ for fixed effect of injection site, $p = 0.001$; $F_{(2, 183)} = 0.1$ for random effect of case, $p = 0.9$; Fig. 4I). These results show that amygdalar boutons in the upper layers of pOFC are even larger than thalamic boutons forming synapses in the middle layers; the latter form a robust pathway in sensory systems that relays information from the thalamus to cortex reliably (Sherman and Guillery, 1998).

2.3.4 Appositions between amygdalar and thalamic projections with inhibitory neurons

A key unanswered question about the amygdalar and thalamic pathways is the nature of their postsynaptic targets in pOFC. With regard to cortical inhibitory neurons, the upper layers (1-3a) of pOFC are populated mostly by two classes of inhibitory neurons: CR-positive (Fig. 2.5A, green) presumed inhibitory neurons, which form synapses on neighboring inhibitory neurons, at least in the upper layers of some areas, and CB-positive (Fig. 2.5A, red) inhibitory neurons which form synapses on the dendrites of nearby pyramidal neurons in layers 2-5 (DeFelipe, 1997). The middle-deep layers (3b-6) contain mostly PV-positive (Fig. 2.5A, blue) inhibitory neurons, which provide strong inhibition by forming synapses on the soma, axon initial segment or proximal dendrites of layer 3 and 5 pyramidal neurons (DeFelipe, 1997).

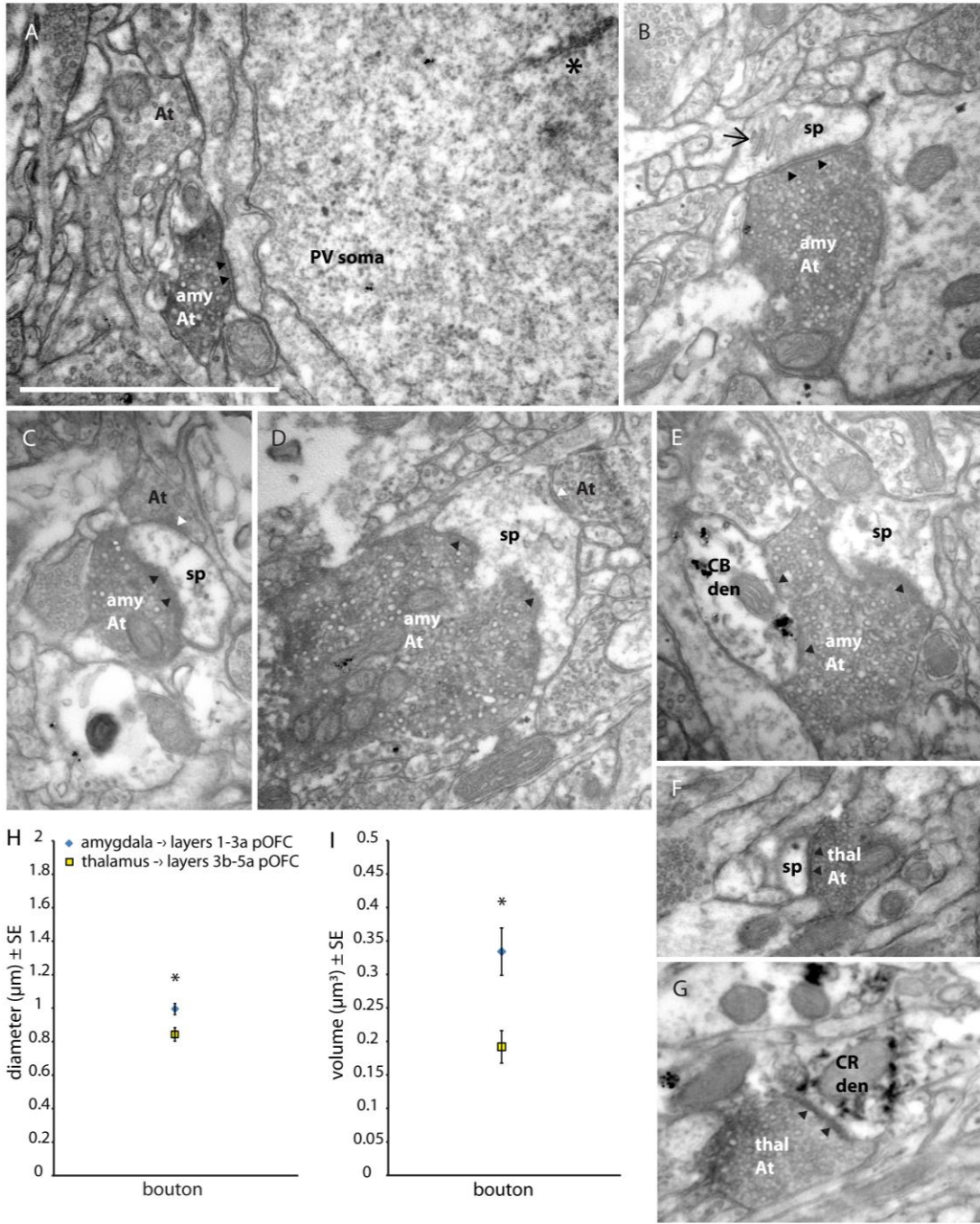


Figure 2.4. Amygdalar terminals in the upper layers of pOFC were larger than thalamic terminals in the middle layers at the synaptic level.

Scale bar in A is 1 μm , and applies to A-G. **A-E**, Amygdalar boutons labeled with DAB in the upper layers of pOFC, forming: **A**, A macular synapse (silhouette arrowheads) with a PV-positive soma labeled with TMB (asterisk); **B**, A macular synapse (black arrowheads) with a spine (sp) containing a spine apparatus (arrow); **C**, A macular synapse (black arrowheads) with a spine (sp), which also receives an unlabeled symmetric synapse (white arrowhead) from a presumed inhibitory bouton (At); **D**, A perforated synapse (black arrowheads) with a spine (sp), which also receives an unlabeled symmetric synapse (white arrowhead) from a presumed inhibitory bouton (At); **E**, Two synapses (black arrowheads) with a spine (sp) and a calbindin-positive dendrite (CB den) labeled with gold (black clumps). **F-G**, Thalamic boutons labeled with DAB forming: **F**, A macular synapse (black arrowheads) with a spine (sp) and **G**, A macular synapse (black arrowheads) with a calretinin-positive dendrite (CR den) labeled with TMB. **H**, Diameters of amygdalar boutons in the upper layers of pOFC (blue) and thalamic boutons in the middle layers of pOFC (yellow), measured in the EM. **I**, Amygdalar axon boutons in the upper layers of pOFC were larger in volume than thalamic terminals in the middle layers of pOFC. Vertical lines indicate standard error (SE). * $p \leq 0.05$.

We first studied the prevalence of appositions between amygdalar fibers and PV, CB, and CR inhibitory neurons in pOFC using laser scanning confocal microscopy ($n = 376$ appositions of 8,035 boutons in 2 cases; Fig. 2.5B, C). Of the three classes of presumed inhibitory neurons, amygdalar projections in the upper layers of pOFC formed appositions mostly with CB (8%, Fig. 2.5F) and CR neurons (8%) and less often with PV neurons (2%). By comparison, in the middle layers of pOFC amygdalar boutons formed fewer appositions with CB (2%, $\chi^2_{(1, n = 2232)} = 41.9, p < 0.00001$; Fig. 2.5F) or CR neurons (3%, $\chi^2_{(1, n = 2771)} = 13.9, p = 0.0002$) and more with PV neurons (4%, $\chi^2_{(1, n = 3203)} = 13.4, p = 0.0003$).

We then studied appositions between thalamic terminals and inhibitory neurons in the middle layers (3b-5a) of pOFC, which are the predominant layers innervated by thalamic afferents ($n = 101$ appositions of 1,226 boutons in 2 cases; Fig. 2.5D, E). Thalamic terminals targeted a greater proportion of inhibitory neurons in the middle layers than amygdalar terminals. Specifically, thalamic axons formed more appositions with PV (11%, $\chi^2_{(1, n = 1498)} = 24.5, p < 0.00001$, Fig. 2.5G), or CR neurons (10%, $\chi^2_{(1, n = 941)} = 15.4, p = 0.0001$), and a similar proportion with CB neurons (3%).

In a case with a more medial injection of tracer (Fig 1H, I; case BO-R), thalamic afferents terminated in significant numbers in the upper layers of pOFC as well ($n = 123$ appositions of 1,156 boutons). Compared to amygdalar axons in the upper layers of pOFC, thalamic axons targeted significantly more CB neurons (14%, $\chi^2_{(1, n = 1834)} = 13.2, p = 0.0003$), a similar proportion of CR neurons (7%), and no boutons formed appositions with PV neurons. Consistent with these findings, midline and paralaminar thalamic

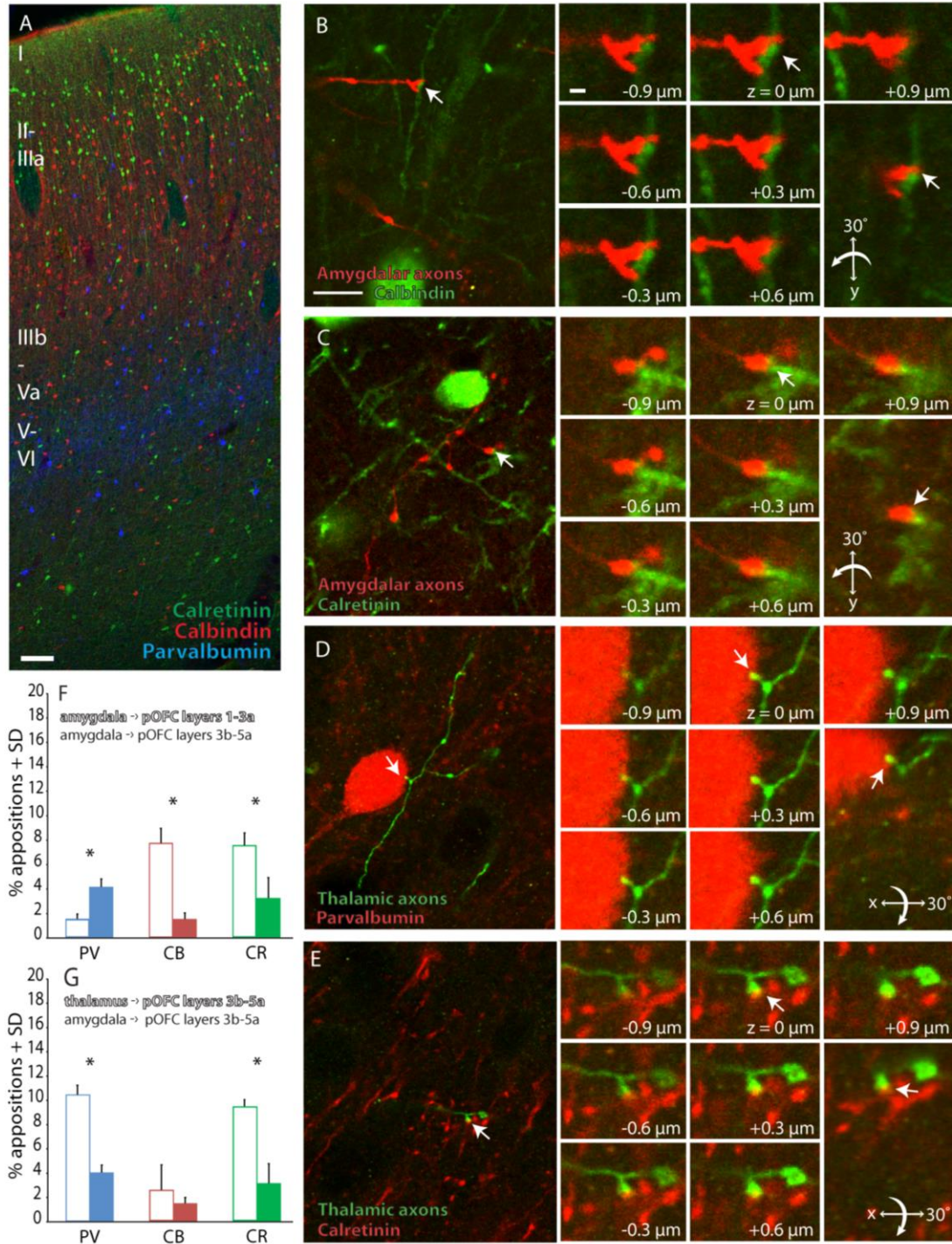


Figure 2.5. Examples of amygdalar and thalamic axons targeting inhibitory neurons in pOFC.

A, Distribution of presumed inhibitory neurons shown in pseudocolor in pOFC, where calretinin neurons (green) and calbindin neurons (red) were found mostly in the upper layers and parvalbumin neurons (blue) were found mostly in the middle – deep layers. Scale bar = 100 μm . **B**, Amygdalar axons (red) in the upper layers of pOFC; one is closely apposed to a dendrite of a calbindin neuron (green, white arrows). Scale bar = 10 μm and applies to left panels of B-E. Right, Sequential optical sections through apposition and 3D rotation through apposition (scale bar = 1 μm and applies to all insets B-E). **C**, Amygdalar axons (red) in the upper layers of pOFC; shows one close apposition with a dendrite of a calretinin neuron (green, white arrows). **D**, Thalamic axon (green) in the middle layers of pOFC; example of a close apposition with a parvalbumin neuron (red, white arrows). **E**, Thalamic axon (green) in the middle layers of pOFC formed a close apposition with a calretinin neuron (red, white arrows). **F**, Amygdalar terminals targeted more calbindin and calretinin inhibitory neurons in the upper layers of pOFC (open bars), and more parvalbumin neurons in the middle layers (filled bars). **G**, Thalamic terminals (open bars) targeted more parvalbumin and calretinin neurons in the middle layers compared to amygdalar terminals (filled bars). Vertical lines indicate standard deviation (SD). * $p \leq 0.05$.

nuclei activate feedforward inhibition in upper cortical layers in mice (Cruikshank et al., 2012). These data show that compared to amygdalar fibers, thalamic fibers targeted a higher proportion of inhibitory neurons in both the upper and middle layers of pOFC.

A few amygdalar axons targeted inhibitory neurons proximally in the upper layers of pOFC, forming significantly more appositions on cell bodies of inhibitory neurons in layers 1-3a ($n = 11$ of 310 appositions: 7 CB-positive, 3 PV-positive, 1 CR-positive) than thalamic axons, which formed no appositions involving a soma ($n = 0$ of 123 appositions; $\chi^2_{(1, n = 433)} = 4.5, p = 0.03$). On the other hand, in the middle layers of pOFC, both amygdalar and thalamic axons formed appositions with cell bodies of presumed inhibitory neurons ($n = 5$ of 224 thalamic appositions; $n = 1$ of 66 amygdalar appositions; all PV-positive; Fig. 2.5D). This suggests that although amygdalar fibers interacted with relatively fewer inhibitory neurons in the upper layers of pOFC, they targeted inhibitory neurons more proximally than the thalamic pathways.

2.3.5 Postsynaptic targets of amygdalar projections in pOFC

We further investigated at the synaptic level the excitatory and inhibitory targets of amygdalar terminals in pOFC. We reconstructed synapses formed between amygdalar axons and elements of postsynaptic neurons in the upper layers (1-3a) of pOFC using electron micrographs from uninterrupted serial sections through the synapse photographed in the EM ($n = 164$ boutons from 2 cases; Fig. 2.6A-C). We identified postsynaptic targets by morphology for excitatory neurons, which have spiny dendrites,

and by morphology and label for CB, CR, or PV for presumed inhibitory neurons, which have smooth or sparsely spiny dendrites (Peters et al., 1991; DeFelipe, 1997).

The majority of amygdalar boutons innervated single spines of presumed excitatory neurons in the upper layers of pOFC (75%, $n = 123$ of 164 boutons; Fig. 2.6D). A smaller proportion (10%, $n = 17$) of amygdalar boutons formed synapses with single dendrites of presumed inhibitory neurons, and only one terminal formed a synapse with a soma. The remainder boutons were multisynaptic (14%, $n = 23$), which were more frequent in the amygdalar pathway than the thalamic (3%, $n = 1$ of 39 boutons; two-tailed Fisher exact test, $p = 0.05$; Fig. 2.6D). Of these multisynaptic amygdalar boutons, the majority formed a synapse with one dendrite and at least one spine (8%, $n = 12$ of 164 boutons) or formed synapses with multiple spines (5%, $n = 9$), and a minority (<1%, $n = 1$) formed synapses with multiple dendrites, or a soma and multiple spines (<1%, $n = 1$).

Some amygdalar boutons in the upper layers of pOFC formed synapses with dendritic shafts of presumed inhibitory neurons (16% of synapses, $n = 31$ of 189 synapses total, formed by 164 labeled boutons). Boutons forming synapses with at least one dendritic shaft or soma (presumed inhibitory neurons) were significantly larger than boutons with only excitatory postsynaptic targets (mean diameter \pm SE, $1.2 \pm 0.094 \mu\text{m}$, $n = 32$ boutons with inhibitory targets from 2 cases; $0.95 \pm 0.033 \mu\text{m}$, $n = 132$ boutons with excitatory targets from 2 cases; hierarchically-nested mixed model ANOVA, $F_{(1, 2.1)} = 18.1$ for fixed effect of target, $p = 0.05$; $F_{(2, 160)} = 0.4$ for random effect of case, $p = 0.6$; Fig. 2.6E). Among labeled dendrites, CB-positive dendrites were the most frequently

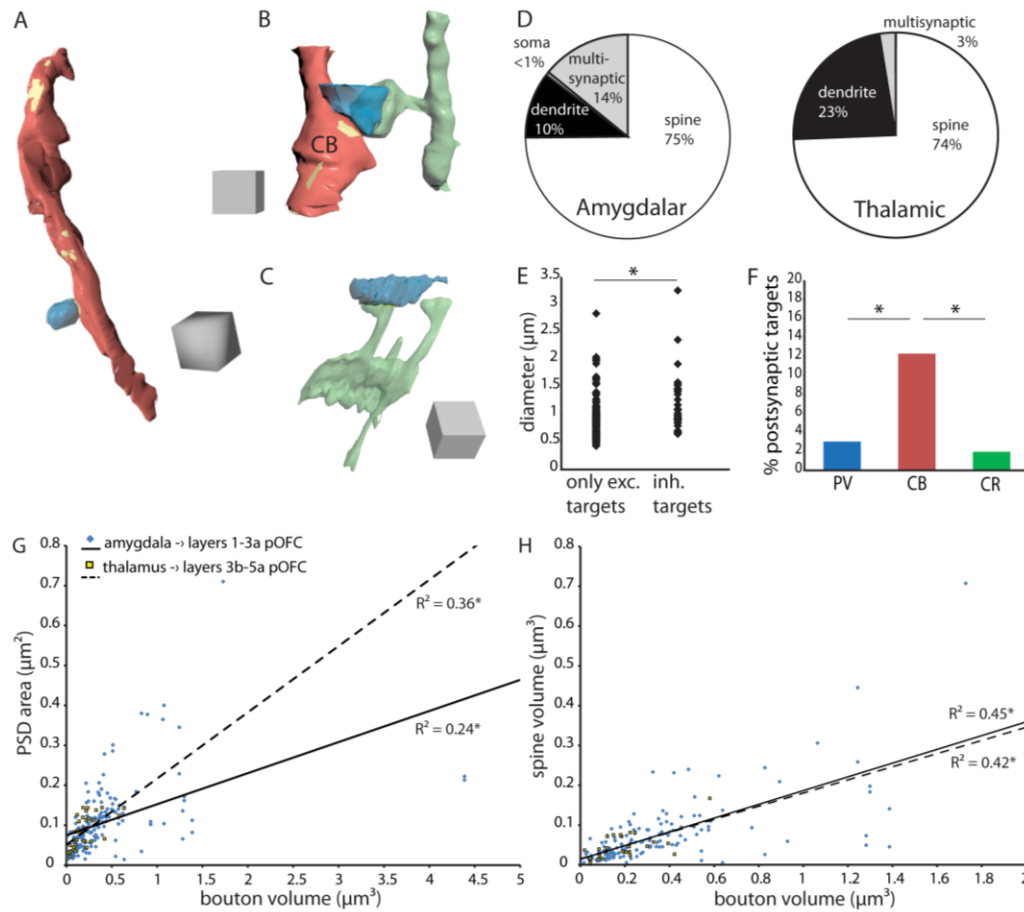


Figure 2.6. Excitatory and inhibitory postsynaptic targets of amygdalar boutons in pOFC.

A-C, Amygdalar boutons (blue) form synapses (yellow) with: **A**, A smooth dendrite of a presumed inhibitory neuron (red); **B**, A smooth dendrite (red) labeled for CB and a spiny dendrite of a presumed excitatory neuron (green); and **C**, A spiny dendrite of a presumed excitatory neuron (green). Scale cubes are $1 \mu\text{m}^3$. **D**, Left, Amygdalar boutons most frequently innervated single spines in the upper layers of pOFC, and a significant proportion were multisynaptic. Right, Thalamic boutons also formed synapses mostly with spines, but thalamic pathways contained fewer multisynaptic boutons in the middle layers of pOFC. **E**, Amygdalar boutons with at least one inhibitory target were larger than amygdalar boutons with only excitatory targets. **F**, Among labeled dendrites, amygdalar boutons mostly formed synapses with calbindin positive dendrites of presumed inhibitory neurons in the upper layers of pOFC. **G**, Amygdalar (blue diamonds, solid line) and thalamic (yellow squares, dashed line) bouton volume was positively correlated with PSD area. **H**, Amygdalar (blue diamonds, solid line) and thalamic (yellow squares, dashed line) bouton volume was positively correlated with spine volume. * $p \leq 0.05$.

innervated (12%, $n = 15$ dendrites of 122 boutons; Fig. 2.6F). Fewer amygdalar boutons formed synapses with PV (3%, $n = 2$ dendrites and 1 soma of 99 boutons; two-tailed Fisher exact test, $p = 0.01$) or CR neurons (2%, $n = 2$ dendrites of 105 boutons, $p = 0.004$). The remainder dendrites and soma were unlabeled ($n = 13$ of 31 dendrites and 2 somata). These data are consistent with the fluorescence data (where 17% of boutons were apposed to a labeled dendrite or soma) but show a relatively greater proportion of synapses with CB neurons, and fewer with CR neurons (compare Fig. 2.5F, 2.6F). A minority of spines were labeled for CB (5%, $n = 6$ of 114 spines), which may belong to a minority of pyramidal neurons that are positive for CB, or only in one instance for PV (1%, $n = 1$ of 94 spines), which likely belongs to a sparsely spiny inhibitory neuron (DeFelipe, 1997). These data at the synaptic level highlight the role of calbindin neurons among inhibitory neurons targeted by the amygdala.

2.3.6 Synaptic specializations of amygdalar and thalamic boutons

The majority of synapses formed by amygdalar boutons were macular (Peters and Kaiserman-Abramof, 1969), with the postsynaptic density forming a complete disk (Fig. 2.4A-C). Some amygdalar synapses were perforated with a discontinuous postsynaptic density (PSD) (21%, $n = 40$ out of 189 synapses; Fig. 2.4D), most of which were on spines (80%, $n = 32$ of 40; the remainder were on dendrites). This was similar to the proportion of thalamic boutons forming perforated synapses in the middle layers (13%, $n = 5$ of 40 synapses, all axo-spinous). Among amygdalar and thalamic boutons, PSD area was significantly correlated with bouton volume (linear regression, amygdala: $n = 178$

boutons, $R^2 = 0.24$, $F_{(1, 176)} = 54.1$, $p < 0.0001$; thalamus: $n = 36$ boutons, $R^2 = 0.36$, $F_{(1, 34)} = 18.8$, $p = 0.0001$; Fig. 2.6G). The lower slope of the correlation between amygdalar bouton volume and PSD area may be due to the greater proportion of multisynaptic amygdalar boutons, compared to the thalamic pathway.

The volume of post-synaptic spines was also significantly correlated with bouton volume (linear regression, amygdala: $n = 145$ boutons, $R^2 = 0.45$, $F_{(1, 143)} = 117.5$, $p < 0.0001$; thalamus: $n = 26$ boutons, $R^2 = 0.42$, $F_{(1, 24)} = 17.3$, $p = 0.003$; Fig. 2.6H). Thalamic boutons in the middle layers targeted a significantly higher proportion of spines containing a spine apparatus (SA) or smooth endoplasmic reticulum (SER, 55%, $n = 16$ of 29 spines; two-tailed Fisher exact test, $p = 0.02$) compared to amygdalar boutons (32%, $n = 50$ out of 156 spines, Fig. 2.4C). SER is found in dendrites and some spines, which at times forms a SA; these components are associated with stable spines (Ostroff et al., 2010). Additionally, a minority of amygdala-targeted spines in pOFC (5%, $n = 7$ of 156 spines, Fig. 2.4C, D) also received a symmetric synapse, presumably from a local inhibitory neuron. These results show that amygdalar boutons formed perforated synapses, larger synapses and targeted larger spines.

2.3.7 Comparison of amygdalar synapses with surrounding neuropil

We next investigated if the prevalence of large amygdalar synapses differs or not from non-labeled synapses in the neuropil. This analysis revealed that amygdalar boutons formed synapses that were significantly larger than those in the surrounding neuropil (mean area \pm SE, $0.11 \pm 0.0064 \mu\text{m}^2$, $n = 178$ amygdalar synapses from 2 cases; $0.84 \pm$

0.0052 μm^2 , n = 165 unlabeled synapses from 1 case; two-tailed t test, $t_{(341)} = 2.6$, p = 0.01).

2.4 Discussion

Novel findings from the system to the synapse revealed that the pathway from the amygdala to pOFC is stronger than to other prefrontal cortices or even the thalamocortical (Fig. 2.7). This conclusion is based on evidence that the amygdalar pathway to pOFC is denser (Ghashghaei et al., 2007), has more large terminals, is largely excitatory, and is distinguished for unique synaptic specializations among other pathways. In aggregate, these features suggest that the amygdala can exert a powerful influence on pOFC.

2.4.1 Specialized amygdalar pathways target preferentially the pOFC: comparison with ACC

We found that pathways from large or restricted amygdalar sites consistently innervated most robustly the pOFC than areas 9/46 or even ACC, which is also strongly linked with the amygdala (Ghashghaei et al., 2007). The amygdalar pathway to pOFC had a significant proportion of large terminals. Large terminals have a higher content of vesicles and mitochondria (Germuska et al., 2006; Zikopoulos and Barbas, 2007b), and are associated with greater synaptic efficacy and highly active synapses (Reichova and Sherman, 2004; Zikopoulos and Barbas, 2007a).

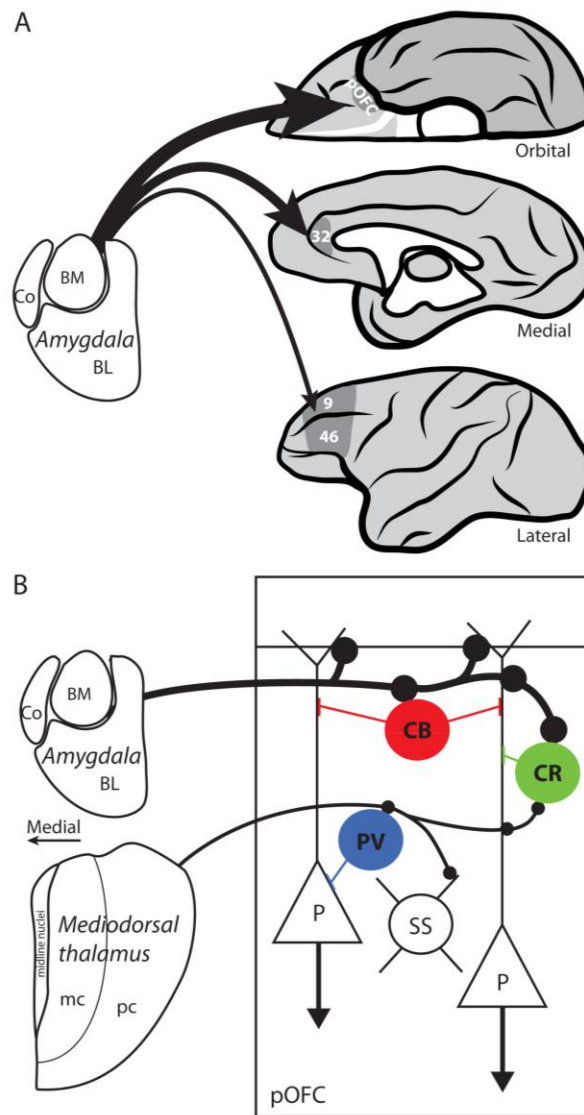


Figure 2.7. Summary of features in amygdalar pathway to pOFC, ACC, and 9/46.

A, Thickness of arrows depicts the relative density and terminal size of amygdalar pathways to pOFC, ACC, and 9/46. **B**, Amygdalar terminals were larger and formed synapses mostly with excitatory neurons in the upper layers of pOFC compared to thalamic axons in the middle layers. Among inhibitory neurons, amygdalar axons targeted CB and CR neurons in the upper layers, while thalamic axons targeted more PV and CR neurons in the middle layers. Large amygdalar synapses may drive excitatory neurons in pOFC, while synapses on CB and CR neurons may reduce background excitation, or noise. Excitatory spiny stellate neurons (SS) are a major target of thalamic pathways.

Among prefrontal areas the pOFC is distinguished for receiving extensive projections from sensory association cortices representing each modality (reviewed in Barbas, 2000). Coupled with robust input from the amygdala, the pOFC is poised to link external cues with internal valuations, reliably convey the salience of task-specific stimuli, quickly form associations related with reward and update them as conditions change (Tremblay and Schultz, 1999; Wallis and Miller, 2003; Simmons and Richmond, 2008; Morrison and Salzman, 2011; Luk and Wallis, 2013; Wilson et al., 2014). The above studies show that responses of neurons in orbitofrontal cortex vary based on task context, suggesting flexible integration of information. It has been hypothesized that processing flexibly the state of a task applies to diverse tasks that test function in orbitofrontal cortex across species (Wilson et al., 2014).

The ACC differs in several ways from the pOFC. While the pOFC is a stronger ‘receiver’ of pathways from the amygdala, the ACC is a stronger ‘sender’ of pathways to the amygdala (Ghashghaei et al., 2007). The emphasis in ACC appears to be in processing the value of actions and outcomes (Kennerley et al., 2006), consistent with its connections with cingulate motor areas (Barbas and Pandya, 1987; Morecraft and Van Hoesen, 1998). Further, the most robust projections of ACC are motor-related, innervating brainstem and spinal autonomic centers (An et al., 1998; Rempel-Clower and Barbas, 1998; Barbas et al., 2003). These efferent autonomic pathways mediate emotional expression, including vocalizations and distress calls in primates (reviewed in Vogt and Barbas, 1988; Devinsky et al., 1995; Hadland et al., 2003).

2.4.2 Specialized amygdalar 'drivers' to the upper layers of pOFC: comparison with the thalamic

The predominance of dense and potentially efficient pathways from the amygdala to the upper layers of pOFC is also unusual and different from thalamic relay pathways. In the latter, upper layer terminations are thought to have a modulatory role (Sherman and Guillery, 1998). Dense pathways from thalamic relay nuclei target most densely the middle cortical layers (layers 3b-5a), a pattern seen also for MD to prefrontal cortex (Giguere and Goldman-Rakic, 1988). These thalamocortical pathways are described as drivers, capable of eliciting action potentials in postsynaptic neurons (Freund et al., 1989; Sommer and Wurtz, 2004). In contrast, amygdalar terminations in the upper layers were not only denser but also larger than the thalamic in the middle layers.

Synaptic specializations further suggest higher strength in the amygdalar pathway than the thalamic to pOFC. This is exemplified by amygdalar innervation of large spines, which are associated with large synapses and large excitatory postsynaptic currents (Harris and Stevens, 1989; Matsuzaki et al., 2001). Multisynaptic amygdalar boutons were more frequent than the thalamic in pOFC; such boutons increase in number after long-term potentiation and learning (Jones et al., 1997; Muller et al., 2000; Geinisman et al., 2001). Finally, some amygdalar terminals formed perforated synapses, which are enriched with AMPA receptors and are thought to participate in more efficient computations (Geinisman, 2000; Nicholson et al., 2006; Nava et al., 2014).

The strong amygdalar pathway to the upper layers provides a circuit mechanism for extended influences in pOFC, by impinging on the apical dendrites and tufts of

pyramidal neurons from layers 2, 3 and 5, as well as calbindin and calretinin inhibitory neurons (DeFelipe, 1997; Callaway, 1998; Douglas and Martin, 1998). The amygdalar pathway to the upper layers of pOFC may thus affect the activity of the entire cortical column, including neurons that project back to the amygdala, as shown in mouse medial prefrontal cortex (Little and Carter, 2013). In rhesus monkeys, neurons in layer 5 and to a lesser extent in layer 3 project to the amygdala (Ghashghaei et al., 2007), and pOFC uniquely targets the purely inhibitory intercalated masses (IM) of the amygdala (Ghashghaei and Barbas, 2002). In turn, IM neurons project to the central amygdalar nucleus, a key output of the amygdala to brainstem and hypothalamic autonomic centers (reviewed in Price, 2003; Barbas et al., 2011). The pOFC projects as well to the central nucleus—albeit to a lesser extent, and through these dual pathways the pOFC may flexibly adjust autonomic drive depending on the circumstances (Ghashghaei and Barbas, 2002). When activated by the robust amygdalar pathways, the pOFC may modify the activity of the amygdala as conditions change (Simmons and Richmond, 2008), adding necessary flexibility in reward learning (John et al., 2013).

2.4.3 Amygdalar drivers and feedforward inhibition: a mechanism for gain control

Like other long distance pathways in primates, the amygdalar pathway to orbitofrontal cortex is excitatory (Miyashita et al., 2007). We found that the amygdala also innervates a higher proportion of excitatory postsynaptic sites than the thalamic, while the opposite applies for inhibitory postsynaptic targets. Among the small proportion of synapses with presumed inhibitory neurons, amygdalar axons innervated

mostly CB and CR neurons in pOFC. CB neurons form synapses on distal dendrites of neighboring pyramidal neurons and mildly modulate them, while CR neurons modulate other inhibitory neurons in the upper layers (DeFelipe et al., 1989; DeFelipe, 1997). This circuit mechanism can enhance signal and reduce weak activity at the fringes of columns of neurons engaged in working memory tasks in monkey lateral prefrontal cortex (Constantinidis and Goldman-Rakic, 2002; Wang et al., 2004). By analogy, amygdalar axons may increase the signal to noise ratio by activating CB and CR inhibitory neurons and simultaneously drive neurons in pOFC through large and efficient synapses on excitatory postsynaptic targets (Fig. 2.7). This circuit mechanism may control gain by enhancing activation by relevant signals and reducing noise to help focus attention on stimuli with affective import. Interestingly, the amygdala, pOFC, and MD have in common robust and overlapping projections to the inhibitory thalamic reticular nucleus (TRN), which is thought to be the brain's vanguard for attention (reviewed in Zikopoulos and Barbas, 2007b). All three pathways extend to the sensory sectors of TRN and may gate sensory stimuli with emotional significance (Zikopoulos and Barbas, 2012). The pathway to TRN provides an alternative route through which the amygdala may influence pOFC via the thalamic MD, to which it also projects (Russchen et al., 1987).

2.4.4 Circuits for flexible behavior and their disruption in psychiatric diseases

Dynamic integration of external sensory stimuli and internal valuations in orbitofrontal cortex based on context (Simmons and Richmond, 2008; Wilson et al., 2014) is likely disrupted in a variety of psychiatric diseases, including obsessive-

compulsive disorder (OCD) and phobias (Barbas et al., 2011; John et al., 2013). Specifically, pathways connecting the amygdala and orbitofrontal cortex have been implicated in the pathology of OCD, characterized by recurrent intrusive thoughts and impulses, leading to repetitive compulsive behaviors (reviewed in Chamberlain et al., 2005; Maia et al., 2008; Arnsten and Rubia, 2012). OCD is thought to arise from excess activation of loops connecting the basal ganglia, the amygdala, ACC, and orbitofrontal cortex (Huey et al., 2008; Maia et al., 2008; Haber and Heilbronner, 2013). Specifically, the orbitofrontal cortex has reduced volume and shows increased activation in OCD patients experiencing symptoms (Breiter and Rauch, 1996; Szeszko et al., 1999; Adler et al., 2000; Kang et al., 2004). Lesions of the connections between orbitofrontal cortex, the thalamus and basal ganglia have been used with some success as therapy for OCD (Maia et al., 2008; Greenberg et al., 2010). Further, the therapeutic effects of deep brain stimulation in a rat OCD model have been attributed to ultimate excitation of presumed inhibitory neurons and decreased firing rates of orbitofrontal neurons (McCracken and Grace, 2007).

The precise circuit neuropathology of OCD is not clearly understood. But based on the above studies our findings suggest a possible pathway mechanism, mediated through a strong excitatory amygdalar pathway to pOFC. Increased excitation from the amygdala in OCD may override the comparatively few synapses on the modulatory CB and CR neurons in pOFC, and compromise the ability to disambiguate the contextual significance of stimuli. Reduced inhibition in orbitofrontal cortex may decrease the

ability to focus only on relevant stimuli and respond also to multiple other stimuli that richly impinge on pOFC.

CHAPTER THREE: SEQUENTIAL PATHWAYS LINK THE PRIMATE AMYGDALA, MEDIODORSAL THALAMUS, AND POSTERIOR ORBITOFRONTAL CORTEX

3.1 Introduction

The amygdala is a critical site for processing the affective content of stimuli (Davis and Whalen, 2001; Baxter and Murray, 2002). The strongest pathways from the amygdala are directed to posterior orbitofrontal cortex (pOFC), where affective signals are integrated with sensory information enabling representation of task state (Davis and Whalen, 2001; Ghashghaei et al., 2007; Wilson et al., 2014). Additionally, the primate amygdala and pOFC are each reciprocally connected with the medial, magnocellular thalamic mediodorsal (MDmc) nucleus (Porrino et al., 1981; Aggleton and Mishkin, 1984; McFarland and Haber, 2002; Miyashita et al., 2007; Izquierdo and Murray, 2010), forming a tri-partite circuit that is necessary for flexible behavior in primates. The organization of the circuit has received limited attention at the level of the system and its synaptic interactions remain unknown.

An unanswered question concerning the tri-partite circuit pertains to the interaction of the amygdalar pathway with neurons in MDmc that project to pOFC. Although the pathway from the thalamus to cortex is often referred to as a 'relay', thalamocortical pathways are heterogeneous. As in other thalamic nuclei, in MDmc there are two types of cortically-projecting excitatory neurons: calbindin (CB), which project to the upper cortical layers, and parvalbumin (PV), which project to the middle cortical

layers (Jones, 1998). The interactions between amygdalar pathways and thalamic projection neurons to pOFC with these dual projection systems in MDmc are unknown. Amygdalar axons may target these classes of projection neurons differentially, and thus influence primarily upper or middle cortical layers through MDmc.

Amygdalar axons projecting to MDmc differ from those projecting to cortex in size and expression of zinc (Miyashita et al., 2007), but their postsynaptic targets and synaptic features in MDmc have not been investigated. These differences between axons in cortex and the thalamus suggest that amygdalar neurons projecting to MDmc and pOFC may arise from distinct neuronal populations in the amygdala, as has been suggested in rats (McDonald, 1987). Identifying the synaptic features of amygdalar axons in MDmc can elucidate its effects on thalamic neurons.

The pathway from the amygdala to MDmc suggests the presence of a sequential pathway through which the amygdala can influence pOFC via two routes: a direct projection to pOFC and an indirect pathway through MDmc (Porrino et al., 1981). Our previous findings show that amygdalar and thalamic pathways in pOFC are complementary. Amygdalar projections terminate most densely in the upper cortical layers and among inhibitory neurons, innervate preferentially CB and calretinin (CR) neurons. In contrast, thalamic pathways to pOFC terminate in the middle layers (McFarland and Haber, 2002) and innervate more PV inhibitory neurons. If projections from MDmc represent a second route for amygdalar input to reach pOFC, the amygdala may have differential effects in pOFC through the direct and indirect pathways.

To understand this important circuit underlying affective reasoning, we addressed

the following questions: 1) How are amygdalar axons and thalamic neurons projecting to pOFC organized in MDmc? 2) What are the synaptic specializations of amygdalar pathways in MDmc, in comparison with those in pOFC? 3) Do cortical and thalamic pathways arise from different neurons in the amygdala? 4) Is there evidence of a sequential pathway connecting the amygdala with neurons in MDmc that project to pOFC? These data are prerequisite to unraveling the neurochemical and synaptic features of this circuit, which is essential for flexible behavior and may be disrupted in psychiatric diseases.

3.2 Materials and Methods

3.2.1 Surgery, tracer injections, and tissue processing

Experiments were conducted on seven rhesus monkeys (*Macaca mulatta*) aged 2-3.5 years of both sexes injected with 1-2 distinct neural tracers (Table 3.1, Fig. 3.1). Experiments were conducted according to the *Guide for the Care and Use of Laboratory Animals* (National Research Council, 2011). Experimental methods were approved by the Institutional Animal Care and Use Committee at Boston University School of Medicine, Harvard Medical School, and New England Primate Research Center. Procedures involving animals were designed to reduce the number of animals needed and minimize animal suffering.

Prior to surgery, magnetic resonance images were obtained following animal sedation with ketamine hydrochloride and propofol anesthesia, in order to calculate

Case - Hemisphere	Injection site – division	Tracer	Sex	Age (years)
BC – Right	A13	FE	M	3
BJ – Right	pOFC – orbital proisocortex	LY	F	2
BK - Right	pOFC – orbital proisocortex	CBL	F	2.5
BM – Left	pOFC – orbital proisocortex	FE	F	3.5
BP – Right	pOFC – orbital proisocortex	FR	F	3.5
BL - Right	Amygdala – cortical, basomedial	FR	M	3
BM - Left	Amygdala –basolateral, lateral	FR	F	3.5
BN - Right	Amygdala – basomedial, basolateral	FE	M	2

Table 3.1. Injection sites in pOFC, amygdala, and thalamus

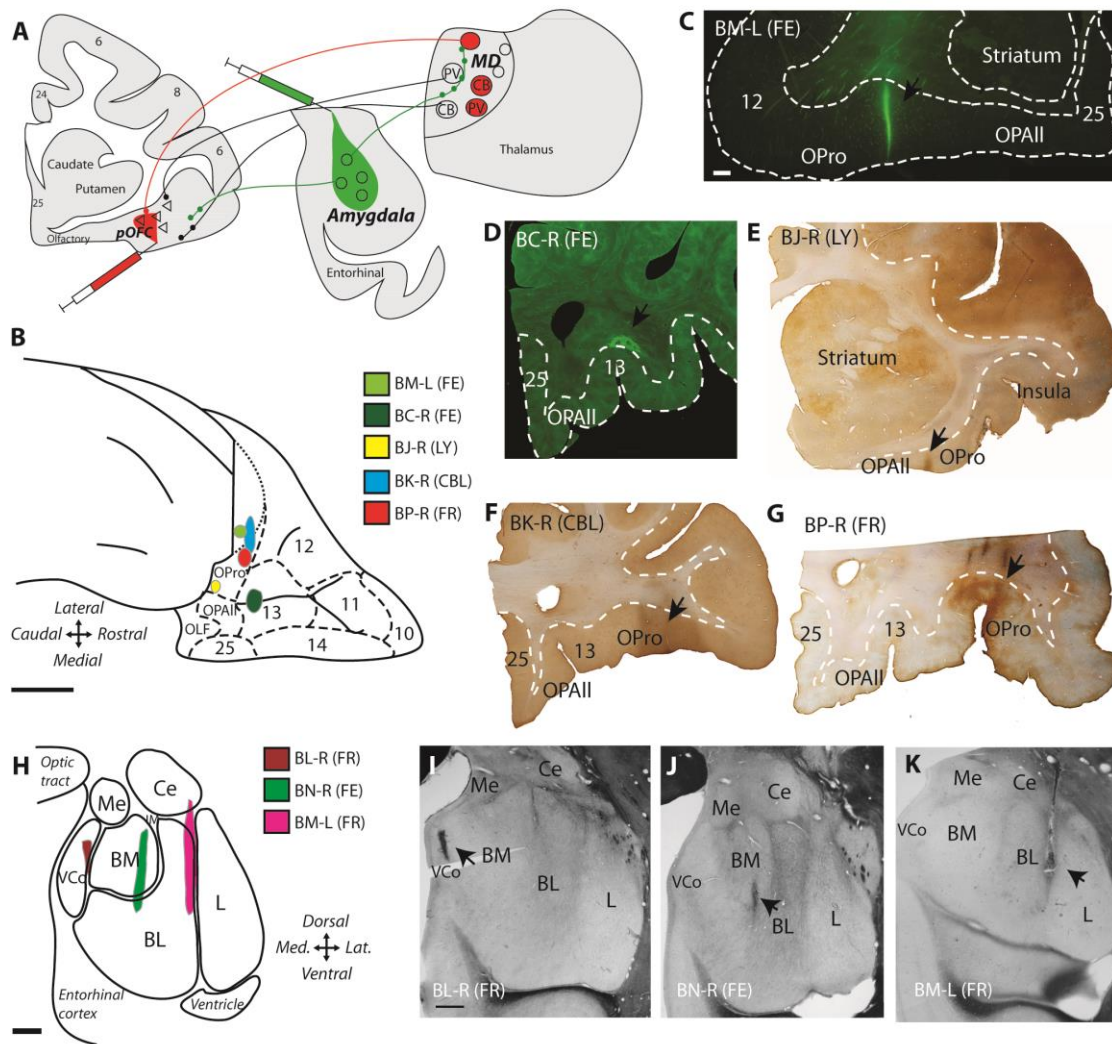


Figure 3.1. Neural tracers used to label pathways in the amygdala and pOFC

A, Experimental design: injection of retrograde tracer in pOFC and anterograde tracer in the amygdala label overlapping zones in MD. **B**, Injection sites in pOFC shown on the orbital surface of a rhesus monkey brain. Scale bar is 5 mm. **C-G**, Coronal sections through pOFC show injection of neural tracer in fluorescence microscopy (C, D) or converted for brightfield microscopy (D-G). Scale bar is 1 mm and applies to C-G. **H**, Injection sites in the amygdala shown schematically. **I-K**, Fresh tissue sections in the amygdala show injection of neural tracers. Scale bar is 1 mm and applies to I-K.

stereotaxic coordinates for the injection sites. Experiments were conducted under sterile conditions, and animals were continuously monitored for respiratory rate, oxygen saturation, heart rate, and temperature. For surgery, the animals were placed under isoflurane anesthesia and positioned in stereotaxic apparatus (Kopf 1430M, David Kopf Instruments; Tujunga, CA, USA), and a small opening was made in the skull and dura. We injected 10% dilutions of Lucifer yellow dextran (LY, 4 μ l, 10 kDa, Invitrogen; Carlsbad, CA, USA), fluoroemerald (FE, fluorescein dextran, 3 μ l, 10kDa or a mixture of 3 kDa and 10 kDa; Invitrogen), fluororuby (FR, tetramethylrhodamine dextran, 3 – 4 μ L, mixture of 3 kDa and 10kDa; Invitrogen) or Cascade Blue dextran (CBL, 6 μ l, mixture of 3 kDa and 10 kDa, Invitrogen) into amygdalar nuclei or pOFC using Hamilton syringes (10 μ l; Reno, NV, USA). After 18 days, the animals were anesthetized with sodium pentobarbital and perfused transcardially with 4% paraformaldehyde, 0.2% glutaraldehyde in 0.1M phosphate buffer saline (PBS), pH 7.4. The brain was removed, cryoprotected in ascending sucrose solutions (10% to 30% sucrose %wt/vol in 0.1M PBS, pH 7.4 with 0.05% sodium azide; Sigma-Aldrich, St. Louis, MO, USA) (Rosene et al., 1986), frozen in isopentane (Fisher Scientific; Pittsburgh, PA, USA), at -80°C, and cut on a freezing microtome (AO Scientific Instruments, Reichert Technologies; Buffalo, NY, USA), in 50 μ m coronal sections forming 10 series. Sections were stored free floating at -20°C in a solution of 30% ethylene glycol, 30% glycerol, 0.05% sodium azide in 0.05 M phosphate buffer, pH 7.4.

3.2.2 *Brightfield and confocal microscopy*

To identify overlap between amygdalar axons and pOFC projection neurons in MD, in one case (BM-L), the thalamus was removed following perfusion and prior to cryoprotection, postfixed for 3 days in 4% paraformaldehyde, embedded in 7% agarose (Electron Microscopy Sciences, Hatfield, PA, USA) and cut on a vibratome at 100 μm . Sections were mounted on glass slides and coverslipped while damp with Prolong Gold Antifade mounting medium (Invitrogen). Areas of overlap between amygdalar axons and pOFC projection neurons in MDmc were imaged using laser scanning confocal microscopy (Fluoview FV-300, Olympus; LSM-510, Carl Zeiss Microscopy; Thornwood, NY, USA) at 63x-100x magnification. Stacks of optical sections 0.3 μm thick were acquired in MDmc to identify appositions between amygdalar axons and projection neurons. Appositions were defined as close contacts between a labeled bouton and labeled dendrite, including an area of colocalization at the point of contact. FE tracer was excited with a 488 nm Argon laser, and FR tracer was excited with a 568 nm Krypton laser (Olympus) or 543 nm Helium Neon laser (Zeiss).

3.2.2.1 Immunohistochemistry: To label pOFC projection neurons and CB, CR, or PV, free floating 50 μm sections containing MD were rinsed in PB, then incubated in 0.01M sodium citrate buffer (pH 8.5) at 35-45°C for 30 minutes (Jiao et al., 1999). A 30 minute incubation with 0.3% hydrogen peroxide in PBS (0.01M phosphate buffer saline, pH 7.4) quenched endogenous peroxidases. Sections were rinsed in PBS and then incubated for one hour at 4°C in 0.05M glycine (Sigma-Aldrich) and pre-blocked for one hour at 4°C in

5% normal goat serum (NGS, Vector Laboratories; Burlingame, CA, USA), 5% bovine serum albumin (BSA, Sigma-Aldrich) and 0.2% Triton-X (Sigma-Aldrich) in 0.01M PBS. Tracers and calcium-binding proteins were bound overnight at 4°C with primary antibodies (FE, FR, CBL, or LY: 1:800 in 1% NGS, 1% BSA, and 0.1% Triton-X in PBS; rabbit polyclonal, Invitrogen; and CB, CR, or PV: 1:2000, mouse monoclonal, Swiss Antibodies; Bellinzona, Switzerland). Primary and secondary antibody penetration was enhanced with eight minute runs (three minutes on, two minutes off, three minutes on) in a temperature-controlled variable wattage microwave oven (150W at 4°C, Pelco Biowave with ColdSpot and ThermoCube, Ted Pella; Redding, CA, USA) during each incubation. Next the tissue was rinsed in PBS and incubated overnight at 4°C in secondary antibodies conjugated with fluorescent label (1:100 in 1% NGS, 1% BSA, and 0.1% Triton-X in PBS; Alexa Fluor 568 goat anti-rabbit or goat anti-mouse IgG and Alexa Fluor 488 goat anti-mouse or goat anti-rabbit IgG, Invitrogen). Sections were rinsed in PB, mounted on gelatin-coated glass slides and coverslipped while damp with Prolong Gold Antifade mounting medium (Invitrogen) or FluorSave reagent (EMD Millipore, Billerica, MA, USA).

For analysis of VGLUT1 and VGLUT2, sections were incubated in sodium citrate buffer, glycine, and blocked as above, and any BDA tracer was blocked using avidin-biotin blocking solution (AB blocking kit, Vector). Sections were then incubated overnight in primary antibodies to VGLUT1 (1:2000 in 1% NGS, 1% BSA, and 0.1% Triton-X in PBS; anti VGLUT1 rabbit polyclonal, MAb Technologies, Stone Mountain, GA, USA) or VGLUT2 (1:2000 in 1% NGS, 1% BSA, and 0.1% Triton-X in PBS; anti

VGLUT2 rabbit polyclonal, MAb Technologies). Sections were rinsed in PBS and then incubated in biotinylated secondary antibodies (1:200 in 1% NGS, 1% BSA, and 0.1% Triton-X in PBS; biotin-SP Fab fragment goat anti-rabbit IgG, Jackson Immuno Research, West Grove, PA, USA) for 2 hours at 4°C. Sections were then incubated for one hour at 25°C with avidin-biotin horseradish peroxidase (AB-HRP, Vectastain Elite ABC kit, Vector) at a 1:100 dilution in PBS, followed by rinses in PBS. VGLUT signal was amplified through incubation in biotinylated tyramide signal amplification solution (1:4000 in PBS, TSA Biotin Kit, Perkin Elmer, Waltham, MA, USA), with 0.005% hydrogen peroxide for 20 minutes at 25°C. This step also ensured that any rabbit binding sites on the primary or secondary antibody were blocked prior to incubation with a second rabbit primary antibody. Sections were then rinsed in PBS and incubated overnight at 4°C in antibodies to label tracers (FE or FR: 1:800 in 1% NGS, 1% BSA, and 0.1% Triton-X in PBS; rabbit polyclonal, Invitrogen). Following rinses in PBS, sections were incubated overnight at 4°C in streptavidin-conjugates to visualize VGLUT (1:100 Alexa Fluor 647 streptavidin, Invitrogen) and secondary antibodies to visualize tracers (1:100 in 1% NGS, 1% BSA, and 0.1% Triton-X in PBS; Alexa Fluor 488-AffiniPure Fab fragment goat anti-rabbit IgG [FE] or Rhodamine Red-X-AffiniPure Fab fragment goat anti-rabbit IgG, Jackson Immuno Research). In control experiments omission of the primary antibodies and incubating in secondary antibody solutions showed no immunolabeling.

3.2.2.2 Data analysis: We analyzed retrogradely labeled pOFC projection neurons in MD

in 4-8 evenly spaced sections labeled for CB or PV through the entire rostral-caudal extent of MD in 3 cases (BJ-R, BK-R, BP-R) (Olszewski, 1952). In one case (BJ-R), an additional series of sections was labeled for CR. One additional case (BC-R) with an injection site confined to deep layers and white matter below area 13 was analyzed for comparison; in this case 2 evenly spaced sections labeled for CB or PV covering central MD were analyzed. For each section, all retrogradely labeled neurons in MD were counted at 20x magnification, and colocalization with CB or PV was determined using an epifluorescence microscope and digital camera (Olympus BX51 and DP70 digital camera, Olympus; Center Valley, PA, USA).

We used laser scanning confocal microscopy (LSM-510, Carl Zeiss Microscopy; Thornwood, NY, USA) to study colocalization between fluorescently labeled tracer and VGLUT1 or VGLUT2. Stacks of optical sections 0.3 μ m thick were acquired in patches of labeled fibers in upper layers 2-3a of pOFC or MDmc at 63x magnification. Alexa 488 conjugates were excited with a 488 nm Argon laser, Rhodamine Red X conjugates with a 543 nm Helium Neon laser, and Alexa 647 conjugates with a 633 nm Helium Neon laser. Images were deconvolved to remove noise and fluorescent halo (AutoDeblur, version X1.4.1, MediaCybernetics, Silver Spring, MD, USA). All labeled boutons were counted, and we used ImageJ and ColocalizeRGB plugin to detect colocalization between labeled boutons and VGLUT1 or 2 (Rasband, 1997-2014). We used χ^2 tests to compare proportions of VGLUT1 or 2 colocalized boutons in pOFC and MDmc.

3.2.3 *Electron microscopy*

3.2.3.1 Immunohistochemistry and embedding: To study pathways in the electron microscope (EM), we used triple immunohistochemistry to identify tracers with DAB (which appears as uniform dark precipitate under EM), and calcium binding proteins (CB or PV) using gold labeling with silver enhancement (forms clumps of round particles) and tetramethylbenzidine (TMB) staining (forms rod-shaped precipitate). Tissue sections were incubated as above in 0.01M sodium citrate, pH 8.5 (30 minutes at 35°C), 0.05 M glycine (one hour at 4°C), and any BDA tracer was blocked with AB blocking solutions. Background binding was blocked with incubation for one hour at 4°C in 5% NGS, 5% BSA, 0.025% Triton X-100 (Roche Applied Sciences; Indianapolis, IN, USA), 0.1% acetylated BSA-c (Aurion; Wageningen, NL), and 3.5% mouse blocking reagent (MOM basic kit, Vector) in PBS. Sections were then bound overnight at 4°C with antibodies for tracers (FE, FR, or LY: 1:800 in 1% NGS, 1% BSA, 0.1% BSA-c, 0.025% Triton X-100, and 8% MOM protein concentrate [MOM basic kit, Vector] in PBS; rabbit polyclonal IgG, Invitrogen) and one of three calcium binding proteins (CB, CR, or PV: 1:2000, mouse monoclonal IgG, Swant). All primary and secondary antibody incubations included an eight minute microwave run as above.

Sections were rinsed in PBS then incubated for six hours at 25°C with biotinylated secondary antibodies for tracers (1:200 in 1% NGS, 1% BSA, 0.1% BSA-c, 0.025% Triton X-100, 8% MOM protein concentrate, and 0.1% cold water fish gelatin [Aurion] in PBS; biotinylated goat anti-rabbit IgG, Vector) and gold-conjugated

secondary antibodies for calcium-binding proteins (1:50 UltraSmall ImmunoGold F(ab) fragment of goat anti-mouse IgG, Aurion). Sections were then postfixed with 3% glutaraldehyde and 1% paraformaldehyde in PB in a microwave oven (2 minutes at 150W, 4°C). Sections were rinsed in glycine (5 minutes) and rinsed in PB (2 x 10 minutes), followed by enhancement conditioning solution (ECS, 1:10, 2 x 10 minutes, Aurion). Gold-conjugated proteins were visualized by silver enhancement for 60-90 minutes (R-Gent SE-EM, Aurion); the tissue was then rinsed in ECS (2 x 10 minutes) and then PB (2 x 10 minutes). Tracers were visualized with DAB as above. For all rinses following silver enhancement 0.1 M PB pH 7.4 was used, and in some pieces of tissue the order of labeling was reversed to control for any attraction between gold and biotin. Any remaining biotin binding sites were blocked with AB blocking solutions, and then any remaining mouse binding sites were blocked with incubation for one hour at 4°C in 3.5% mouse blocking reagent, 5% NGS, 5% BSA, 0.025% Triton X-100, and 0.1% BSA-c in PB.

Sections were incubated overnight at 4°C with antibody for a second calcium binding protein (CB, PV, or CR: 1:2000 in 1% NGS, 1% BSA, 0.1% BSA-c, 0.025% Triton X-100, and 8% MOM protein concentrate in PB; mouse monoclonal IgG, Swant), followed by rinses in PB and incubation for 1-2 hours at 25°C in biotinylated secondary antibody (1:200 in 1% NGS, 1% BSA, 0.1% BSA-c, 0.025% Triton X-100, and 8% MOM protein concentrate in PB; biotinylated goat anti-mouse IgG, Vector), then rinsed in PB and incubated in AB-HRP as above. These calcium-binding proteins were visualized with TMB staining as follows: sections were first incubated for 15 minutes in

0.005% TMB (Sigma-Aldrich), 0.004% ammonium chloride (Sigma-Aldrich), and 5% ammonium paratungstate (Sigma-Aldrich) in 0.1M PB, pH 6.0, and then incubated for one to five minutes in the same solution plus 0.005% hydrogen peroxide (Sigma-Aldrich) until staining appeared. The staining was stabilized by incubating sections for 10 minutes in a solution of 0.05% DAB (SigmaFast DAB tablet, Sigma-Aldrich), 0.02% cobalt chloride (Sigma-Aldrich), 0.004% ammonium chloride (Sigma-Aldrich), and 0.005% hydrogen peroxide (Sigma-Aldrich) in 0.1M PB, pH 6.0. Finally sections were rinsed in PB and postfixed in 6% glutaraldehyde and 2% paraformaldehyde in PB with a microwave oven (150W at 15°C) until sample temperature reached 30-35 °C (Jensen and Harris, 1989). We conducted control experiments on tissue by omitting primary antibodies and incubating in secondary antibody solutions and no immunolabeling was observed.

Sections were rinsed in PB (3 x 20 minutes) and postfixed for 15 minutes in 1% osmium tetroxide (Electron Microscopy Sciences) with 1.5% potassium ferrocyanide (Electron Microscopy Sciences) in PB with a microwave oven (100W at 12°C, 2 minutes on, 2 minutes off, 2 minutes on) and rinsed in PB (3 x 2 minutes) and water (3 x 2 minutes). Sections were then rinsed in 50% ethanol (3 x 5 minutes), stained with 1% uranyl acetate (30 minutes in 70% ethanol, Electron Microscopy Sciences), and dehydrated in a series of ethanols (90%, 95%, 100%; 3 x 5 minutes each). For embedding, sections were infiltrated with propylene oxide (2 x 7 minutes, Electron Microscopy Sciences), and then a 1:1 mixture of araldite (Electron Microscopy Sciences) and propylene oxide (one hour). Sections were infiltrated with araldite overnight,

followed by flat embedding in araldite in aclar (Ted Pella). Aclar-embedded tissue was cured for 48 hours at 60°C. Small columns of tissue 500-750 µm wide were cut from each section, divided by layer, and re-embedded in araldite blocks and cured for 48 hours at 60°C.

3.2.3.2 Serial sectioning and data analysis: To reconstruct postsynaptic sites, araldite blocks containing embedded tissue from MDmc were sectioned at 50 nm using an ultramicrotome (Leica Ultracut UCT, Leica Microsystems; Buffalo Grove, IL, USA) and collected on pioloform coated copper slot grids, to form series of approximately 75-150 sections. Using 80 kV transmission EM at 16000x-26000x (JEOL 100CX; Jeol, Peabody, MA, USA), we exhaustively sampled a few sections to identify approximately 10-30 labeled boutons in each series. Each bouton was photographed in serial sections through at least 20 sections. Boutons that were complete in the series were photographed in serial sections covering the entire bouton, while boutons that were not complete were photographed in at least 20 sections. We analyzed labeled boutons using Reconstruct to trace bouton profiles and postsynaptic sites (Fiala, 2005). Synapses, axon terminals, and postsynaptic sites were identified using classical criteria, (Peters et al., 1991). We compared mean diameters of amygdalar boutons in MD with those in pOFC using a two-tailed t test.

3.3 Results

3.3.1 Thalamic projection neurons targeting pOFC

We first investigated the organization and types of thalamic neurons that project to pOFC. Unlike the cortex, in the primate thalamus CB and PV neurons form two classes of excitatory projection neurons: CB neurons are thought to project diffusely to the upper layers of cortex, while PV neurons project focally to the middle layers (Jones and Hendry, 1989; for discussion see Jones, 1998). Injections of tracers covering all cortical layers in pOFC labeled projection neurons retrogradely in the thalamic MD nucleus (Fig. 3.1). We then labeled tissue through the thalamus for CB or PV, to study the proportion of projection neurons that were double-labeled (Fig. 3.2A-C).

Among double-labeled neurons in MD, in each case there was a consistent trend of a greater proportion of CB-positive projection neurons (mean \pm SEM, $36.1 \pm 7.5\%$ CB-positive of all retrogradely labeled neurons; $13.8 \pm 3.0\%$ PV-positive; $n = 3$ cases; two-tailed t test, $t_{(2)} = 2.4$, $p = 0.1$; Fig. 3.2C). To investigate the identity of the remaining retrogradely labeled neurons, in one case we also double-labeled for CR and found that 3.1% of retrogradely labeled neurons were positive for CR. The remaining projection neurons in MD that were directed to pOFC were unlabeled; this may represent lightly labeled CB or PV neurons that did not reach threshold to determine possible colocalization. Alternatively, there may be thalamic projection neurons that do not colocalize with any of the known calcium binding proteins (CB, PV, or CR), a question that remains to be addressed in future studies.

In one additional case, the tracer was confined to the deep layers (layer 6) of

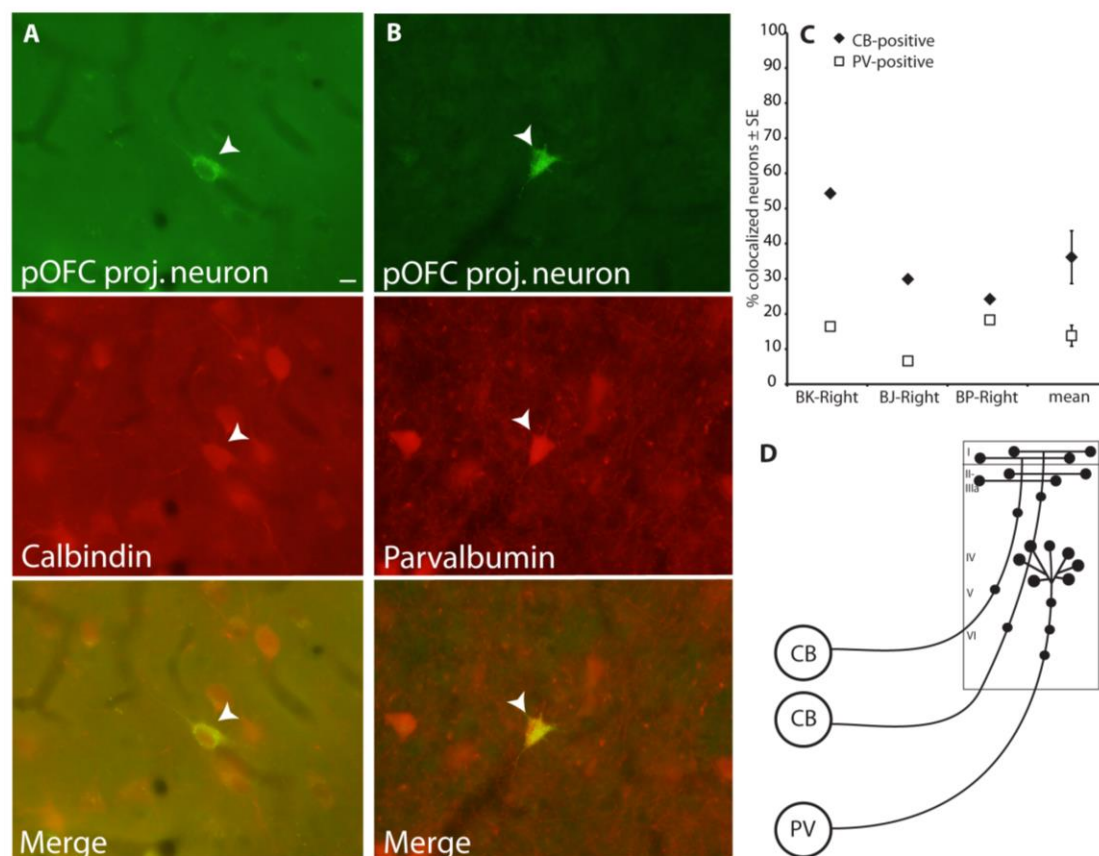


Figure 3.2. Neurons in MD projecting to pOFC colocalized with CB or PV.

Scale bar is 10 μ m and applies to A and B. **A**, Thalamic MD neuron projecting to pOFC (upper panel, white arrowhead) that is also positive for CB (middle panel), merged images (bottom panel). **B**, Thalamic MD neuron projecting to pOFC (upper panel, white arrowhead) that is also positive for PV (middle panel), merged images (bottom panel). **C** Thalamic neurons projecting to pOFC more frequently colocalized with CB than PV, in all cases analyzed. **D**, Schematic depicting CB thalamocortical neurons terminating diffusely in the upper cortical layers, while PV thalamocortical neurons terminate focally in the middle cortical layers. Vertical lines indicate standard error of the mean (SE).

pOFC and the white matter below (case BC-R, Fig. 3.1). In this case, 38% of double-labeled neurons in MD were PV-positive, and comparatively fewer (29%) were CB-positive. This evidence suggests that in MD, PV thalamic neurons target the middle and deep cortical layers preferentially, while CB-positive neurons project diffusely to the upper as well as to the deep layers of cortex. Previous studies have shown that MD terminals are densest in the middle to deep layers of pOFC, and comparatively less dense in the upper cortical layers (Giguere and Goldman-Rakic, 1988; McFarland and Haber, 2002). However, we found a higher proportion of CB projection neurons in this MD pathway. The relatively low density of MD terminals in the upper layers, but high proportion of CB neurons projecting to pOFC, suggests that thalamic CB neurons send divergent, diffuse projections to cortex so that cortical injections label more of them in MD, as depicted schematically in Figure 3.2D.

3.3.2 Amygdalar pathways form synapses with excitatory projection neurons in MDmc

We next investigated the organization of amygdalar pathways to MDmc. The rationale is based on evidence that amygdalar axons innervate MDmc, the sector of the thalamus that projects robustly to pOFC and to a lesser extent to other prefrontal cortices (Porrino et al., 1981; Ray and Price, 1993; Dermon and Barbas, 1994; Miyashita et al., 2007; Xiao et al., 2009). The type of MD neurons targeted by the amygdala remains unknown. To address this issue, we labeled the amygdalar pathway to MDmc using anterograde tracers, and identified its postsynaptic targets in the EM by morphology and for the presence of label for CB or PV in thalamic neurons (Fig. 3.3).

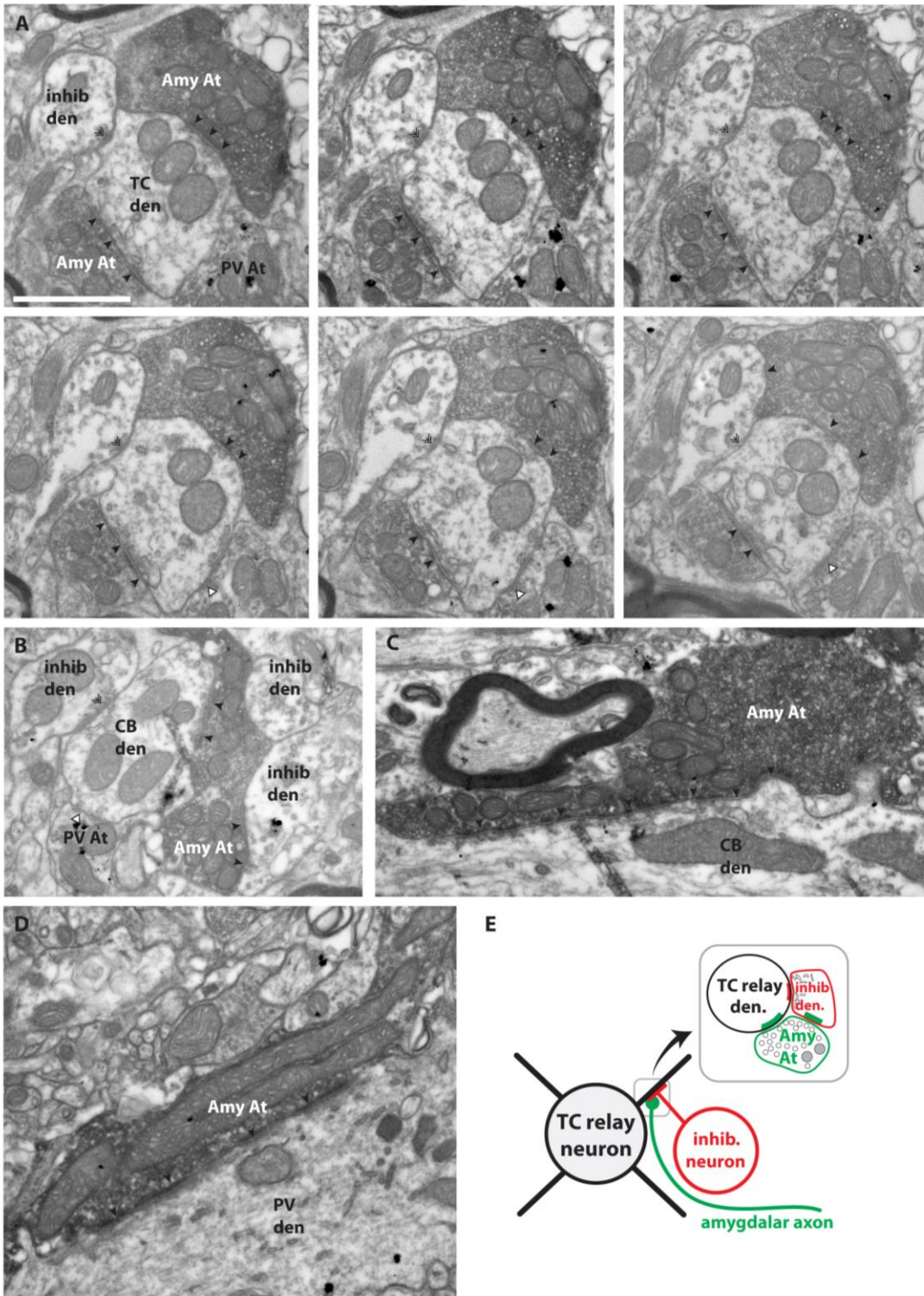


Figure 3.3. Amygdalar axon terminals formed synapses on MDmc thalamic relay dendrites.

Scale bar is 1 μm and applies to panels A-D. **A**, Amygdalar axon terminal forming a synaptic triad in MDmc, where the amygdalar terminal (Amy At, black arrowheads), forms excitatory synapses with both the central, thalamocortical relay dendrite (TC den) and a vesicle-containing dendrite of a local inhibitory neuron (inhib den). The central relay dendrite receives symmetric, inhibitory synapses from both the inhibitory dendrite (double arrowheads) and a PV inhibitory axon terminal (PV At, silhouette arrowheads). **B**, Amygdalar axon terminal forming excitatory, asymmetric synapses (black arrowheads) with a TMB-labeled CB relay dendrite and an inhibitory axon dendrite. The relay dendrite receives symmetric synapses from an inhibitory dendrite (double arrowhead) and a PV axon terminal (silhouette arrowhead). **C**, Amygdalar axon terminal forming a large excitatory, asymmetric synapse (black arrowheads) with a TMB-labeled CB relay dendrite. **D**, Amygdalar axon terminal forming an excitatory, asymmetric synapse (black arrowheads) with a gold-labeled PV relay dendrite. **E**, Schematic depicting the organization of a synaptic triad, where an excitatory afferent innervates a proximal dendrite of a thalamic relay neuron as well as dendrites of local inhibitory neurons. The relay dendrite also receives symmetric synapses from the same local inhibitory neuron.

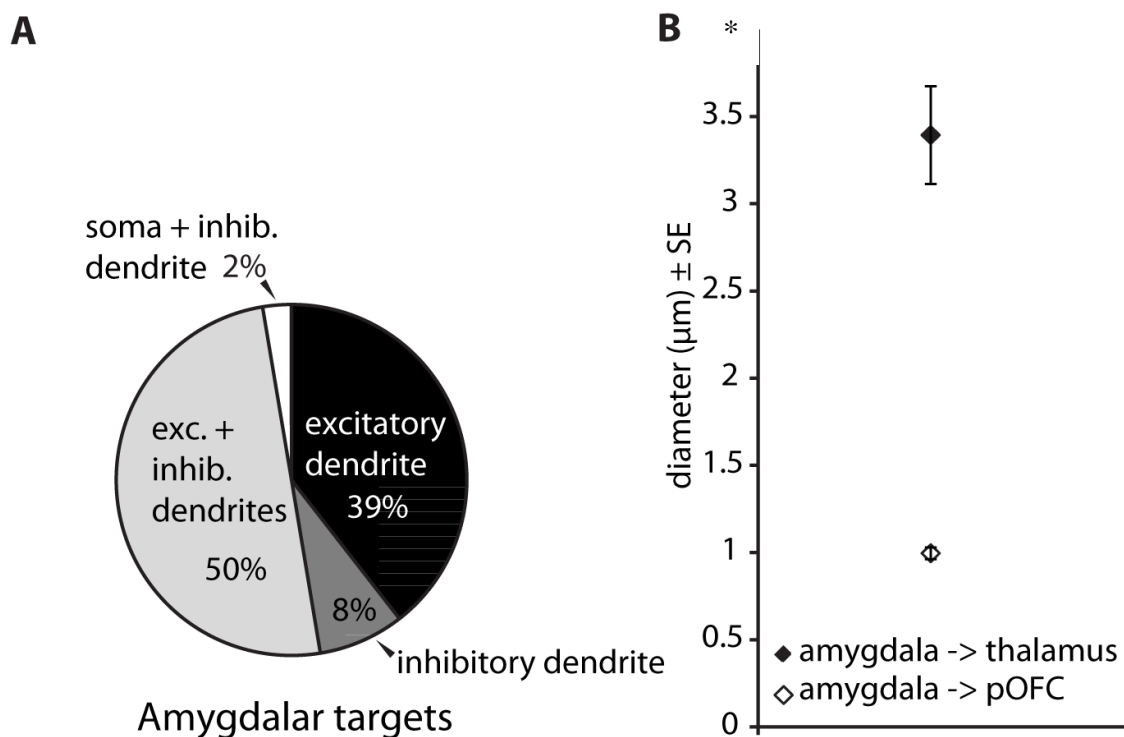


Figure 3.4. Amygdalar axon terminals in MDmc were larger than those in the cortex and frequently multisynaptic.

A, Postsynaptic targets of amygdalar axons in MDmc. Vertical lines indicate standard error of the mean (SE). **B**, Amygdalar axon terminals in MDmc were larger in diameter than amygdalar terminals in cortex. $*p \leq 0.05$.

We identified thalamic excitatory neurons that project to the cortex by morphology and the presence of CB or PV. The primate thalamus also contains local inhibitory neurons which can be identified morphologically; dendrites of local inhibitory neurons contain vesicles and form symmetric dendro-dendritic synapses (Fig. 3.3A) (Peters et al., 1991).

We investigated the postsynaptic targets of the amygdalar pathway in MDmc and found that the majority of amygdalar axons formed at least one synapse with an excitatory dendrite (89%, $n = 34$ of 38 boutons). Amygdalar synapses more frequently innervated CB dendrites in MDmc (68%, $n = 21$ of 31 labeled dendrites, the remainder innervated PV dendrites; Fig 3.3B-D). This finding suggests that amygdalar input to MDmc preferentially influences upper cortical layers through synapses on CB thalamic projection neurons, which target both upper and deep cortical layers, in contrast to PV neurons which terminate in focal middle layer projections.

Some amygdalar boutons formed more than one synapse. Most formed synapses with both excitatory and inhibitory neurons (50%, $n = 19$ of 38; Fig. 3.4A). Of these boutons, the majority formed synaptic triads that could be identified in the series ($n = 14$ of 19; Fig 3.3A-E). In this arrangement, the inhibitory dendrites are postsynaptic to the excitatory amygdalar bouton, and are also presynaptic to the same excitatory relay neuron as the amygdalar bouton (Fig. 3.3E) (Peters et al., 1991). Synaptic triads have been described in sensory thalamic nuclei, including retinal afferents entering the lateral geniculate nucleus to relay visual signals to cortex (Famiglietti and Peters, 1972; reviewed in Jones, 1985) as well as in higher order thalamic nuclei including the ventral

anterior nucleus (Ilinsky and Kultas-Ilinsky, 1990).

3.3.3 Amygdalar boutons in MDmc were larger than those in pOFC

The amygdalar pathway to MDmc had another synaptic specialization.

Amygdalar axons formed large boutons in MDmc (mean diameter \pm SE, $3.4 \pm 0.28 \mu\text{m}$, range $1.1 \mu\text{m}$ to $7.0 \mu\text{m}$, $n = 38$ boutons from 2 cases, Fig. 3.4B). These boutons were significantly larger than amygdalar boutons that innervate pOFC ($0.99 \pm 0.033 \mu\text{m}$, range $0.43 \mu\text{m}$ to $3.3 \mu\text{m}$, $n = 164$ boutons from 2 cases; two-tailed t test, $t_{(200)} = 16.1$, $p < 0.0001$). All amygdalar boutons in MDmc also contained multiple mitochondria, and can be classified as RL boutons (round, large) which contain round vesicles and mitochondria and form asymmetric (excitatory) synapses in the thalamus (Ilinsky and Kultas-Ilinsky, 1990). RL boutons target proximal dendrites of thalamic relay neurons, in comparison with small excitatory boutons (round small, RS) which target more distal dendrites, do not contain mitochondria, and are characteristic of most corticothalamic terminals (Ilinsky and Kultas-Ilinsky, 1990; Schwartz et al., 1991).

3.3.4 Amygdalar axons in pOFC and MDmc colocalize with vesicular glutamate transporters

The morphological differences between amygdalar axons in MDmc and those to cortex suggest that amygdalar pathways to MDmc and to pOFC may originate from separate populations in the amygdala. While both of these pathways are glutamatergic and excitatory, we investigated whether they could be further distinguished by the

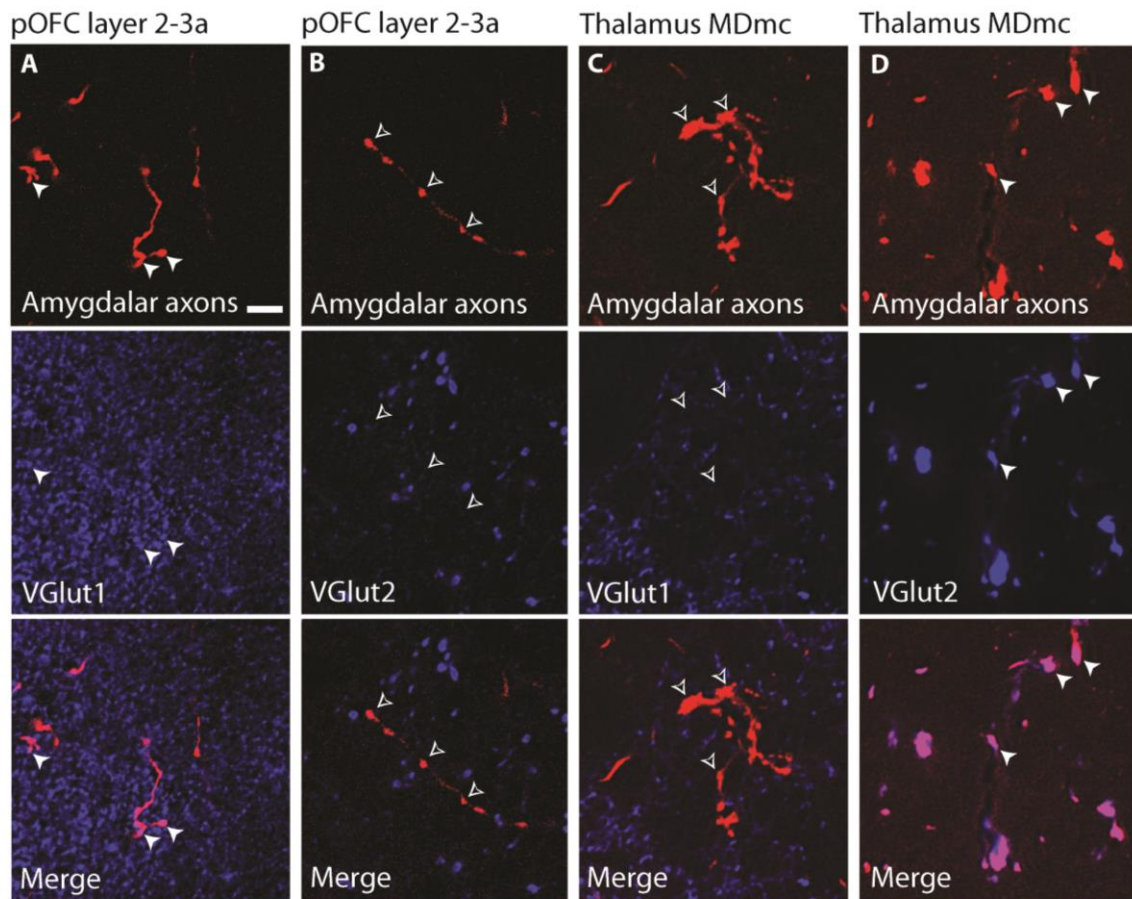


Figure 3.5. Amygdalar axons in MDmc and pOFC express different glutamate transporters.

Scale bar is 10 μm and applies to all panels. **A-B**, Amygdalar axons (upper panel, white arrowheads) in upper layers of pOFC colocalized with VGLUT1 (middle panel), but not with VGLUT2 (middle panel, silhouette arrowheads), merged images (bottom panel). **C-D**, Amygdalar axons in MDmc (upper panel, white arrowheads) colocalized with VGLUT2 (middle panel), but not with VGLUT1 (middle panel, silhouette arrowheads), merged images (bottom panel).

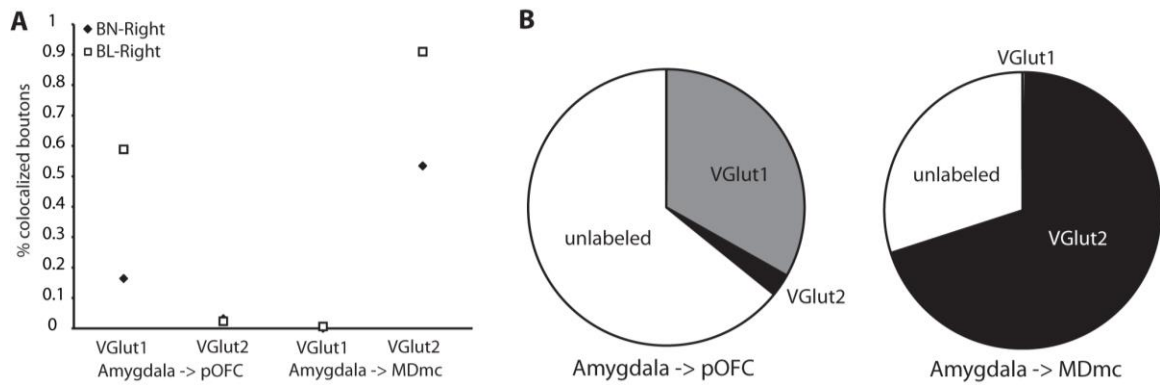


Figure 3.6. Amygdalar axons in MDmc expressed VGLUT2 more frequently, while those in pOFC expressed more VGLUT1.

A, Scatterplot depicting the proportion of amygdalar boutons in each case which colocalized with VGLUT1 or 2 in MDmc or pOFC. **B**, Overall proportion of amygdalar boutons that colocalized with VGLUT1 or 2 in MDmc or pOFC.

expression of vesicular glutamate transporter 1 or 2 (VGLUT1 or VGLUT2). Corticocortical and corticothalamic axons express VGLUT1, while thalamocortical axons express primarily VGLUT2, in primates (Hackett et al., 2011). The nature of glutamate transporters in amygdalar axons remains unexplored. To address this issue, we used immunofluorescence to identify colocalization between labeled amygdalar axons and VGLUT1 or 2, in pOFC and MDmc (n = 1626 boutons from 2 cases; Fig. 3.5). We found that in the upper layers of pOFC, amygdalar axons colocalized more frequently with VGLUT1 (33% VGLUT1, n = 161 of 485 boutons from 2 cases; 3% VGLUT2, n = 16 of 611 boutons from 2 cases; $\chi^2_{(1, n=1096)} = 186.7$, $p < 0.0001$; Fig 3.5A-B, 3.6). The remainder boutons were unlabeled and may represent boutons that were lightly labeled by VGLUT1 or 2 and which did not meet the threshold for colocalization. In contrast, in MDmc amygdalar axons colocalized most frequently with VGLUT2 (70% VGLUT2, n = 179 of 257 boutons from 2 cases; 0.4% VGLUT1, n = 1 of 273 boutons from 2 cases; $\chi^2_{(1, n=530)} = 283.3$, $p < 0.0001$; the remainder were unlabeled; Fig. 3.5C-D, 3.6). This demonstrates that amygdalar axons in cortex differ chemically from amygdalar axons in MDmc. This evidence, along with morphological differences between the two pathways, supports the idea that amygdalar projections to cortex and MDmc arise from distinct neurons in the amygdala, as has been proposed in rats (McDonald, 1987).

3.3.5 Amygdalar axons target projection neurons in MDmc that project to pOFC

The amygdala projects to MDmc which projects to pOFC, but it is not known if this pathway is sequential in view of evidence that other subcortical structures also

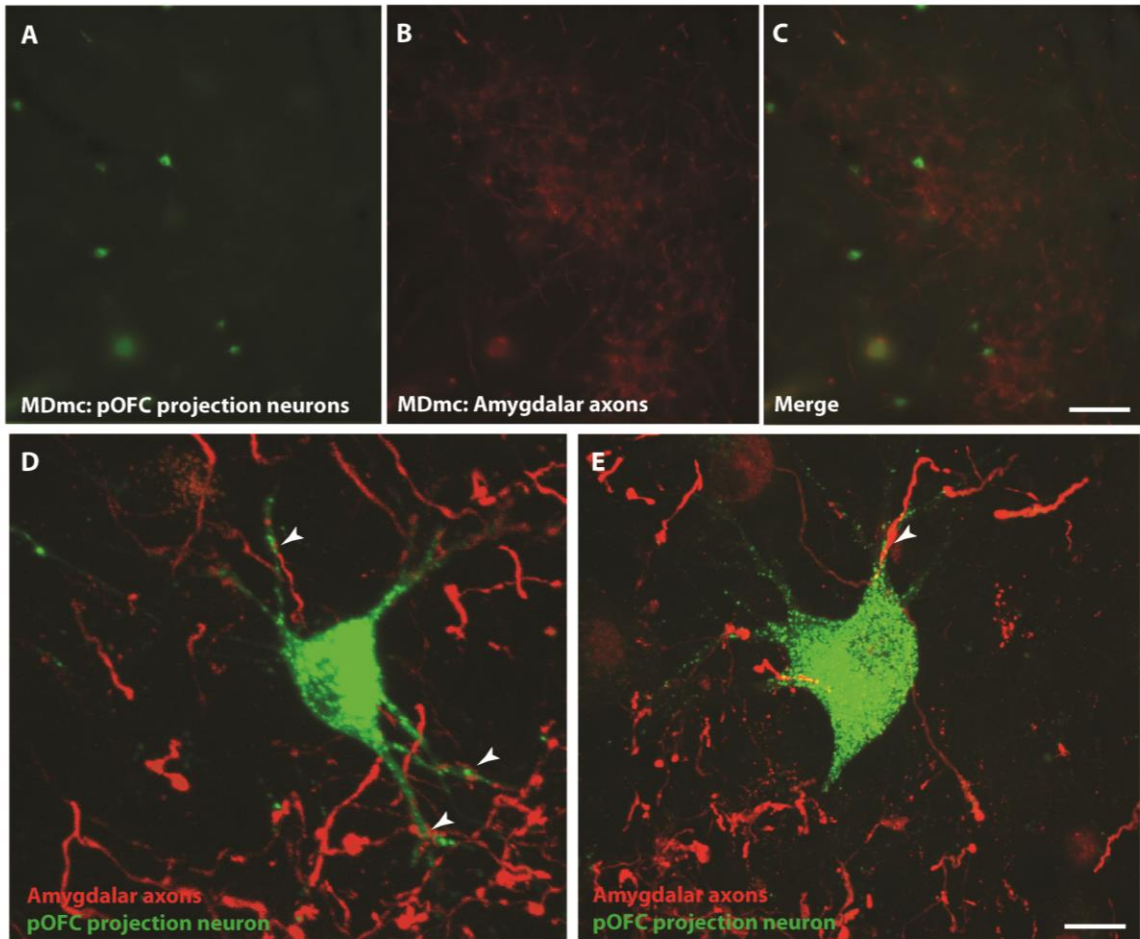


Figure 3.7. In MDmc, neurons projecting to pOFC overlapped with amygdalar axons.

A-C, Neurons in MDmc projecting to pOFC (left panel), overlapped with patches of labeled amygdalar axons (middle panel), merged images (right panel). Scale bar is 100 μm and applies of A-C. D-E, Laser scanning confocal microscopy shows close appositions (white arrowheads) between pOFC projection neurons and amygdalar axons in MDmc. Scale bar is 20 μm and applies to D-E.

project to MD (Russchen et al., 1987; Erickson et al., 2004; Rovo et al., 2012). To address this issue, we injected retrograde neural tracers in pOFC and anterograde tracers in the amygdala simultaneously. We first identified whether the projection systems overlap or not in MDmc. We found that amygdalar axons in MDmc terminated in dense patches, many of which overlapped with retrogradely labeled pOFC projection neurons (Fig 3.7A-C). Using laser scanning confocal microscopy to analyze areas of overlap, we found labeled amygdalar axons forming close appositions with labeled pOFC projection neurons in MDmc (Fig. 3.7D-E). Only the cell body and proximal dendrites of retrogradely-labeled pOFC projection neurons were labeled by this method, so only proximal targets of amygdalar axons could be identified. This finding provides evidence of a sequential pathway through MD, which includes strong proximal inputs on relay neurons. Thus, in addition to sending signals to pOFC directly, the amygdala sends signals indirectly to pOFC through MDmc.

3.4 Discussion

In addition to a strongly excitatory pathway to cortex, the amygdala has a powerful influence on MDmc through large synapses forming synaptic triads. Amygdalar pathways to cortex and thalamus may originate from separate neurons in the amygdala, as shown in morphological differences and differential expression of glutamate transporters. We provide direct evidence for the first time that amygdalar axons target neurons in the thalamic MDmc that project to pOFC, establishing a second, indirect route for signals from the amygdala to reach pOFC (Fig 3.8).

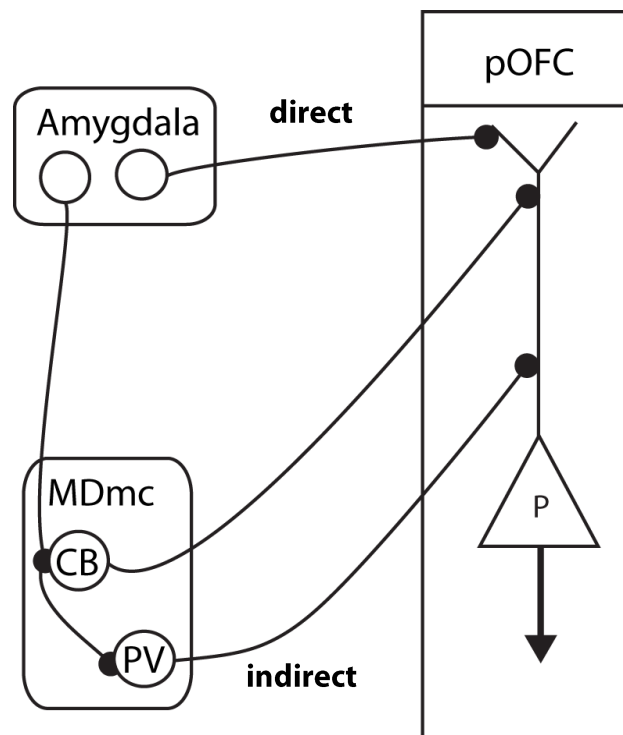


Figure 3.8. Amygdalar signals reach pOFC directly, and indirectly through the thalamus.

Direct projections target upper layers, while indirect projections through the thalamus may target upper and middle layers through CB and PV thalamic neurons, to enhance cortical signaling of affective content.

3.4.1 Direct and indirect routes connect amygdala with pOFC

The primate amygdala sends a strong projection to MDmc. This amygdalar pathway was distinguished for its very large terminals enriched with mitochondria, which are characteristic of efficient synapses (Germuska et al., 2006; Zikopoulos and Barbas, 2007a). The MD is also reciprocally connected with pOFC (Giguere and Goldman-Rakic, 1988; Dermon and Barbas, 1994). But since other inputs converge on MDmc as well, and neurons in MD project to other areas (Russchen et al., 1987; Erickson et al., 2004; Rovo et al., 2012), a pathway connecting the amygdala with pOFC through MD was uncertain. We show for the first time the existence of a sequential pathway between the basolateral amygdala to pOFC, through MDmc. This second, indirect route may allow the amygdala to activate thalamic afferents to pOFC, in addition to a direct amygdalar pathway to pOFC. These two pathways differ in their laminar distribution, interactions with inhibitory neurons, and synaptic features.

Previous studies have shown that amygdalar axons in pOFC terminate most densely in the upper cortical layers (Porrino et al., 1981; Ghashghaei et al., 2007), and among inhibitory neurons innervate mostly CB and CR neurons. In contrast, thalamic axons target predominantly the middle cortical layers and more PV inhibitory neurons than the amygdalar pathway. While thalamocortical neurons that terminate in the middle cortical layers are classically considered to be drivers (Jones, 1998; Sherman and Guillery, 1998), we previously found that amygdalar terminals in the upper layers of pOFC are even larger than the thalamic, innervate more excitatory neurons, and may act as specialized drivers in the upper layers of pOFC. Combined with our findings that

amygdalar axons in MD target neurons projecting to pOFC, this evidence suggests that the amygdala can drive signal to either upper or middle layers of pOFC through the direct or indirect pathways.

The amygdala likely reaches different layers of pOFC through connections with CB and PV thalamic projection neurons. In the thalamus, these calcium-binding proteins mark parallel pathways for excitatory projection neurons: CB neurons are thought to terminate in the upper layers of cortex, while PV neurons terminate in the middle layers (Jones and Hendry, 1989). Here we found that amygdalar axons innervate both classes of thalamic projection neurons, though more synapses were formed with CB neurons. This finding suggests that the amygdala preferentially activates thalamic input to the upper layers of pOFC through the thalamus as well as directly. Additional evidence of this preference emerged from the fact that more CB neurons in MD project to pOFC. These findings suggest that whereas each thalamic PV neuron terminates in a dense focal projection in the middle cortical layers, each thalamic CB neuron terminates in a diffuse arbor covering the upper cortical layers and partially overlaps with parvalbumin axons in the middle to deep cortical layers, as shown schematically in Figure 3.2C. Further, we provide evidence for the presence of calretinin-positive pOFC projection neurons in MD, a novel thalamocortical pathway.

The predominance of CB-positive projection neurons to pOFC may be a specialized projection to limbic cortices. The thalamus develops earlier than the cortex (Finlay and Darlington, 1995), and in primates, limbic cortices complete development earlier than the six-layered eulaminar cortices (Rakic, 2002). This may coincide more

closely with the developmental timeline of CB neurons, which develop earlier than PV neurons in the human thalamus (Kultas-Ilinsky et al., 2004). Additionally, the lack of a well-developed layer 4 in limbic cortices could influence the thalamic input to the middle layers from PV-positive thalamic neurons. Study of the proportions of CB and PV thalamic projection neurons directed to other areas is needed to address these questions further.

3.4.2 Divergence of amygdalar pathways to the cortex and to the thalamus

In addition to targeting different layers and inhibitory neurons in pOFC, amygdalar axons in the direct and indirect pathways differ morphologically. Amygdalar axons that innervated MD were larger than those that terminate in cortex. The two amygdalar pathways also differed in their expression of vesicular glutamate transporters: amygdala – thalamic terminals expressed mostly VGLUT2, while amygdala – cortical terminals were more frequently VGLUT1-positive. These transporters are necessary for filling vesicles with glutamate, and maintain the readily releasable pool of vesicles at axon terminals of excitatory glutamatergic neurons (Weston et al., 2011). Compared to VGLUT1 terminals, VGLUT2 thalamocortical terminals have a higher vesicle release probability, and show paired-pulse depression, where sequential spikes elicit smaller synaptic responses (Weston et al., 2011). This suggests that VGLUT2 terminals from the amygdala are highly efficient and likely elicit action potentials in their postsynaptic targets in MD, ensuring transmission of signals. These chemical differences are also consistent with previous evidence indicating that the pathways from the amygdala to

thalamus and amygdala to cortex may be distinct in both rats and monkeys (McDonald, 1987; Miyashita et al., 2007).

The morphological and chemical differences found here suggest that neurons in the amygdala that project to the thalamus or cortex may also differ physiologically. Two types of excitatory projection neurons have been described in the basolateral amygdala of cats and rats: bursting and regular-spiking, which may have pyramidal or spiny stellate morphology (Rainnie et al., 1993; Pare et al., 1995). Bursting neurons are larger, with a lower input resistance, and thus may be less excitable (Rainnie et al., 1993). There is evidence that neurons with these physiological properties have different targets in the hippocampal system, where bursting neurons in the subiculum project to presubiculum, while regular spiking subicular neurons project to entorhinal cortex (reviewed in O'Mara et al., 2001). Amygdalar axons in MD are much larger than those in cortex, and may arise from larger cells in the amygdala, as has been suggested for cortical neurons that project to the pulvinar thalamic nucleus (Rockland, 1996). Thus, the large terminals in MD may belong to large neurons in the amygdala that are bursting neurons. In monkeys, visual stimuli with affective content can elicit burst firing in amygdalar neurons (Gonzalez Andino and Grave de Peralta Menendez, 2012). If these neurons project to the thalamus, this provides a mechanism for salient stimuli to activate thalamic neurons, and transmit saliency signals to cortex.

These two classes of amygdalar projection neurons may also have a different developmental time scale. VGLUT2 appears first in rats, and in mice some cerebellar and hippocampal axons express VGLUT2 early in development, and switch to VGLUT1

as they mature (Miyazaki et al., 2003; Wojcik et al., 2004). Amygdalar axons in MD may mature earlier, as the thalamus develops earlier than cortex in primates (Finlay and Darlington, 1995), which would more closely parallel the development of VGLUT2.

3.4.3 Amygdalar axons form synaptic triads in MDmc

Our findings also revealed for the first time in primates that amygdalar axons formed synaptic triads with projection neurons in MDmc. This type of arrangement is akin to the organization seen in the sensory relay thalamic nuclei. While studies have found large amygdalar boutons forming excitatory synapses in MD in rats and monkeys, (Kuroda and Price, 1991; Miyashita et al., 2007) amygdalar boutons forming synaptic triads have not previously been demonstrated. The robust projection from the amygdala to MD raises the question of the nature of signals transmitted by this exceptionally strong pathway. The type of signals conveyed can best be understood for the sensory thalamic relay nuclei. For example, retinal pathways form synaptic triads with thalamic neurons projecting to visual cortex in cats (Famiglietti and Peters, 1972; Jones, 1985). This synaptic specialization connects glutamatergic afferents with dendrites of both excitatory thalamic projection neurons and local inhibitory neurons (Peters et al., 1991; Steriade et al., 1997). In a synaptic triad, an excitatory afferent forms synapses on a dendrite of a thalamic relay neuron and a vesicle-filled dendrite of a local inhibitory neuron, which forms an inhibitory synapse on the relay dendrite (Famiglietti and Peters, 1972). This unique arrangement produces disynaptic inhibition on the same part of the relay dendrite, with a short latency.

The situation is more complex for MD, a high order thalamic nucleus, which receives multiple afferents. In addition to excitatory afferents from the cortex and brainstem, and inhibitory afferents from the thalamic reticular nucleus, MD also receives inhibitory input from the basal ganglia (Russchen et al., 1987; Giguere and Goldman-Rakic, 1988; Carpenter, 1989; Xiao et al., 2009; Zikopoulos and Barbas, 2012). Large excitatory terminals in MD are comparatively rare. For example, at least in rats, few afferents form exclusively large excitatory terminals in MDmc (Kuroda and Price, 1991). Afferents from prefrontal cortex form only small terminals that lack mitochondria, while axons from piriform cortex form both large and small terminals (Kuroda and Price, 1991). Consistent with this pattern, in monkey parvicellular MD, prefrontal afferents form mostly small terminals and only a few large terminals (Schwartz et al., 1991). Large excitatory terminals are especially relevant to thalamic activity, as they target more proximal dendrites of relay neurons than smaller terminals (Ogren and Hendrickson, 1979; Ilinsky and Kultas-Ilinsky, 1990).

We provide evidence that amygdalar axons in MDmc terminate in large, mitochondria-containing boutons, forming synaptic triads, which may give the amygdala privileged access to proximal dendrites of relay neurons, ensuring transmission of signals to pOFC. The presence of triads in this pathway provides evidence that the amygdala acts as a sensory ganglion to transmit signals on the emotional environment to MD and from there to prefrontal cortex.

The functional significance of synaptic triads is not known, but their structure suggests a unique relay mechanism: afferents depolarize both relay dendrites and local

inhibitory neurons, so that the relay dendrite is initially depolarized followed by hyperpolarization (Steriade and Deschenes, 1984). Inhibitory dendrites are interconnected, resulting in disinhibition of the relay dendrite following hyperpolarization, allowing for a short window when the relay neuron is depolarized and preventing summation while transmitting high frequency signals to cortex (Steriade and Deschenes, 1984). Synaptic triads may allow thalamic relay neurons to transmit amygdalar signals undistorted to cortex, even at high frequencies.

3.4.4 Role of thalamus in emotion

Thalamic MD neurons play an important role in processing affective content: lesions of MD impair conditioned fear learning, and neurons in MDmc fire differentially in response to stimuli associated with reward, similar to neurons in the amygdala and OFC (Oyoshi et al., 1996; Li et al., 2004). However, thalamic neurons differ from cortical and amygdalar neurons in their physiological properties. Unlike the amygdala, thalamic projection neurons may switch between firing in bursting or tonic modes, which elicit different network effects (Steriade et al., 1997; Jones, 2009). Generally, burst firing is associated with synchronized oscillations generated during sleep, while a switch to tonic firing is essential to transmit signals undistorted to cortex (Jones, 2009). In MD, burst firing of thalamocortical neurons inhibits extinction learning, while tonic firing promotes extinction learning (Lee et al., 2012).

The nature of signals sent through the sequential pathway from the amygdala to MDmc and pOFC is not known, but other thalamic pathways may offer clues. Another

sequential pathway involves afferents from the superior colliculus, which innervate another part of MD, the lateral sector that projects to the frontal eye fields (FEF) in monkeys (Sommer and Wurtz, 2004). In this pathway, it has been suggested that MD acts as high pass filter, as high frequency signals are passed from the superior colliculus to FEF, and signals sent along this pathway are thought to represent corollary discharges related to planned saccades (Sommer and Wurtz, 2004). By analogy, amygdalar neurons may send corollary signals through MDmc, signaling affective content, in order to recruit relevant cortical areas and ensure that signals arriving via direct projections are received. A similar role has been proposed for the pulvinar thalamic nucleus: amygdalar connections with pulvinar projection neurons may activate visual cortices to coordinate cortical processing of visual stimuli with emotional relevance (Pessoa and Adolphs, 2010).

Thalamic MD lesions in primates lead to deficits in reinforcer devaluation, which requires updating the value of rewards, as well as impaired performance on memory-related delayed non-match to sample tasks (Markowitsch, 1982; Zola-Morgan and Squire, 1985; Izquierdo and Murray, 2010; reviewed in Mitchell and Chakraborty, 2013). Deficits in reward processing may be related to loss of the sequential amygdalar pathway to MDmc and pOFC in lesioned animals. Disruptions in the sequential pathway also change social behavior: mice with selective deletion of VGLUT2, which likely disconnects the pathway from the amygdala to pOFC through MDmc, show increased risk taking behavior and decreased avoidance (Wallen-Mackenzie et al., 2009). Conversely, increasing activity in MD produces the opposite behavioral changes

including anxiety-like symptoms, supporting a role of the sequential pathway in emotional behavior (Rotge et al., 2012). Our findings suggest that the strong, efficient excitatory pathway from the amygdala to MD activates cortically projecting neurons, including those that project widely to the upper layers of cortex, and may be necessary for recruiting cortical areas during tasks with affective import. Further, the amygdala can interact with neurons that project to pOFC, in addition to sending direct projections to pOFC, and these two routes may converge in pOFC to enhance cortical processing of emotional stimuli.

CHAPTER FOUR: CONCLUSION

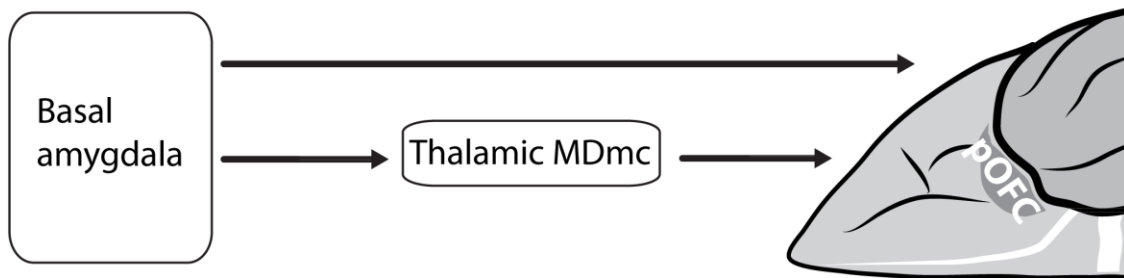
4.1 Amygdalar and thalamic pathways converge in pOFC

Amygdalar and thalamic pathways converge in pOFC, in circuits that are essential for flexible emotional behavior. The following are highlights of key novel findings shown schematically in Figure 4.1. We provide evidence that amygdalar and thalamic pathways target different layers in pOFC: amygdalar projections terminate mostly in the upper cortical layers, while thalamic pathways terminate in the middle cortical layers. The laminar pattern of termination is relevant to the function of a pathway. For example, different cortical layers contain different proportions of inhibitory neurons. In line with this, we found that amygdalar pathways in pOFC targeted mostly CB and CR inhibitory neurons in the upper cortical layers, while thalamic axons in the middle layers targeted more inhibitory neurons overall, and especially more PV neurons.

Further specializations in the amygdalar pathway to pOFC, especially large bouton size and prevalence of multisynaptic boutons, suggest that this pathway is synaptically efficient. Driving inputs to the upper cortical layers represent an unusual termination pattern, as cortical ‘drivers’ are typically thalamocortical pathways that terminate in the middle cortical layers. The strong and driver-like pathway from the amygdala to the upper layers may drive emotionally relevant signals from the amygdala to pOFC, for integration with sensory information to form a representation of task state (Wilson et al., 2014). Amygdalar axons in pOFC also preferentially innervate CB and CR neurons, which are suited to reduce noise at the fringes of active columns, and enhance signal (Wang et al., 2004).

1. Are amygdalar pathways to pOFC different from other inputs?

- Amygdalar pathway to pOFC has larger, more multisynaptic boutons than thalamic pathway and targets fewer inhibitory neurons
- May be a synaptically efficient driver of cortical neurons



2. Is there an indirect pathway through MD? How is it different from the direct pathway?

- There is a sequential pathway connecting the amygdala, MDmc, and pOFC
- Amygdalar pathways to MD and pOFC may be separate in the amygdala
- Amygdalar axons form large synapses in synaptic triads on thalamic relay neurons

Figure 4.1. Synaptic specializations in amygdalar pathways to pOFC and MD.

4.2 Sequential pathways link the amygdala with pOFC through MDmc

Previous studies suggested that there is overlap of amygdalar and pOFC pathways in MDmc (Porrino et al., 1981). However, other cortical and subcortical pathways project to MD, and a sequential pathway connecting pOFC and the amygdala through MDmc was uncertain (Russchen et al., 1987). We provide direct evidence for a sequential pathway linking the amygdala with thalamic neurons in MDmc that project to pOFC, forming a second, indirect route for amygdalar signals to reach pOFC.

Amygdalar axons in MD differ morphologically and neurochemically from those to cortex: amygdalar axon terminals in MD were larger in diameter and colocalized more frequently with the vesicular glutamate transporter VGLUT2. These features suggest that amygdalar axons in MD form highly efficient synapses. Further, these specializations between the two pathways indicate that they are distinct in the amygdala. Amygdalar axons in MDmc also formed more synapses with thalamic CB neurons, which project widely to the upper layers of cortex. This indirect pathway to pOFC may reinforce the direct amygdalar input to the upper layers of pOFC ensuring transmission of signals.

Interestingly, amygdalar pathways in MD formed synaptic triads. This specialization connects excitatory afferents, dendrites of excitatory thalamic relay neurons and local inhibitory neurons, and was first described in sensory thalamic nuclei (Famiglietti and Peters, 1972). We found that a significant proportion of amygdalar axons formed triads with excitatory thalamic relay neurons, akin to those connecting sensory afferents with thalamic relay neurons. This suggests that the amygdala may act

as a sensor of the value of stimuli, relaying signals with emotional import through the thalamic MDmc to prefrontal cortex.

4.3 Functional implications

We demonstrate here for the first time that signals from the amygdala follow two routes to cortex, one directly to pOFC and another through the thalamic MDmc. Both pathways show features of efficient synapses, suggesting high priority for signals with affective significance. The two routes may serve to enhance cortical processing of emotional content. Direct amygdalar projections to cortex may convey the affective content of stimuli for integration with sensory information in cortex. The indirect pathway through the thalamus may be necessary to activate cortical columns to strengthen amygdalar signals in pOFC. Further, both pathways may activate feedforward inhibition to reduce noise, or weak activation at the fringes of active columns, to eliminate distractors and focus attention on emotionally salient stimuli.

BIBLIOGRAPHY

- Abbott LF, Chance FS (2005) Drivers and modulators from push-pull and balanced synaptic input. *Progress in Brain Research* 149:147-155.
- Adler CM, McDonough-Ryan P, Sax KW, Holland SK, Arndt S, Strakowski SM (2000) fMRI of neuronal activation with symptom provocation in unmedicated patients with obsessive compulsive disorder. *Journal of Psychiatric Research* 34:317-324.
- Aggleton JP, Mishkin M (1984) Projections of the amygdala to the thalamus in the cynomolgus monkey. *Journal of Comparative Neurology* 222:56-68.
- Aggleton JP, Burton MJ, Passingham RE (1980) Cortical and subcortical afferents to the amygdala of the rhesus monkey (*Macaca mulatta*). *Brain Research* 190:347-368.
- An X, Bandler R, Ongur D, Price JL (1998) Prefrontal cortical projections to longitudinal columns in the midbrain periaqueductal gray in macaque monkeys. *Journal of Comparative Neurology* 401:455-479.
- Arnsten AF, Rubia K (2012) Neurobiological circuits regulating attention, cognitive control, motivation, and emotion: disruptions in neurodevelopmental psychiatric disorders. *Journal of the American Academy of Child and Adolescent Psychiatry* 51:356-367.
- Bachevalier J, Loveland KA (2006) The orbitofrontal-amygdala circuit and self-regulation of social-emotional behavior in autism. *Neuroscience & Biobehavioral Reviews* 30:97-117.
- Barbas H (2000) Connections underlying the synthesis of cognition, memory, and emotion in primate prefrontal cortices. *Brain Research Bulletin* 52:319-330.
- Barbas H (2007) Flow of information for emotions through temporal and orbitofrontal pathways. *Journal of Anatomy* 211:237-249.
- Barbas H, Pandya DN (1987) Architecture and frontal cortical connections of the premotor cortex (area 6) in the rhesus monkey. *Journal of Comparative Neurology* 256:211-218.
- Barbas H, Pandya DN (1989) Architecture and intrinsic connections of the prefrontal cortex in the rhesus monkey. *Journal of Comparative Neurology* 286:353-375.
- Barbas H, De Olmos J (1990) Projections from the amygdala to basoventral and mediodorsal prefrontal regions in the rhesus monkey. *Journal of Comparative Neurology* 300:549-571.

- Barbas H, Zikopoulos B, Timbie C (2011) Sensory pathways and emotional context for action in primate prefrontal cortex. *Biological Psychiatry* 69:1133-1139.
- Barbas H, Saha S, Rempel-Clower N, Ghashghaei T (2003) Serial pathways from primate prefrontal cortex to autonomic areas may influence emotional expression. *BMC Neuroscience* 4:25.
- Baxter MG, Murray EA (2002) The amygdala and reward. *Nature Reviews Neuroscience* 3:563-573.
- Bechara A, Damasio H, Damasio AR (2000) Emotion, decision making and the orbitofrontal cortex. *Cerebral Cortex* 10:295-307.
- Breiter HC, Rauch SL (1996) Functional MRI and the study of OCD: from symptom provocation to cognitive-behavioral probes of cortico-striatal systems and the amygdala. *Neuroimage* 4:S127-S138.
- Callaway EM (1998) Local circuits in primary visual cortex of the macaque monkey. *Annual Review of Neuroscience* 21:47-74.
- Carpenter MB (1989) Connectivity patterns of thalamic nuclei implicated in dyskinesia. *Stereotactic and Functional Neurosurgery* 52:79-119.
- Cavada C, Company T, Tejedor J, Cruz-Rizzolo RJ, Reinoso-Suarez F (2000) The anatomical connections of the macaque monkey orbitofrontal cortex. A review. *Cerebral Cortex* 10:220-242.
- Chamberlain SR, Blackwell AD, Fineberg NA, Robbins TW, Sahakian BJ (2005) The neuropsychology of obsessive compulsive disorder: the importance of failures in cognitive and behavioural inhibition as candidate endophenotypic markers. *Neuroscience & Biobehavioral Reviews* 29:399-419.
- Cohen J (1988) *Statistical Power Analysis for the Behavioral Sciences*. Hillsdale, NJ: Lawrence Erlbaum Associates, Inc.
- Constantinidis C, Goldman-Rakic PS (2002) Correlated discharges among putative pyramidal neurons and interneurons in the primate prefrontal cortex. *Journal of Neurophysiology* 88:3487-3497.
- Cruikshank SJ, Ahmed OJ, Stevens TR, Patrick SL, Gonzalez AN, Elmaleh M, Connors BW (2012) Thalamic control of layer 1 circuits in prefrontal cortex. *Journal of Neuroscience* 32:17813-17823.
- Davis M, Whalen PJ (2001) The amygdala: vigilance and emotion. *Molecular Psychiatry* 6:13-34.

- De Olmos JS (1990) Amygdala. In: *The Human Nervous System* (Paxinos G, ed), pp 583-710. San Diego: Academic Press, Inc.
- DeFelipe J (1997) Types of neurons, synaptic connections and chemical characteristics of cells immunoreactive for calbindin-D28K, parvalbumin and calretinin in the neocortex. *Journal of Chemical Neuroanatomy* 14:1-19.
- DeFelipe J, Farinas I (1992) The pyramidal neuron of the cerebral cortex: morphological and chemical characteristics of the synaptic inputs. *Progress in Neurobiology* 39:563-607X.
- DeFelipe J, Hendry SH, Jones EG (1989) Synapses of double bouquet cells in monkey cerebral cortex visualized by calbindin immunoreactivity. *Brain Research* 503:49-54.
- Dermon CR, Barbas H (1994) Contralateral thalamic projections predominantly reach transitional cortices in the rhesus monkey. *Journal of Comparative Neurology* 344:508-531.
- Devinsky O, Morrell MJ, Vogt BA (1995) Contributions of anterior cingulate cortex to behaviour. *Brain* 118:279-306.
- Dombrowski SM, Hilgetag CC, Barbas H (2001) Quantitative architecture distinguishes prefrontal cortical systems in the rhesus monkey. *Cerebral Cortex* 11:975-988.
- Douglas RJ, Martin KA (1998) Neocortex. In: *The Synaptic Organization of the Brain*, Fourth Edition (Shepherd GM, ed), pp 459-509. New York: Oxford University Press.
- Erickson SL, Melchitzky DS, Lewis DA (2004) Subcortical afferents to the lateral mediodorsal thalamus in cynomolgus monkeys. *Neuroscience* 129:675-690.
- Famiglietti EV, Jr., Peters A (1972) The synaptic glomerulus and the intrinsic neuron in the dorsal lateral geniculate nucleus of the cat. *Journal of Comparative Neurology* 144:285-334.
- Fiala JC (2005) Reconstruct: a free editor for serial section microscopy. *Journal of Microscopy* 218:52-61.
- Finlay BL, Darlington RB (1995) Linked regularities in the development and evolution of mammalian brains. *Science* 268:1578-1583.
- Freneau RT, Jr. et al. (2001) The expression of Vesicular glutamate transporters defines two classes of excitatory synapses. *Neuron*.

- Freund TF, Martin KA, Soltesz I, Somogyi P, Whitteridge D (1989) Arborisation pattern and postsynaptic targets of physiologically identified thalamocortical afferents in striate cortex of the macaque monkey. *Journal of Comparative Neurology* 289:315-336.
- Gabbott PL, Bacon SJ (1996) Local circuit neurons in the medial prefrontal cortex (areas 24a,b,c, 25 and 32) in the monkey: II. Quantitative areal and laminar distributions. *Journal of Comparative Neurology* 364:609-636.
- Gaffan D, Murray EA (1990) Amygdalar interaction with the mediodorsal nucleus of the thalamus and the ventromedial prefrontal cortex in stimulus reward associative learning in the monkey. *Journal of Neuroscience* 10:3479-3493.
- Geinisman Y (2000) Structural synaptic modifications associated with hippocampal LTP and behavioral learning. *Cerebral Cortex* 10:952-962.
- Geinisman Y, Berry RW, Disterhoft JF, Power JM, Van der Zee EA (2001) Associative learning elicits the formation of multiple-synapse boutons. *Journal of Neuroscience* 21:5568-5573.
- Germuska M, Saha S, Fiala JC, Barbas H (2006) Synaptic distinction of laminar specific prefrontal-temporal pathways in primates. *Cerebral Cortex* 16:865-875.
- Ghashghaei HT, Barbas H (2002) Pathways for emotions: Interactions of prefrontal and anterior temporal pathways in the amygdala of the rhesus monkey. *Neuroscience* 115:1261-1279.
- Ghashghaei HT, Hilgetag CC, Barbas H (2007) Sequence of information processing for emotions based on the anatomic dialogue between prefrontal cortex and amygdala. *Neuroimage* 34:905-923.
- Giguere M, Goldman-Rakic PS (1988) Mediodorsal nucleus: Areal, laminar, and tangential distribution of afferents and efferents in the frontal lobe of rhesus monkeys. *Journal of Comparative Neurology* 277:195-213.
- Goldman-Rakic PS, Porrino LJ (1985) The primate mediodorsal (MD) nucleus and its projection to the frontal lobe. *Journal of Comparative Neurology* 242:535-560.
- Gonzalez Andino SL, Grave de Peralta Menendez R (2012) Coding of saliency by ensemble bursting in the amygdala of primates. *Frontiers in Behavioral Neuroscience* 6:38.
- Greenberg BD, Rauch SL, Haber SN (2010) Invasive circuitry-based neurotherapeutics: stereotactic ablation and deep brain stimulation for OCD. *Neuropsychopharmacology* 35:317-336.

- Greenberg BD, Ziemann U, Harmon A, Murphy DL, Wassermann EM (1998) Decreased neuronal inhibition in cerebral cortex in obsessive-compulsive disorder on transcranial magnetic stimulation. *Lancet* 352:881-882.
- Haber SN, Heilbronner SR (2013) Translational research in OCD: circuitry and mechanisms. *Neuropsychopharmacology* 38:252-253.
- Haber SN, Kunishio K, Mizobuchi M, Lynd-Balta E (1995) The orbital and medial prefrontal circuit through the primate basal ganglia. *Journal of Neuroscience* 15:4851-4867.
- Hackett TA, Takahata T, Balaram P (2011) VGLUT1 and VGLUT2 mRNA expression in the primate auditory pathway. *Hearing Research* 274:129-141.
- Hadland KA, Rushworth MF, Gaffan D, Passingham RE (2003) The effect of cingulate lesions on social behaviour and emotion. *Neuropsychologia* 41:919-931.
- Harris KM, Stevens JK (1989) Dendritic spines of CA 1 pyramidal cells in the rat hippocampus: serial electron microscopy with reference to their biophysical characteristics. *Journal of Neuroscience* 9:2982-2997.
- Herry C, Ciocchi S, Senn V, Demmou L, Muller C, Luthi A (2008) Switching on and off fear by distinct neuronal circuits. *Nature* 454:600-606.
- Hosokawa T, Kato K, Inoue M, Mikami A (2007) Neurons in the macaque orbitofrontal cortex code relative preference of both rewarding and aversive outcomes. *Neuroscience Research* 57:434-445.
- Huey ED, Zahn R, Krueger F, Moll J, Kapogiannis D, Wassermann EM, Grafman J (2008) A psychological and neuroanatomical model of obsessive-compulsive disorder. *Journal of Neuropsychiatry and Clinical Neurosciences* 20:390-408.
- Ilinsky IA, Kultas-Ilinsky K (1990) Fine structure of the magnocellular subdivision of the ventral anterior thalamic nucleus (VAmc) of *Macaca mulatta*: I. Cell types and synaptology. *Journal of Comparative Neurology* 294:455-478.
- Ilinsky IA, Jouandet ML, Goldman-Rakic PS (1985) Organization of the nigrothalamocortical system in the rhesus monkey. *Journal of Comparative Neurology* 236:315-330.
- Izquierdo A, Murray EA (2005) Opposing effects of amygdala and orbital prefrontal cortex lesions on the extinction of instrumental responding in macaque monkeys. *European Journal of Neuroscience* 22:2341-2346.

- Izquierdo A, Murray EA (2007) Selective bilateral amygdala lesions in rhesus monkeys fail to disrupt object reversal learning. *Journal of Neuroscience* 27:1054-1062.
- Izquierdo A, Murray EA (2010) Functional interaction of medial mediodorsal thalamic nucleus but not nucleus accumbens with amygdala and orbital prefrontal cortex is essential for adaptive response selection after reinforcer devaluation. *Journal of Neuroscience* 30:661-669.
- Jensen FE, Harris KM (1989) Preservation of neuronal ultrastructure in hippocampal slices using rapid microwave-enhanced fixation. *Journal of Neuroscience Methods* 29:217-230.
- Jiao Y, Sun Z, Lee T, Fusco FR, Kimble TD, Meade CA, Cuthbertson S, Reiner A (1999) A simple and sensitive antigen retrieval method for free-floating and slide-mounted tissue sections. *Journal of Neuroscience Methods* 93:149-162.
- John YJ, Bullock D, Zikopoulos B, Barbas H (2013) Anatomy and computational modeling of networks underlying cognitive-emotional interaction. *Frontiers in Human Neuroscience* 7:101.
- Jones EG (1985) *The Thalamus*. New York (NY): Plenum Press.
- Jones EG (1998) Viewpoint: the core and matrix of thalamic organization. *Neuroscience* 85:331-345.
- Jones EG (2009) Synchrony in the Interconnected Circuitry of the Thalamus and Cerebral Cortex. *Annals of the New York Academy of Sciences* 1157:10-23.
- Jones EG, Hendry SHC (1989) Differential calcium binding protein immunoreactivity distinguishes classes of relay neurons in monkey thalamic nuclei. *European Journal of Neuroscience* 1:222-246.
- Jones TA, Klintsova AY, Kilman VL, Sirevaag AM, Greenough WT (1997) Induction of multiple synapses by experience in the visual cortex of adult rats. *Neurobiology of Learning and Memory* 68:13-20.
- Kang DH, Kim JJ, Choi JS, Kim YI, Kim CW, Youn T, Han MH, Chang KH, Kwon JS (2004) Volumetric investigation of the frontal-subcortical circuitry in patients with obsessive-compulsive disorder. *Journal of Neuropsychiatry and Clinical Neurosciences* 16:342-349.
- Kennerley SW, Walton ME, Behrens TE, Buckley MJ, Rushworth MF (2006) Optimal decision making and the anterior cingulate cortex. *Nature Neuroscience* 9:940-947.

- Kim JJ, Lee MC, Kim J, Kim IY, Kim SI, Han MH, Chang KH, Kwon JS (2001) Grey matter abnormalities in obsessive-compulsive disorder: statistical parametric mapping of segmented magnetic resonance images. *British Journal of Psychiatry* 179:330-334.
- Kultas-Ilinsky K, Ilinsky IA (1991) Fine structure of the ventral lateral nucleus (VL) of the *Macaca mulatta* thalamus: cell types and synaptology. *Journal of Comparative Neurology* 314:319-349.
- Kultas-Ilinsky K, Fallet C, Verney C (2004) Development of the human motor-related thalamic nuclei during the first half of gestation, with special emphasis on GABAergic circuits. *Journal of Comparative Neurology* 476:267-289.
- Kuroda M, Price JL (1991) Synaptic organization of projections from basal forebrain structures to the mediodorsal thalamic nucleus of the rat. *Journal of Comparative Neurology* 303:513-533.
- Lacerda AL, Dalgalarondo P, Caetano D, Camargo EE, Etchebehere EC, Soares JC (2003) Elevated thalamic and prefrontal regional cerebral blood flow in obsessive-compulsive disorder: a SPECT study. *Psychiatry Research* 123:125-134.
- Lee S, Ahmed T, Kim H, Choi S, Kim DS, Kim SJ, Cho J, Shin HS (2012) Bidirectional modulation of fear extinction by mediodorsal thalamic firing in mice. *Nature Neuroscience* 15:308-314.
- Li XB, Inoue T, Nakagawa S, Koyama T (2004) Effect of mediodorsal thalamic nucleus lesion on contextual fear conditioning in rats. *Brain Research* 1008:261-272.
- Little JP, Carter AG (2013) Synaptic Mechanisms Underlying Strong Reciprocal Connectivity between the Medial Prefrontal Cortex and Basolateral Amygdala. *Journal of Neuroscience* 33:15333-15342.
- Luk CH, Wallis JD (2013) Choice coding in frontal cortex during stimulus-guided or action-guided decision-making. *Journal of Neuroscience* 33:1864-1871.
- Maia TV, Cooney RE, Peterson BS (2008) The neural bases of obsessive-compulsive disorder in children and adults. *Development and Psychopathology* 20:1251-1283.
- Malkova L, Gaffan D, Murray EA (1997) Excitotoxic lesions of the amygdala fail to produce impairment in visual learning for auditory secondary reinforcement but interfere with reinforcer devaluation effects in rhesus monkeys. *Journal of Neuroscience* 17:6011-6020.

- Markowitsch HJ (1982) Thalamic mediodorsal nucleus and memory: A critical evaluation of studies in animals and man. *Neuroscience & Biobehavioral Reviews* 6:351-380.
- Matsuzaki M, Ellis-Davies GC, Nemoto T, Miyashita Y, Iino M, Kasai H (2001) Dendritic spine geometry is critical for AMPA receptor expression in hippocampal CA1 pyramidal neurons. *Nature Neuroscience* 4:1086-1092.
- McCracken CB, Grace AA (2007) High-frequency deep brain stimulation of the nucleus accumbens region suppresses neuronal activity and selectively modulates afferent drive in rat orbitofrontal cortex in vivo. *Journal of Neuroscience* 27:12601-12610.
- McDonald AJ (1987) Organization of amygdaloid projections to the mediodorsal thalamus and prefrontal cortex: a fluorescence retrograde transport study in the rat. *Journal of Comparative Neurology* 262:46-58.
- McFarland NR, Haber SN (2002) Thalamic relay nuclei of the basal ganglia form both reciprocal and nonreciprocal cortical connections, linking multiple frontal cortical areas. *Journal of Neuroscience* 22:8117-8132.
- Medalla M, Barbas H (2012) The anterior cingulate cortex may enhance inhibition of lateral prefrontal cortex via m2 cholinergic receptors at dual synaptic sites. *Journal of Neuroscience* 32:15611-15625.
- Medalla M, Lera P, Feinberg M, Barbas H (2007) Specificity in inhibitory systems associated with prefrontal pathways to temporal cortex in primates. *Cerebral Cortex* 17 Suppl 1:i136-i150.
- Mesulam MM, Mufson EJ, Levey AI, Wainer BH (1983) Cholinergic innervation of cortex by the basal forebrain: cytochemistry and cortical connections of the septal area, diagonal band nuclei, nuclei, nucleus basalis (Substantia Innominata), and hypothalamus in the rhesus monkey. *Journal of Comparative Neurology* 214:170-197.
- Mitchell AS, Chakraborty S (2013) What does the mediodorsal thalamus do? *Frontiers in Systems Neuroscience* 7:37.
- Mitchell AS, Browning PG, Baxter MG (2007) Neurotoxic lesions of the medial mediodorsal nucleus of the thalamus disrupt reinforcer devaluation effects in rhesus monkeys. *Journal of Neuroscience* 27:11289-11295.
- Miyashita T, Ichinohe N, Rockland KS (2007) Differential modes of termination of amygdalothalamic and amygdalocortical projections in the monkey. *Journal of Comparative Neurology* 502:309-324.

- Miyazaki T, Fukaya M, Shimizu H, Watanabe M (2003) Subtype switching of vesicular glutamate transporters at parallel fibre-Purkinje cell synapses in developing mouse cerebellum. *European Journal of Neuroscience* 17:2563-2572.
- Morecraft RJ, Van Hoesen GW (1998) Convergence of limbic input to the cingulate motor cortex in the rhesus monkey. *Brain Research Bulletin* 45:209-232.
- Morrison SE, Salzman CD (2010) Re-valuing the amygdala. *Current Opinion in Neurobiology* 20:221-230.
- Morrison SE, Salzman CD (2011) Representations of appetitive and aversive information in the primate orbitofrontal cortex. *Annals of the New York Academy of Sciences* 1239:59-70.
- Muller D, Toni N, Buchs PA (2000) Spine changes associated with long-term potentiation. *Hippocampus* 10:596-604.
- Muly EC, Senyuz M, Khan ZU, Guo JD, Hazra R, Rainnie DG (2009) Distribution of D-1 and D-5 dopamine receptors in the primate and rat basolateral amygdala. *Brain Structure & Function* 213:375-393.
- Murray EA (2007) The amygdala, reward and emotion. *Trends in Cognitive Sciences* 11:489-497.
- National Research Council (2011) *Guide for the Care and Use of Laboratory Animals: Eighth Edition: The National Academies Press.*
- Nava N, Chen F, Wegener G, Popoli M, Nyengaard JR (2014) A new efficient method for synaptic vesicle quantification reveals differences between medial prefrontal cortex perforated and nonperforated synapses. *Journal of Comparative Neurology* 522:284-297.
- Nicholson DA, Trana R, Katz Y, Kath WL, Spruston N, Geinisman Y (2006) Distance-dependent differences in synapse number and AMPA receptor expression in hippocampal CA1 pyramidal neurons. *Neuron* 50:431-442.
- O'Mara SM, Commins S, Anderson M, Gigg J (2001) The subiculum: a review of form, physiology and function. *Progress in Neurobiology* 64:129-155.
- Ogren MP, Hendrickson AE (1979) The structural organization of the inferior and lateral subdivisions of the Macaca monkey pulvinar. *Journal of Comparative Neurology* 188:147-178.
- Olszewski J (1952) *The Thalamus of the Macaca mulatta . An Atlas for Use with the Stereotaxic Instrument.* Basel, Switzerland: Karger,S.

- Ostroff LE, Cain CK, Bedont J, Monfils MH, Ledoux JE (2010) Fear and safety learning differentially affect synapse size and dendritic translation in the lateral amygdala. *Proceedings of the National Academies of the Sciences of the United States of America* 107:9418-9423.
- Otis TS (2001) Vesicular glutamate transporters in cognition. *Neuron* 29:11-14.
- Oyoshi T, Nishijo H, Asakura T, Takamura Y, Ono T (1996) Emotional and behavioral correlates of mediodorsal thalamic neurons during associative learning in rats. *Journal of Neuroscience* 16:5812-5829.
- Pare D, Papez HC, Dong J (1995) Bursting and oscillating neurons of the cat basolateral amygdaloid complex in vivo: electrophysiological properties and morphological features. *Journal of Neurophysiology* 74:1179-1191.
- Pare D, Royer S, Smith Y, Lang EJ (2003) Contextual inhibitory gating of impulse traffic in the intra-amygdaloid network. *Annals of the New York Academy of Sciences* 985:78-91.
- Pessoa L, Adolphs R (2010) Emotion processing and the amygdala: from a 'low road' to 'many roads' of evaluating biological significance. *Nature Reviews Neuroscience* 11:773-783.
- Peters A, Kaiserman-Abramof IR (1969) The small pyramidal neuron of the rat cerebral cortex. The synapses upon dendritic spines. *Zeitschrift für Zellforschung und mikroskopische Anatomie* 100:487-506.
- Peters A, Palay SL, Webster HD (1991) The fine structure of the nervous system. Neurons and their supporting cells. New York: Oxford University Press.
- Pitkanen A, Amaral DG (1994) The distribution of GABAergic cells, fibers, and terminals in the monkey amygdaloid complex: an immunohistochemical and in situ hybridization study. *Journal of Neuroscience* 14:2200-2224.
- Pitkanen A, Kempainen S (2002) Comparison of the distribution of calcium-binding proteins and intrinsic connectivity in the lateral nucleus of the rat, monkey, and human amygdala. *Pharmacology, Biochemistry and Behavior* 71:369-377.
- Porrino LJ, Crane AM, Goldman-Rakic PS (1981) Direct and indirect pathways from the amygdala to the frontal lobe in rhesus monkeys. *Journal of Comparative Neurology* 198:121-136.
- Price JL (2003) Comparative aspects of amygdala connectivity. *Annals of the New York Academy of Sciences* 985:50-58.

- Price JL, Amaral DG (1981) An autoradiographic study of the projections of the central nucleus of the monkey amygdala. *Journal of Neuroscience* 1:1242-1259.
- Price JL, Russchen FT, Amaral DG (1987) The limbic region. II. The amygdaloid complex. In: *Handbook of Chemical Neuroanatomy. Vol.5, Integrated Systems of the CNS, Part I.* (Björklund A, Hökfelt T, Swanson LW, eds), pp 279-381. Amsterdam: Elsevier.
- Quirk GJ, Repa C, LeDoux JE (1995) Fear conditioning enhances short-latency auditory responses of lateral amygdala neurons: parallel recordings in the freely behaving rat. *Neuron* 15:1029-1039.
- Rainnie DG, Asprodini EK, Shinnick-Gallagher P (1993) Intracellular recordings from morphologically identified neurons of the basolateral amygdala. *Journal of Neurophysiology* 69:1350-1362.
- Rakic P (2002) Neurogenesis in adult primate neocortex: an evaluation of the evidence. *Nature Reviews Neuroscience* 3:65-71.
- Rasband WS (1997-2014) ImageJ. In. Bethesda, MD, USA: U.S. National Institutes of Health.
- Rauch SL, Jenike MA, Alpert NM, Baer L, Breiter HC, Savage CR, Fischman AJ (1994) Regional cerebral blood flow measured during symptom provocation in obsessive-compulsive disorder using oxygen 15-labeled carbon dioxide and positron emission tomography. *Archives of General Psychiatry* 51:62-70.
- Ray JP, Price JL (1993) The organization of projections from the mediodorsal nucleus of the thalamus to orbital and medial prefrontal cortex in macaque monkeys. *Journal of Comparative Neurology* 337:1-31.
- Reichova I, Sherman SM (2004) Somatosensory corticothalamic projections: distinguishing drivers from modulators. *Journal of Neurophysiology* 92:2185-2197.
- Rempel-Clower NL, Barbas H (1998) Topographic organization of connections between the hypothalamus and prefrontal cortex in the rhesus monkey. *Journal of Comparative Neurology* 398:393-419.
- Richter MA, de Jesus DR, Hoppenbrouwers S, Daigle M, Deluce J, Ravindran LN, Fitzgerald PB, Daskalakis ZJ (2012) Evidence for cortical inhibitory and excitatory dysfunction in obsessive compulsive disorder. *Neuropsychopharmacology* 37:1144-1151.

- Rockland KS (1996) Two types of corticopulvinar terminations: round (type 2) and elongate (type1). *Journal of Comparative Neurology* 368:57-87.
- Rogan MT, Staubli UV, LeDoux JE (1997) Fear conditioning induces associative long-term potentiation in the amygdala. *Nature* 390:604-607.
- Romanski LM, Clugnet MC, Bordi F, LeDoux JE (1993) Somatosensory and auditory convergence in the lateral nucleus of the amygdala. *Behavioral Neuroscience* 107:444-450.
- Rosene DL, Roy NJ, Davis BJ (1986) A cryoprotection method that facilitates cutting frozen sections of whole monkey brains from histological and histochemical processing without freezing artifact. *Journal of Histochemistry and Cytochemistry* 34:1301-1315.
- Rotge JY, Aouizerate B, Amestoy V, Lambrecq V, Langbour N, Nguyen TH, Dovero S, Carroit L, Tignol J, Bioulac B, Burbaud P, Guehl D (2012) The associative and limbic thalamus in the pathophysiology of obsessive-compulsive disorder: an experimental study in the monkey. *Translational Psychiatry* 2:e161.
- Rovo Z, Ulbert I, Acsady L (2012) Drivers of the primate thalamus. *Journal of Neuroscience* 32:17894-17908.
- Rudebeck PH, Murray EA (2008) Amygdala and orbitofrontal cortex lesions differentially influence choices during object reversal learning. *Journal of Neuroscience* 28:8338-8343.
- Russchen FT, Amaral DG, Price JL (1987) The afferent input to the magnocellular division of the mediodorsal thalamic nucleus in the monkey, *Macaca fascicularis* *Journal of Comparative Neurology* 256:175-210.
- Schwartz ML, Dekker JJ, Goldman-Rakic PS (1991) Dual mode of corticothalamic synaptic termination in the mediodorsal nucleus of the rhesus monkey. *Journal of Comparative Neurology* 309:289-304.
- Shelton L, Becerra L, Borsook D (2012) Unmasking the mysteries of the habenula in pain and analgesia. *Progress in Neurobiology* 96:208-219.
- Sherman SM, Guillery RW (1998) On the actions that one nerve cell can have on another: distinguishing "drivers" from "modulators". *Proceedings of the National Academy of Sciences of the United States of America* 95:7121-7126.
- Simmons JM, Richmond BJ (2008) Dynamic changes in representations of preceding and upcoming reward in monkey orbitofrontal cortex. *Cerebral Cortex* 18:93-103.

- Sommer MA, Wurtz RH (2004) What the brain stem tells the frontal cortex. I. Oculomotor signals sent from superior colliculus to frontal eye field via mediodorsal thalamus. *Journal of Neurophysiology* 91:1381-1402.
- Steriade M, Deschenes M (1984) The thalamus as a neuronal oscillator. *Brain Research* 8:1-63.
- Steriade M, Jones EG, McCormick DA (1997) *Thalamus - Organisation and function*. Oxford: Elsevier Science.
- Szeszko PR, Robinson D, Alvir JM, Bilder RM, Lencz T, Ashtari M, Wu H, Bogerts B (1999) Orbital frontal and amygdala volume reductions in obsessive-compulsive disorder. *Archives of General Psychiatry* 56:913-919.
- Tai Y, Yi H, Ilinsky IA, Kultas-Ilinsky K (1995) Nucleus reticularis thalami connections with the mediodorsal thalamic nucleus: a light and electron microscopic study in the monkey. *Brain Research Bulletin* 38:475-488.
- Tremblay L, Schultz W (1999) Relative reward preference in primate orbitofrontal cortex. *Nature* 398:704-708.
- Vogt BA, Barbas H (1988) Structure and connections of the cingulate vocalization region in the rhesus monkey. In: *The Physiological Control of Mammalian Vocalization* (Newman JD, ed), pp 203-225. New York: Plenum Publ. Corp.
- Wallen-Mackenzie A, Nordenankar K, Fejgin K, Lagerstrom MC, Emilsson L, Fredriksson R, Wass C, Andersson D, Egecioglu E, Andersson M, Strandberg J, Lindhe O, Schioth HB, Chergui K, Hanse E, Langstrom B, Fredriksson A, Svensson L, Roman E, Kullander K (2009) Restricted cortical and amygdaloid removal of vesicular glutamate transporter 2 in preadolescent mice impacts dopaminergic activity and neuronal circuitry of higher brain function. *Journal of Neuroscience* 29:2238-2251.
- Wallis JD, Miller EK (2003) Neuronal activity in primate dorsolateral and orbital prefrontal cortex during performance of a reward preference task. *European Journal of Neuroscience* 18:2069-2081.
- Wang XJ, Tegner J, Constantinidis C, Goldman-Rakic PS (2004) Division of labor among distinct subtypes of inhibitory neurons in a cortical microcircuit of working memory. *Proceedings of the National Academy of Sciences of the United States of America* 101:1368-1373.
- Waring AE, Means LW (1976) The effect of medial thalamic lesions on emotionality, activity, and discrimination learning in the rat. *Physiology and Behavior* 17:181-186.

- West EA, DesJardin JT, Gale K, Malkova L (2011) Transient inactivation of orbitofrontal cortex blocks reinforcer devaluation in macaques. *Journal of Neuroscience* 31:15128-15135.
- Weston MC, Nehring RB, Wojcik SM, Rosenmund C (2011) Interplay between VGLUT isoforms and endophilin A1 regulates neurotransmitter release and short-term plasticity. *Neuron* 69:1147-1159.
- Wilson RC, Takahashi YK, Schoenbaum G, Niv Y (2014) Orbitofrontal cortex as a cognitive map of task space. *Neuron* 81:267-279.
- Wojcik SM, Rhee JS, Herzog E, Sigler A, Jahn R, Takamori S, Brose N, Rosenmund C (2004) An essential role for vesicular glutamate transporter 1 (VGLUT1) in postnatal development and control of quantal size. *Proceedings of the National Academies of the Sciences of the United States of America* 101:7158-7163.
- Xiao D, Zikopoulos B, Barbas H (2009) Laminar and modular organization of prefrontal projections to multiple thalamic nuclei. *Neuroscience* 161:1067-1081.
- Zikopoulos B, Barbas H (2006) Prefrontal projections to the thalamic reticular nucleus form a unique circuit for attentional mechanisms. *Journal of Neuroscience* 26:7348-7361.
- Zikopoulos B, Barbas H (2007a) Parallel driving and modulatory pathways link the prefrontal cortex and thalamus. *PLoS One* 2:e848.
doi:810.1371/journal.pone.0000848.
- Zikopoulos B, Barbas H (2007b) Circuits for multisensory integration and attentional modulation through the prefrontal cortex and the thalamic reticular nucleus in primates. *Reviews in the Neurosciences* 18 417-438.
- Zikopoulos B, Barbas H (2012) Pathways for emotions and attention converge on the thalamic reticular nucleus in primates. *Journal of Neuroscience* 32:5338-5350.
- Zola-Morgan S, Squire LR (1985) Amnesia in monkeys after lesions of the mediodorsal nucleus of the thalamus. *Annals of Neurology* 17:558-564.

CURRICULUM VITAE



